

THE DETECTION OF PHARMACEUTICAL DRUG COMPOUNDS FROM INTACT  
BIOLOGICAL TISSUE BY MATRIX-ASSISTED LASER DESORPTION  
IONIZATION (MALDI) QUADRUPOLE ION TRAP MASS SPECTROMETRY

By

CHRISTOPHER D. REDDICK

A DISSERTATION PRESENTED TO THE GRADUATE SCHOOL  
OF THE UNIVERSITY OF FLORIDA IN PARTIAL FULFILLMENT  
OF THE REQUIREMENTS FOR THE DEGREE OF  
DOCTOR OF PHILOSOPHY

UNIVERSITY OF FLORIDA

1997

To my parents

## ACKNOWLEDGMENTS

Of all the people who have contributed to this work, no two people deserve more credit than my parents George and Sue Reddick. Growing up, my parents never pushed me to succeed or forced me down a path I did not want to travel. Instead they simply loved me the best that they could and encouraged me in all of my endeavors big and small. I am also thankful to my parents for being the best role models a boy could have. While other kids were searching for role models in the movies or on TV, I only had to look across the dinner table every night to find mine. Of all of the things my parents have done for me over the years, their unconditional support has been their greatest gift. And for that I will always be thankful.

At the University of Florida my sincerest thanks first go to my research advisor Dr. Rick Yost for taking a young man with practically no mass spec experience into a research group full of all-stars. Throughout my tenure in Rick's research group I could always count on him for advice, feedback, and that extra shot of confidence when things weren't going quite as planned. Most of all, I would like to thank Rick for allowing me the freedom to work at my own pace and to really enjoy graduate school. I would also like to thank the members of my committee, Dr. Dave Powell, Dr. Jim Winefordner, Dr. Jim Deyrup, and Dr. Howard Johnson, for their time and effort in helping me complete this dissertation.

Probably the most difficult job I have ever undertaken has been designing and constructing the instrument for this dissertation. No one person was more instrumental in helping me accomplish this goal than Joe Shalosky, the Chemistry Department machine shop supervisor. Joe is an expert machinist. But more importantly he is an excellent teacher with endless patience. I would like to thank Joe for his time, effort, and most importantly for the lively conversations we had during the long hours in the machine shop. I would also like to thank Donna Balkcom for helping me navigate through the graduate system at UF.

Without a doubt, every member of the Yost group has added in one way or another to my experience at UF. I would like to first thank past Yost group members Uli Bernier, Rafael Vargas, Jon Jones, and Tony Annachino for making the early years in Rick's group fun. Thanks also go out to all of the members of the Burrito Brothers lunch crew, past and present. No matter how bad the day was going, our daily trip to Burrito Brothers always seemed to make things better. I especially would like to thank Scott Quarmby for his help with the electronics for the instrument and in general for being a friend. Working with Scott over the past four years has truly been educational. More recently, I would like to thank Rick Troendle for being my co-pilot on the instrument during my last few months of research. Rick's optimism and enthusiasm gave me a real boost during the final push to graduate. The research for this dissertation was funded by Bristol-Myers Squibb. I would like to thank Drs. Ira Rosenberg, Mike Lee, and Mark Hail for their enthusiasm and support throughout the project.

Finally, I would like to thank my longtime friend and mentor at ALCOA, Robin Khosah, for encouraging me to become a scientist and to get my Ph.D.

## TABLE OF CONTENTS

	<u>page</u>
ACKNOWLEDGMENTS .....	iii
ABSTRACT .....	vii
1 INTRODUCTION .....	1
Development of Laser Desorption Mass Spectrometry .....	2
Matrix-Assisted Laser Desorption Ionization (MALDI) .....	6
MALDI Theory and Mechanism .....	12
MALDI Sample Preparation .....	14
MALDI Matrices .....	17
Overview of Dissertation .....	18
2 FUNDAMENTAL INVESTIGATIONS OF MALDI OF DRUG COMPOUNDS IN TISSUE USING A TIME-OF-FLIGHT MASS SPECTROMETER .....	22
Instrument Description .....	23
MALDI Optimization Experiments with Matrigel .....	25
Matrigel Sample Preparation .....	25
Optimization of the MALDI Matrix Concentration .....	27
Optimization of the MALDI Matrix Solvent Polarity .....	32
Optimization of the MALDI Matrix "Soak Time" .....	39
Spatial Resolution Experiments with Spiperone in Matrigel .....	40
3 DESIGN AND CONSTRUCTION OF A NOVEL LASER DESORPTION QUADRUPOLE ION TRAP MASS SPECTROMETER .....	51
The Quadrupole Ion Trap Mass Spectrometer .....	51
Background History .....	51
Ion Trap Theory .....	56
Operation of the Ion Trap .....	63
Ion isolation .....	65
Tandem mass spectrometry (MS/MS) .....	70
Ion detection .....	70
Mass range extension .....	72
Coupling LDI to the Ion Trap .....	76

MALDI Inside the Ion Trap .....	76
MALDI Using an External Source Configuration .....	82
Instrument Design .....	92
Vacuum Manifold and Pumping System .....	92
Ion Source .....	95
DC Quadrupole Deflector Assembly .....	100
Laser Setup .....	102
Software Control .....	106
4 MALDI OF DRUG COMPOUNDS IN TISSUE USING A QUADRUPOLE ION TRAP MASS SPECTROMETER .....	109
Instrument Calibration & Optimization .....	109
EI of Perfluorotributylamine Calibration Gas .....	109
Instrument Simulation using SIMION V6.0 .....	115
High Mass Calibration using a Peptide Mixture.....	121
Analysis of Spiperone from Rat Cerebral Tissue.....	122
MALDI MS and MS/MS of Standard Spiperone .....	125
Preparation of the Cerebral Tissue.....	128
MALDI Analysis of Cerebral Tissue .....	129
Analysis of Taxol from Mouse Ovarian Tumor Tissue .....	131
MALDI MS and MS/MS of Standard Taxol.....	132
Preparation of the Ovarian Tumor Tissue .....	137
MALDI Analysis of Ovarian Tumor Tissue .....	137
Analysis of Polymyxin B <sub>1</sub> from Human Plasma .....	141
MALDI MS and MS/MS of Standard Polymyxin B <sub>1</sub> .....	142
MALDI Analysis of Human Plasma .....	144
LD/CI as an Alternative to MALDI .....	147
Initial LD/CI Experiments with Trimethylphenylammonium bromide .....	151
LD/CI of Spiperone in Rat Cerebral Tissue .....	156
5 CONCLUSIONS AND FUTURE WORK .....	157
LIST OF REFERENCES .....	164
BIOGRAPHICAL SKETCH.....	172

Abstract of Dissertation Presented to the Graduate School  
of the University of Florida in Partial Fulfillment of the  
Requirements for the Degree of Doctor of Philosophy

THE DETECTION OF PHARMACEUTICAL DRUG COMPOUNDS FROM INTACT  
BIOLOGICAL TISSUE BY MATRIX-ASSISTED LASER DESORPTION  
IONIZATION (MALDI) QUADRUPOLE ION TRAP MASS SPECTROMETRY

By

Christopher D. Reddick

August 1997

Chairman: Richard A. Yost  
Major Department: Chemistry

The aim of the work presented in this dissertation was to investigate the use of matrix-assisted laser desorption ionization (MALDI) for detecting pharmaceutical drug compounds from intact biological tissues. This research was also designed to evaluate the potential of laser desorption ionization on a quadrupole ion trap for future laser microprobe applications. Research efforts on this project were focused in three major areas: fundamental studies, instrumentation, and applications.

In the first stage of the project, experiments were performed to evaluate and optimize the MALDI process for drugs in a model tissue matrix (matrigel) using a commercial MALDI-time-of-flight instrument. Two central nervous system drug compounds, spiperone and ephedrine, were studied using the MALDI matrix 2,5-dihydroxybenzoic acid. Results of these initial experiments showed that the concentration of the matrix solution, the polarity of the matrix solvent, and the crystallization speed of

the matrix were all important in increasing the production of analyte ion signal from the model tissue.

In the second stage of the project, a novel laser desorption quadrupole ion trap instrument was constructed for analyzing drug compounds from more complex tissues. The instrument was constructed using a Finnigan series 4500 electron ionization/chemical ionization source, a DC quadrupole deflector, and a Finnigan ITS40 quadrupole ion trap mass analyzer. The advantage of this instrument over current laser microprobe instruments is that it is capable of performing multiple stages of mass spectrometry ( $MS^n$ ) for detecting trace levels of analytes from complex tissues such as brain and liver.  $MS^n$  can also be used to determine the structure of drug compounds in tissue.

In the final stage of the project, the new instrument was used to analyze several pharmaceutical drug compounds from tissue samples obtained directly from test species. MALDI spectra were obtained for the antipsychotic drug compound spiperone from incubated rat cerebral tissue. Experiments were also performed on samples of human plasma spiked with the peptide antibiotic polymyxin B<sub>1</sub>. Finally, MALDI was used to detect the anticancer drug taxol in ovarian tumor tissue from mice that had been administered the drug intravenously prior to removal of the tumor. The amount of the drug compounds detected with the new instrument was determined to be in the low picogram range.



## CHAPTER 1 INTRODUCTION

In the past decade, research aimed at deciphering the human genome has rapidly identified numerous disease targets. Using new sequencing methods and amplification techniques such as the polymerase chain reaction (PCR), biologists and biochemists can now identify disease causing mutations in specific regions of proteins and DNA.<sup>1</sup> The natural outcome of this research has been an increase in the demand on the part of physicians and healthcare providers for new therapeutic drug compounds and medications.<sup>2</sup> To meet this challenge, pharmaceutical companies have responded by exploiting new analytical methodologies aimed at increasing the efficiency of their drug discovery and development programs.<sup>3</sup>

One of the most important, yet challenging steps in the pharmaceutical drug development process is elucidating the mechanism of drug action.<sup>4</sup> Information about the biological activity of drug candidates can be used to optimize a lead candidate and can also give early clues as to a drug's metabolic pathway and possible toxicity. Traditionally, drug action and metabolic profiling studies have been carried out on physiological fluids (bile, urine, plasma) using standard techniques such as chromatography<sup>5</sup>, nuclear magnetic resonance spectrometry (NMR)<sup>6</sup>, fluorescence spectroscopy<sup>7</sup>, and chromatography coupled mass spectrometric techniques.<sup>8</sup> However, in order to fully elucidate the mechanism of drug action at the cellular and subcellular levels it is necessary to know the specific site of reactivity, or drug location in the body, as well as the chemical structure of

the drug compound at that specific site.<sup>9</sup> To achieve these two goals analytically requires techniques with high sensitivity, spatial and molecular resolution, and the ability to probe into the subunits of biological matrices.<sup>10</sup>

### Development of Laser Desorption Mass Spectrometry

The combination of laser desorption ionization (LDI) and mass spectrometry is an ideal technique for the analysis of biological materials. By using a focused laser beam, specific regions of biological samples can be sampled with spatial resolution in the submicrometer regime.<sup>11</sup> In addition, the high energy deposition afforded by the focused laser radiation ( $10^6 - 10^8 \text{ W/cm}^2$ ) allows for the vaporization and simultaneous ionization of a wide range of thermally labile and nonvolatile biomolecules. LDI also has the advantage over surface desorption techniques such as fast atom bombardment (FAB) and secondary ion mass spectrometry (SIMS) of being able to probe through the cellular matrix of biological samples.<sup>12</sup> And finally, LDI requires no separation and limited sample preparation prior to analysis. Coupling LDI with mass spectrometry provides a sensitive and selective technique capable of totally characterizing molecular species from tissues by determining their mass, relative abundance, and most importantly their structure (using MS/MS techniques).<sup>13</sup>

The development of laser desorption mass spectrometry began shortly after the introduction of the laser in the early 1960s.<sup>14</sup> The appeal of being able to rapidly heat a solid sample with a coherent light beam to cause the ejection of electrons, neutrals and especially ions led to an early marriage between the laser and mass spectrometer. The first application of the laser in mass spectrometry was made in 1963 when Honig and

Woolston<sup>15</sup> adapted a pulsed ruby laser to a double-focusing mass spectrograph for the elemental analysis of metal surfaces, semiconductors, and insulators.

Several years later Conzemius and coworkers<sup>16</sup> revisited the technique. In their work, a commercial laser was adapted to a double-focusing mass spectrometer of the Mattauch-Herzog type, equipped with both electrical and photoplate detection. The system had limited spatial resolution (~150  $\mu\text{m}$ ) and was used mainly for measuring concentration profiles of trace elemental species in metal systems and thin films.

To date, LDI sources have been coupled with every type of mass analyzer design including single and double focusing sector<sup>17</sup>, quadrupole<sup>18</sup>, time-of-flight<sup>19</sup>, and ion trap mass spectrometers.<sup>20</sup> Probably the most widely cited laser desorption mass spectrometer for biological applications is the Laser Microprobe Mass Analyzer (LAMMA).<sup>21</sup> This instrument, introduced commercially in 1977, is based on a time-of-flight mass spectrometer and uses a Q-switched, frequency-multiplied Nd:YAG sampling laser, a He-Ne spotting laser, and a modified laser focusing microscope system capable of achieving spatial resolution as low as 0.5  $\mu\text{m}$  (Figure 1-1). The LAMMA was originally developed for high sensitivity molecular analysis of thin histological sections, but has been primarily used for *in situ* determination of physiological cations in organ tissues.<sup>22-25</sup>

Vandeputte and Savor<sup>26</sup> used the LAMMA to study the localization of aluminum in livers of aluminum maltol treated rabbits. This model was developed to study long-term aluminum toxicity. In their work, aluminum maltol was administered to adult male rabbits intravenously three times a week for 8-30 weeks. Liver sections were fixed in 10% buffered formalin, embedded in paraffin, and mounted on copper grids. While the LAMMA was not used to image aluminum in the liver sections, significant accumulations

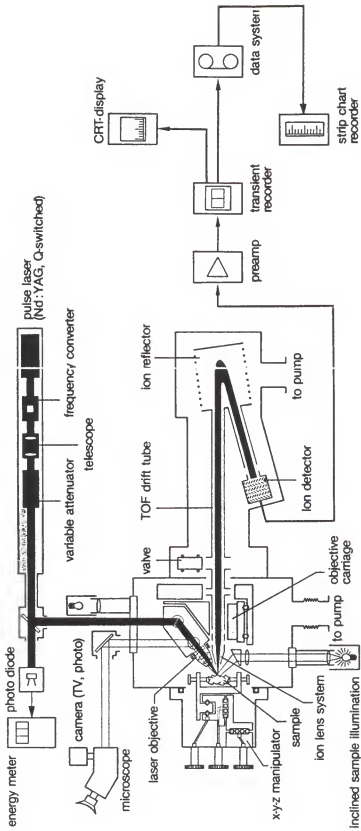


Figure 1-1. Schematic of the Laser Microprobe Mass Analyzer (LAMMA).<sup>27</sup>

of aluminum were detected in electron-dense deposits in cells found in pathological lesions of the liver tissue. Improving on this work, Verbueken and coworkers<sup>28</sup> used the LAMMA to analyze kidney sections from rats treated with the immunosuppressive drug cyclosporin. Instead of looking for metabolites of cyclosporin in the kidney sections, the LAMMA was used to pin-point and determine the chemical composition of numerous intrarenal crystalline deposits. Results of this work revealed the microcrystalline structures to consist of calcium oxalate, sodium urate, and calcium phosphate. Similar deposits in human kidney sections were also characterized by the LAMMA.

Applications of laser desorption mass spectrometry for the analysis of molecular species from biological matrices have not been widely reported in the scientific literature. This is due primarily to the fact that many biomolecules of interest undergo thermal degradation at the high laser irradiances needed to vaporize and ionize regions of tissue.<sup>29</sup> The laser desorption of molecular species from tissues occurs both resonantly and nonresonantly.<sup>30</sup> In resonant desorption, the direct resonant excitation of the analyte molecules channels energy into vibrational modes which can lead to photodissociation. In the case of nonresonant desorption, the high irradiances required for desorption occur very close to the point of plasma generation, which can also lead to molecular decomposition. In either case, the intense energy deposition from the incident laser irradiation destroys the molecule.<sup>31</sup> The problem of performing laser desorption out of tissues is further complicated because the traditional laser microprobe instruments do not have the selectivity and sensitivity to detect analyte fragments in the presence of the intense background noise from the tissue.<sup>32</sup>

### Matrix-Assisted Laser Desorption Ionization (MALDI)

In 1985, Hillenkamp and Karas<sup>33</sup> reported laser desorption of intact  $(M+H)^+$  ions for the dipeptide, Trp-Trp (M.W. 390) using a pulsed nitrogen laser. In this work, a low concentration of the analyte was mixed with a liquid matrix consisting of a low molecular weight, UV-absorbing compound. It was observed that a strong resonance absorption of the matrix compound at the wavelength of the incident laser radiation promoted a soft desorption, at low laser irradiance, of the dipeptide without fragmentation. Expanding on this pioneering work, Hillenkamp and Karas went on to demonstrate the production of intact molecular ions for several proteins with masses up to 67,000 Da (Figure 1-2).<sup>34</sup> Matrix-assisted laser desorption ionization or MALDI, as the technique is now termed, revolutionized the field of laser desorption mass spectrometry by providing a means of producing intact molecular ions for thermally labile biomolecules.

Since its introduction, MALDI has been used primarily to study neat samples of biomolecules including peptides, proteins, glycoproteins, glycosides, nucleosides, nucleic acids, and oligosaccharides with masses between 10,000 to 300,000 Da.<sup>35-38</sup> In the work presented here, MALDI was used to produce intact molecular ions for small pharmaceutical drug compounds (300 - 1200 Da) directly from intact biological tissues. While the literature is lacking in this specific area, there have been reports of similar uses of MALDI for detecting molecular species embedded in other types of solid materials.

Hercules and coworkers<sup>39</sup> used MALDI to detect various compounds directly from polyamide thin layer chromatography (TLC) plates. The compounds analyzed included polyaromatic hydrocarbons (PAHs), alkaloids, and amino acids. The MALDI spectra

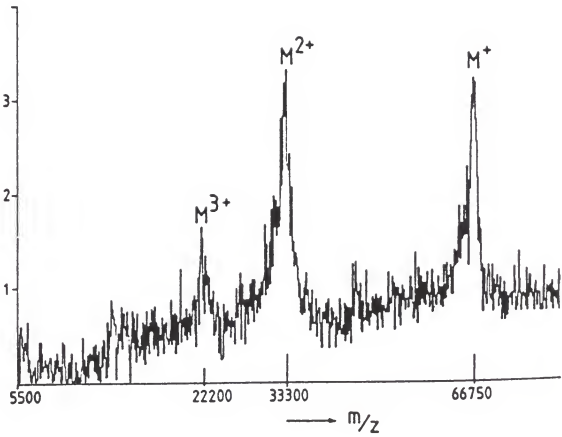


Figure 1-2. MALDI spectrum of 100 pmol of Bovine Albumin (M.W. 67,000) using nicotinic acid matrix.<sup>34</sup>

were obtained using a Q-switched, pulsed Nd:YAG laser (265 nm) with a power output of 18  $\mu\text{J}$  and a spot size of  $\sim 5 \mu\text{m}$ . Samples were prepared by spotting 0.2  $\mu\text{L}$  of the sample mixtures onto TLC plates so that approximately 50  $\mu\text{g}$  of each compound was deposited. Separations were performed using methanol/water and methylene chloride/methanol as the mobile phases. After the separation, the plates were allowed to dry at room temperature and the spots were visualized with UV fluorescence. MALDI was performed by depositing a drop of concentrated matrix solution directly on top of each of the separated spots. Two matrices were evaluated: DHB and sinnapinic acid.

Of particular note in this study was the detection of the antibacterial drug compound erythromycin (M.W. 735).<sup>39</sup> Abundant  $(\text{M}+\text{H})^+$  and  $(\text{M}+\text{Na})^+$  ions were obtained for MALDI of erythromycin from the polyamide TLC plates. Background ions from the TLC plate were also observed below  $m/z$  150, but were found not to interfere with the molecular ion species observed. Higher laser irradiances were needed to obtain MALDI spectra from the TLC plates than from a standard metal substrate. This was believed to be due to a combination of scattering and absorption by the TLC plates. Also, reducing the plate thickness from 250  $\mu\text{m}$  to 100  $\mu\text{m}$  was found to increase the production of molecular ion signal for all of the compounds studied, including erythromycin.

More recently, MALDI has been applied to the analysis of proteins separated by gel electrophoresis and electroblotted onto membranes.<sup>40-43</sup> Gels currently in use are too fragile for most manipulations, and it is increasingly common for separated proteins to be electroblotted onto more robust polymer membranes by the application of an orthogonal electric field.<sup>44</sup> Several groups have reported MALDI of proteins from poly(vinylidene difluoride) (PVDF) membranes up to 67,000 Da. Vestling and Fenselau<sup>45</sup> have



demonstrated the usefulness of MALDI for providing molecular weights for several proteins, including horse heart cytochrome c, lysozyme, and bovine trypsin using  $\alpha$ -cyano-4-hydroxycinnamic acid (M.W. 171) as the UV-absorbing matrix. In this work, the proteins were transferred to PVDF membranes, washed with water to remove contaminants, and allowed to dry. 1.0  $\mu$ L of the matrix solution (100 mM in 50:50 methanol/toluene) was then applied to each spot on the membrane. Spectra were obtained by scanning across the membranes with a focused beam from a pulsed 337 nm nitrogen laser (Figure 1-3).

Hillenkamp and coworkers<sup>46</sup> used infrared MALDI at 2.94  $\mu$ m to desorb proteins directly from PVDF, polypropylene (PP), nitrocellulose, and polyamide blot membranes. A variety of methods were employed to add the matrix to the blots. Soaking the dried membranes in organic solutions containing the matrix compound (succinic acid) was found to provide the most intense molecular ion signals for all of the proteins tested. Membrane thickness and surface area were also found to influence the production of protein signals. The results obtained for IR-MALDI were compared with those obtained by UV-MALDI at 355 nm using DHB as the matrix (Figure 1-4). In all cases, IR-MALDI showed superior results. The increase in molecular ion signal with IR desorption versus UV desorption was believed to be related to the different penetration depths of the laser radiation at the two wavelengths (3-5  $\mu$ m vs. 200-300 nm, respectively).

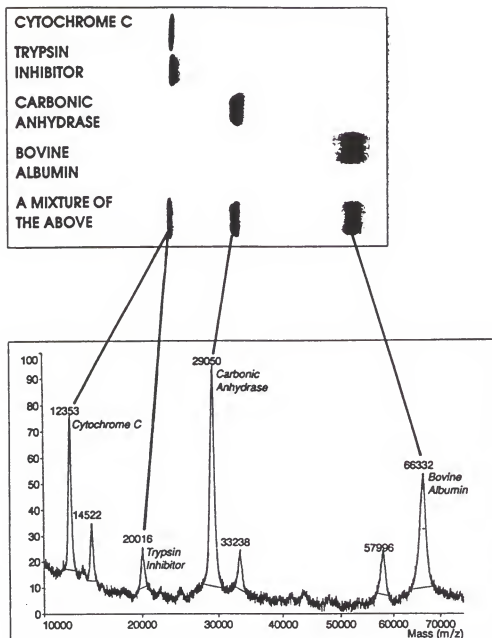


Figure 1-3. MALDI spectrum of Cytochrome C, Trypsin Inhibitor, Carbonic Anhydrase, and Bovine Albumin electroblotted onto a PVDF membrane using  $\alpha$ -cyano-4-hydroxycinnamic acid.<sup>45</sup>

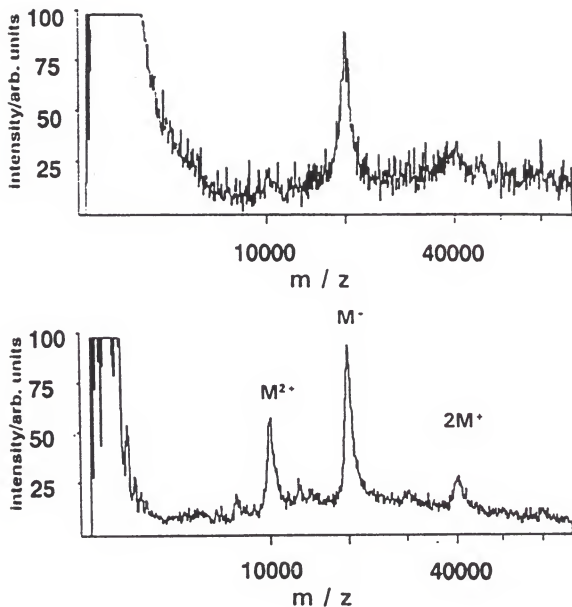


Figure 1-4. Comparison of UV (top) and IR (bottom) MALDI spectra of Soybean Trypsin Inhibitor (M.W. 19,979) electroblotted onto a PVDF membrane. Both spectra were obtained using saturated DHB in ethanol.<sup>46</sup>

### MALDI Theory and Mechanism

Although significant work has been done in the area of MALDI, the actual mechanism of how MALDI works is still not fully understood.<sup>47</sup> In general, MALDI involves rapidly depositing energy into a solid lattice of analyte embedded in matrix crystals using short (3-300 ns), intense ( $10^6$  W/cm<sup>2</sup>) laser pulses. Part of the deposited energy is reemitted through fluorescence. Another portion is channeled into vibrational modes of the matrix molecules. Some of the matrix molecules decompose from these vibrational states; others transfer their energy to the crystal lattice causing rapid heating to the phase-transition temperature. An expanding gas-phase plume is then formed containing highly excited matrix molecules with entrained analyte molecules (Figure 1-5). It has been suggested that the lack of degradation of the analyte molecules during the initial laser desorption event is due to a frequency mismatch between the lattice vibrations in the matrix crystals and the intermolecular vibrations in the encapsulated analyte molecules.<sup>48</sup>

The production of analyte ions in MALDI can be divided into at least three different processes<sup>49</sup>, which depending on the wavelength and irradiance, contribute to a varying extent to the overall ionization of the analyte. In the first process, preformed analyte ions in the solid matrix are volatilized into the gas phase during the initial laser desorption event. Analyte molecules in their ionized form in the condensed-phase have been shown to give rise to gas-phase ions extremely easily. The presence of abundant (M+Na)<sup>+</sup> and (M+K)<sup>+</sup> ions in MALDI are thought to result from preformed adducts between the analyte molecules and salts from the matrix solvent.<sup>50</sup> The second process

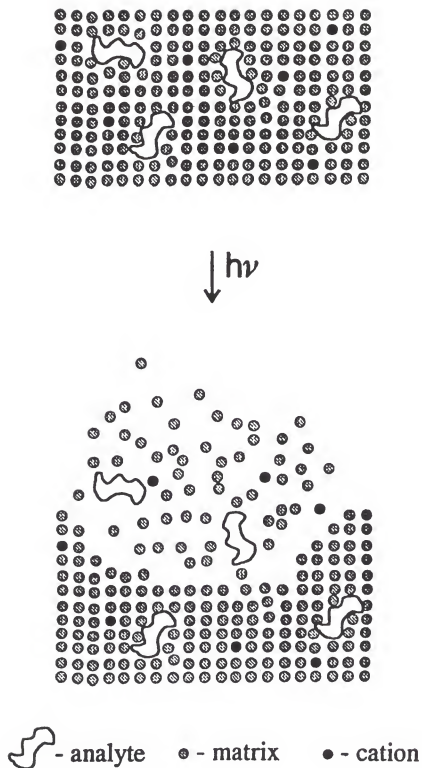
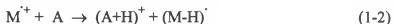


Figure 1-5. Diagram showing the formation of the supersonic gas-phase plume of matrix and analyte molecules during MALDI.<sup>51</sup>

involves direct photoionization and photofragmentation of individual molecules (photon-molecule interactions, comparable to gas-phase photoionization). This process plays an increasingly important role at higher laser irradiance. The final ionization process involves protonation reactions by collisions of highly excited matrix ions and ground-state analyte molecules. As one of the elemental steps of energy transfer from matrix to analyte molecules, the formation of intermediate radical ions has been proposed.



These radicals are photoionized in the condensed phase and react with ground-state analyte molecules in the dense gas-phase plume formed just above the solid surface, resulting in subsequent ionization by proton transfer reactions.



Rapid adiabatic cooling in the expanding jet prevents the intact analyte ions from fragmenting.

### MALDI Sample Preparation

One of the advantages of MALDI is that the preparation of samples is simple, fast, and requires relatively little material. Traditionally, a 5-10 mg/mL solution of the matrix material is prepared in water or water/organic solvent. For analysis of polar biomolecules, methanol, acetone, and acetonitrile have been used. It is important to note that the selection of the solvent system can have a dramatic effect on the crystal formation and therefore on the quality of the resulting MALDI spectra. A suitable amount of the analyte

solution ( $10^{-5}$  -  $10^{-6}$  M) is then mixed with 5-10  $\mu\text{L}$  of the matrix solution to yield a molar ratio of  $10^2$  -  $10^6$  (matrix-to-analyte). For large peptides and proteins, 0.1% trifluoroacetic acid is added to aid the solubilization of the analyte.<sup>52</sup> For analysis, a drop (0.5-1.0  $\mu\text{L}$ ) of the matrix/analyte mixture is then applied to the sample probe (typically stainless steel or copper) and allowed to dry at room temperature. Passing a stream of warm air or nitrogen over the droplet to speed crystallization of the sample is sometimes performed.<sup>52</sup>

Several improvements in sample preparation have been reported for MALDI with the aim of increasing the sensitivity, shot-to-shot-reproducibility, and resolution of the technique. Vorm and Mann<sup>53</sup> described a sample preparation procedure which decouples matrix and sample handling. In this technique, the matrix solution is applied to the sample probe in a solvent that evaporates very rapidly, leaving a thin layer of very small matrix crystals. A small volume of analyte solution (0.3-1.0  $\mu\text{L}$ ) is then added on top of the matrix surface and allowed to dry. An alternative to this approach is to electrospray the matrix/analyte solution as a fine mist by applying a small potential between the sample syringe and the sample probe. Caprioli et al.<sup>54</sup> demonstrated MALDI of the neurotransmitter Substance P from dialysis probes using this technique. With both techniques, increases in sensitivity (subfemtomole) and TOF mass resolution were reported, believed to result from the very flat, homogeneous crystal layers that formed. Hercules et al.<sup>55</sup> showed that the choice of matrix compound and the speed of drying of the matrix/analyte mixture has the most pronounced affect on the crystal structure and therefore on the quality of the resulting spectra (Figure 1-6). In their work, an increase of



Figure 1-6. Scanning electron images showing the crystal formations for various matrices and drying speeds: Ferulic acid (top left), Ferulic acid with accelerated drying (middle left), Ferulic acid/Fruuctose with accelerated drying (bottom left), DHB (top right), DHB with accelerated drying (middle right), and DHB/Fruuctose/5-methylsalicylic acid (bottom right).<sup>55</sup>



ca. 50% in signal intensity and a 30–40% increase in resolution were obtained using DHB with accelerated drying.

For MALDI of drug compounds from intact tissue in this dissertation research, both the standard droplet method and the electrospray deposition method were used. Descriptions of the sample preparation procedures for these experiments are presented in chapter 2. A possible alternative for performing MALDI of biological tissues is to freeze the sections and use the ice crystals as the absorbing matrix. Williams and coworkers<sup>56</sup> have reported MALDI from frozen matrices using an IR laser (266 nm) for the analysis of single- and double-stranded DNA up to 29,000 Da. Samples were cooled to ~ 253K using a liquid nitrogen cold finger attached to a copper sample stage.

In general, the two most important factors in preparing samples for MALDI are analyte/matrix solubilization and crystal formation. Regardless of the technique chosen, the analyte must be made to dissolve in the matrix solvent and the resulting crystal lattice that forms upon drying must be flat and homogeneous in order for quality MALDI spectra to be obtained.

### MALDI Matrices

The basic prerequisites for a compound to work as a matrix in MALDI are as follows.<sup>49</sup> First, the compound must exhibit a strong spectral absorbance at the wavelength of the incident laser radiation. For most of the MALDI experiments reported in the literature, UV lasers including N<sub>2</sub> (337 nm)<sup>57</sup>, eximer (193, 248, 308, and 351 nm)<sup>52</sup>, frequency-doubled eximer-pumped dye (220–300 nm)<sup>52</sup>, and Q-switched, frequency-tripled and quadrupled Nd:YAG (355 and 266 nm, respectively)<sup>58</sup> have been used. IR-

MALDI has also been reported using TEA-Co<sub>2</sub> (10.6  $\mu\text{m}$ ) and Er:YAG (3  $\mu\text{m}$ ) lasers.<sup>59</sup> The second requirement is that the matrix compound must be chemically compatible with the analyte of interest. Generally, this means that the matrix compound should be soluble in the same solvents as the analyte. The matrix compound should not however undergo any sort of chemical reaction with the analyte in solution. Finally, matrices should be acidic so as to promote ionization of the analyte molecules via proton-transfer reactions. Russell and coworkers<sup>60</sup> investigated the affect of matrix acidity on the production of analyte (M+H)<sup>+</sup> ion yield using a series of *p*-substituted anilines as the matrices. Results of their work showed a linear increase in ion yield with increasing excited state acidity of the matrix compound.

Matrices in MALDI can generally be classified based on their absorbance wavelength and on their application to either biomolecules or more recently synthetic polymers. A list of current matrices and their use in various applications is given in Table 1-1. For all of the work presented in this dissertation, 2,5-dihydroxybenzoic acid (DHB) was used as the MALDI matrix compound.

### Overview of Dissertation

Research efforts on this project were focused in three major areas: fundamental studies, instrument development, and applications. In the first stage of the project experiments were performed to optimize the MALDI process using matrigel, a model tissue matrix. The goals of these initial experiments were to elucidate the mechanism of MALDI for drug compounds in tissue and to determine the effect of MALDI on the spatial distribution of drug compounds in tissue. MALDI was demonstrated for the

Table 1-1. Typical MALDI matrices and their use in various applications.<sup>61</sup>

Matrix	Application(s)
<i>trans</i> -2,5-Dimethoxycinnamic Acid	Higher mass biopolymers, glycoproteins, peptides, polymers
<i>a</i> -Cyano-4-hydroxycinnamic Acid	Organic compounds from 200-1000 Da, glycoproteins
2,5-Dihydroxybenzoic Acid	Polymers, polypeptides, oligosaccharides, glycopeptides
2-(4-Hydroxyphenylazo)-benzoic Acid	Low molecular weight compounds, sulfonic acids, dyes
2,4,6-Trihydroxyacetophenone	Oligonucleotides, polymers, biopolymers
2,4-Dihydroxyacetophenone	Biopolymers, oligonucleotides, mass range 400-60,000 Da
2,6-Dihydroxyacetophenone	Biopolymers, oligonucleotides, mass range 400-60,000 Da
5-Chlorosalicylic Acid	Water insoluble polymers
5-Methoxysalicylic Acid	Used in combination with DHB for better resolution
1,8,9-Trihydroxyanthracene	Non-polar compounds and polymers
<i>trans</i> -Indole-acrylic Acid	Polythymidines and polyuridines
Indoleacetic Acid	Oligonucleotides
N-(3-Indoleacetyl)-L-leucine	Oligonucleotides, polycytidines, polyuridines
Anthranilic Acid	Oligosaccharides, glycopeptides, glycoproteins
3-Hydroxypicolinic Acid	Oligonucleotides, polycytidines, polyuridines
Nicotinic Acid	Proteins and peptides
Vanillic Acid	Proteins and peptides
Pyrazine-2-carboxylic Acid	Proteins and peptides
3-Aminopyrazine-2-carboxylic Acid	Proteins and peptides
Ferrulic Acid	Proteins, peptides, amino acids
Caffeic Acid	Proteins
3-Nitrobenzyl alcohol	Used for FAB and flow MALDI
Nitrophenyl octyl ether	Polymers up to 10 kDa (salt)

central nervous system drug compounds spiperone and ephedrine from matrigel using a Finnigan MAT Lasermat MALDI-time-of-flight instrument. The matrix concentration, matrix solvent polarity, and the “soak time” of the matrix solution were found to be important in the production of analyte molecular ion signal.

Spatial resolution experiments were also performed with spiperone in matrigel. Results of these experiments revealed that addition of the MALDI matrix solution as a droplet caused significant migration of the analyte. An electrospray apparatus was constructed and used to spray the matrix solution on top of the tissue as a fine mist. With this method, the migration of spiperone in matrigel was prevented. The results of this initial work are presented in Chapter 2.

Chapter 3 describes the design and construction of a novel laser desorption quadrupole ion trap mass spectrometer designed specifically to detect and potentially map trace levels of drug compounds in complex tissues such as brain, liver, and tumor tissue. The instrument was constructed using a modified Finnigan MAT model 4500 electron ionization (EI)/chemical ionization (CI) ion source and a Finnigan ITS40 quadrupole ion trap mass analyzer. A DC quadrupole deflector was incorporated to allow the ion trap to be positioned  $90^\circ$  off-axis with the ion source. This configuration was used to allow light from a nitrogen laser to be directed perpendicularly onto the surface of the sample held within the ion source. The off-axis design will also allow a microscope objective to be incorporated for future imaging experiments. Included in chapter 3 is an introduction to the quadrupole ion trap mass spectrometer, complete with a historical review and discussion of its theory and operation.

Chapter 4 presents the application of the new instrument for the analysis of drug compounds in tissue obtained from test animals. The chapter begins with the calibration experiments performed using perfluorotributylamine (FC43) and a peptide mixture. Simulation experiments were also performed with SIMION V6.0 to optimize the various instrumental parameters for MALDI. In the first application experiment, spiperone was detected from a thin section of rat cerebral tissue using DHB as the MALDI matrix. The sample was prepared by incubating the tissue section in a  $10^{-4}$  M solution of spiperone. Results of these experiments showed that the MS/MS capabilities of the ion trap were necessary to confirm the presence of spiperone in the more complex brain tissue. In the second experiment, MALDI was performed on thin sections of rat ovarian tumor tissue containing the anticancer drug taxol. In contrast to the previous experiments in which the drug compound was mixed with the tissue after it had been removed from the animal, taxol was injected directly into the rat approximately 1 hr before being sacrificed. Based on the initial loading of taxol in the tumor, the spot size of the laser, and the thickness of the tissue section, the amount of taxol detected was determined to be approximately 280 pg. MALDI MS/MS spectra were also obtained for the peptide antibiotic polymyxin B<sub>1</sub> mixed with human plasma.

Chapter 5 concludes the dissertation with a discussion of the results obtained from the experiments presented in this work. Also included in this final chapter are suggestions for instrumental improvements and a discussion of future applications and experiments.

## CHAPTER 2

### FUNDAMENTAL INVESTIGATIONS OF MALDI OF DRUG COMPOUNDS IN TISSUE USING A TIME-OF-FLIGHT MASS SPECTROMETER

In the first stage of this project, experiments were performed to investigate the use of MALDI to detect drug compounds from a model tissue matrix. The goals of these initial experiments were threefold: to elucidate the mechanism of MALDI for drugs in tissue, to optimize the MALDI process to increase the production of analyte molecular ion signal, and to evaluate the usefulness of MALDI for potentially imaging drug compounds from more complex biological matrices.

To avoid using large quantities of tissue from test animals for these initial optimization experiments, a commercially available model tissue matrix (matrigel), was used instead. Matrigel (Collaborative Biomedical Products) is a collection of extracellular membranes underlying cells *in vivo* extracted from Engelbreth-Holm-Swarm (EHS) mouse sarcoma.<sup>62</sup> Matrigel's minor components are laminin, collagen type IV, heparin sulfate proteoglycans, entactin, nodogen, tissue plasminogen activator, and other naturally occurring growth factors.<sup>63</sup> Matrigel proved to be an ideal model tissue matrix for these experiments because of its unique physical properties. In its frozen storage state matrigel was a solid. As it warmed to room temperature it became a liquid, enabling drug compounds to be easily mixed in with it. At room temperature the matrigel/drug mixture solidified, locking the embedded drug compounds into position.

### Instrument Description

The instrument used for this work was a Finnigan MAT Lasermat MALDI-time-of-flight (TOF) mass spectrometer (Hemel Hemstead, UK) (Figure 2-1). The Lasermat was used to perform the initial optimization experiments while the laser desorption ion trap instrument was being constructed. Although the Lasermat was originally designed to perform routine analysis of peptides and proteins,<sup>64</sup> it required no modifications for MALDI of drugs in tissue.

With the Lasermat, light from a pulsed nitrogen laser (337 nm) was used to desorb ions from samples deposited onto a 35 mm stainless steel sample plate having a target area 2.0 mm in diameter. The nitrogen laser produced 3 ns pulses of approximately 100  $\mu\text{J}$  in energy. Although the laser can fire at a repetition rate of 20 Hz, the system was operated at 1 Hz. The laser beam was focused down to a spot size of approximately 0.1 mm by 0.3 mm using a single fused-silica lens (50 mm focal length). The laser power density was adjusted from  $10^6 - 10^7 \text{ W/cm}^2$  using a rotating polarizer under computer control. Control of the laser beam aim was achieved using a rotating fused-silica wedge.

The ion source of the Lasermat consists of five stainless steel lenses which were used to direct and accelerate the desorbed ions down the length of the 0.5 m flight tube. Very high potentials ( $\pm 20 \text{ kV}$ ) and small distances between the lenses were maintained to ensure that ions were ejected into the flight tube at the same time. Detection of the desorbed ions was achieved with a discrete dynode electron multiplier situated at the end of the flight tube. Mass determination was made by measuring the flight time ( $t$ ) of the

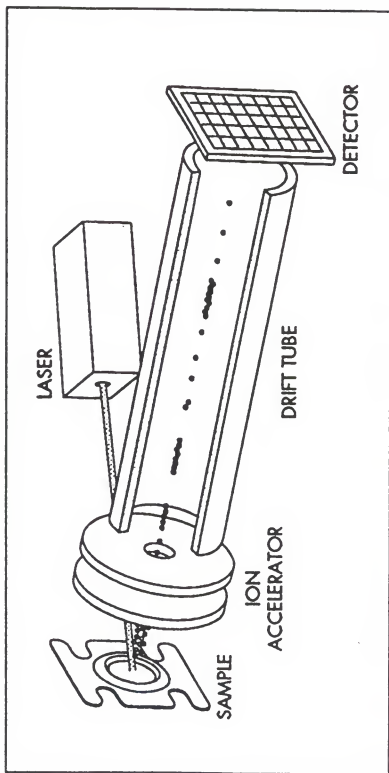


Figure 2-1. Schematic of the Finnigan Laser-matrix MALDI-TOF mass spectrometer.<sup>64</sup>



desorbed ions of given mass-to-charge ( $m/z$ ) down the flight tube of known length ( $l$ ), after being accelerated in the extraction field to a common energy ( $E$ ).<sup>65</sup>

$$\frac{m}{z} = 2E \frac{t^2}{l} \quad (2-1)$$

### MALDI Optimization Experiments with Matrigel

#### Matrigel Sample Preparation

The test compounds chosen for this work were the central nervous system (CNS) drug compounds spiperone (M.W. 395) and ephedrine (M.W. 165) (Figure 2-2). Spiperone and ephedrine proved to be ideal model compounds for this initial work because they were both soluble in matrigel and because they have been studied extensively in previous work in our laboratory.<sup>62,66</sup> Standards of spiperone in matrigel (100 ppm) were prepared by mixing 0.1 mg of solid spiperone (Sigma Chemical Co.) with 1.0 mL of matrigel after it melted from its frozen storage state. The mixture was vortexed until all of the spiperone had visibly dissolved in the matrigel. After mixing, the spiperone-matrigel mixture was allowed to gel at room temperature. Standards of ephedrine in matrigel (100 ppm) were prepared in the same manner by mixing 0.1 mL of a standard solution of ephedrine (1 mg/mL) (Alltech Associates, Inc.) with 1.0 mL of matrigel.

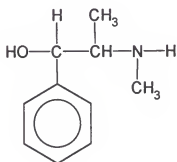
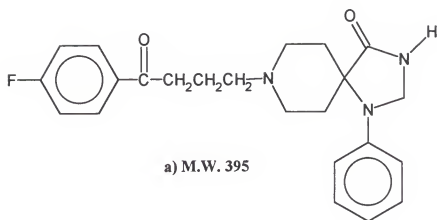


Figure 2-2. Structures and molecular weights of the central nervous system (CNS) drug compounds studied: a) spiperone and b) ephedrine.

### Optimization of the MALDI Matrix Concentration

Before analyzing the matrigel samples by MALDI, LDI reference spectra were acquired for spiperone and ephedrine in matrigel without the addition of a matrix solution (Figure 2-3 and Figure 2-4). The LDI spectra for both compounds were dominated primarily by ions from the matrigel tissue. The presence of these background ions suggested that some of the components of the matrigel tissue absorbed strongly in the ultraviolet region. Most of the background ions were identified as low molecular weight amino acids from the collagen in the matrigel. Abundant sodium and potassium ions were also detected due to the salt content of the matrigel tissue. For the matrigel sample containing spiperone,  $(M+Na)^+$  and  $(M+K)^+$  adduct ions were also detected. The lack of abundant  $(M+H)^+$  ions for either spiperone or ephedrine with laser desorption alone was due to the inability of the laser to desorb and ionize those analyte molecules located below the tissue surface. Higher laser powers were employed to try to probe into the matrigel tissue. However, no  $(M+H)^+$  ion signal was detected even at the maximum laser power setting of the instrument. After analysis, observation of the matrigel surface under magnification revealed no evidence of laser ablation or crater formation. No attempt was made to focus the laser beam more tightly to provide higher irradiance levels because of the complicated design of the Lasermat optics system.

After trying LDI unsuccessfully, MALDI was performed using 2,5-dihydroxybenzoic acid (DHB) as the UV-absorbing matrix (Figure 2-5). In the first experiment, 1.0  $\mu$ L of the matrigel standard containing spiperone was deposited onto the center of a Lasermat sample plate using an Eppendorf micro-pipette and allowed to air dry

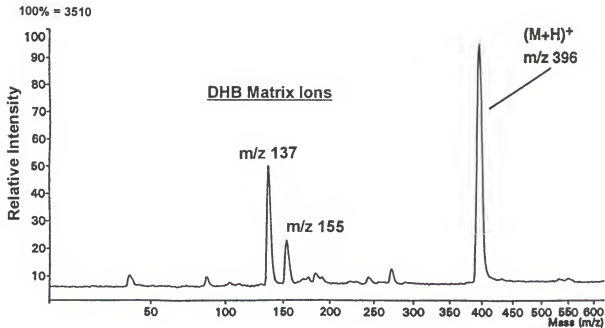
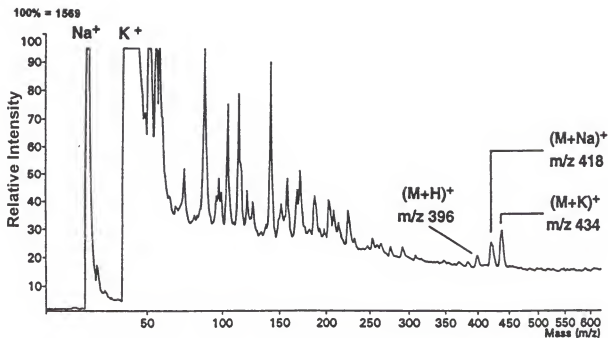


Figure 2-3. Comparison of the LDI spectrum (top) and the MALDI spectrum (bottom) using DHB (0.25 M) for 100 ppm of spiperone in matrigel.

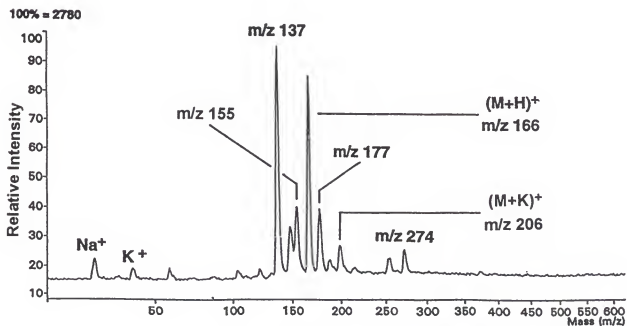
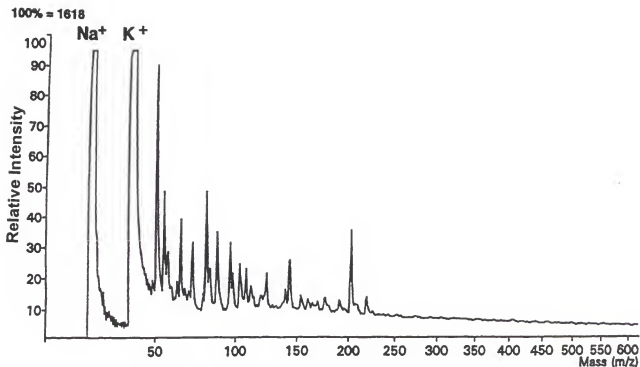


Figure 2-4. Comparison of the LDI spectrum (top) and the MALDI spectrum (bottom) using DHB (0.25 M) for 100 ppm of ephedrine in matrigel.

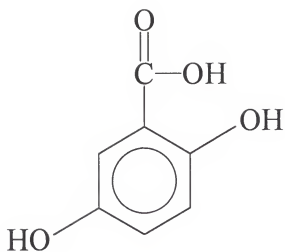


Figure 2-5. Structure of the MALDI matrix compound 2,5-dihydroxybenzoic acid (DHB), M.W. 154.

at room temperature. The amount of drug compound deposited was determined to be 100 ng. With larger amounts of matrigel (>3  $\mu\text{L}$ ), the sample did not dry completely. After drying, the sample was washed with successive drops of water to remove any undissolved analyte molecules from the tissue surface. 1.0  $\mu\text{L}$  of a 0.01 M DHB matrix solution prepared in 30% acetonitrile/70% water was then added directly on top of the sample. Upon drying, the DHB matrix solution crystallized on top of the matrigel, forming needles of several hundred micrometers in length pointing inward from the rim of the sample area. While the first sample continued to dry, two more matrigel samples containing spiperone were prepared for MALDI using the same volume of DHB matrix solution (1.0  $\mu\text{L}$ ), but at increasing concentrations of 0.15 M and 0.25 M. The same sample preparation procedure was repeated for the matrigel samples containing ephedrine.

As can be seen in Figures 2-3 and 2-4, switching from LDI to MALDI resulted in a dramatic increase in the production of the  $(\text{M}+\text{H})^+$  peak for both spiperone and ephedrine in matrigel. For spiperone, the area of the  $(\text{M}+\text{H})^+$  peak increased from 400 using the 0.01 M DHB matrix solution to 3439 using the most concentrated matrix solution. For ephedrine, the  $(\text{M}+\text{H})^+$  peak area increased from 349 using the 0.01 M solution to 2363 with the 0.25 M DHB matrix solution. The MALDI spectra for the matrigel samples also included several intense peaks corresponding to the DHB matrix. The two most abundant peaks corresponded to the  $(\text{M}+\text{H})^+$  ion at  $m/z$  155 and for the  $(\text{M}+\text{H} - \text{H}_2\text{O})^+$  ion at  $m/z$  137. Less intense peaks at  $m/z$  177 and  $m/z$  274 were also seen for the  $(\text{M} - \text{H}_2\text{O} + \text{K})^+$  ion and the  $(2\text{M} - 2\text{H}_2\text{O} + \text{H})^+$  ion respectively.

The increase in the  $(\text{M}+\text{H})^+$  peak area observed for both compounds using MALDI is believed to have resulted from a two-step process. In the first step, the embedded

analyte molecules were extracted out of the matrigel and into the solvent of the DHB matrix solution (Figure 2-6). In the second step, the extracted analyte molecules became encapsulated in the matrix crystal layer that formed on the surface of the matrigel as the solvent evaporated. Increasing the concentration of the matrix solution further increased the production of  $(M+H)^+$  ions by providing an excess of surrounding matrix molecules to promote the desorption and protonation of the extracted analyte molecules.

In addition to increasing the production of the  $(M+H)^+$  ion signal, addition of the DHB matrix was also found to reduce the sodium and potassium adduct ions and suppress the background ions from the matrigel which complicated the spectra. Under magnification it was observed that with the less concentrated DHB matrix solution, the crystal layer that formed did not completely cover the matrigel surface. This allowed the incident laser to interact more directly with the matrigel, resulting in the production of matrigel ions in addition to analyte and DHB matrix ions. With increasing DHB concentration, the matrigel surface became completely covered with matrix crystals. In this way, the incident laser only came into direct contact with the matrix crystals containing the extracted analyte molecules. With the most concentrated DHB solution the resulting spectra were dominated by  $(M+H)^+$  ions and DHB matrix ions.

#### Optimization of the MALDI Matrix Solvent Polarity

In the next set of experiments the polarity of the matrix solvent mixture was optimized to see if more of the drug compounds could be made to partition out of the matrigel tissue and into the MALDI matrix solution. As before, samples of spiperone or ephedrine in matrigel (100 ppm) were prepared and deposited onto Lasermat sample



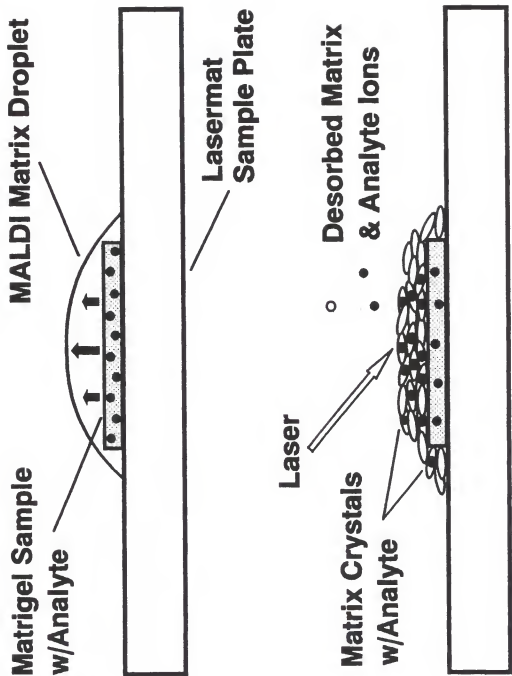


Figure 2-6. Diagram illustrating the MALDI mechanism for drug compounds in matrigel.

plates for analysis. For these experiments, the DHB matrix solution was prepared at 0.25 M since this gave the best results from the previous experiments. The polarity of the DHB solvent was varied in each case by using different percentages of acetonitrile and water. Five solvent mixtures were used ranging from 100% acetonitrile to 100% water. The polarity of each solvent mixture was calculated using the solvent polarity parameter defined as:

$$P' = \phi_a P_a + \phi_b P_b \quad (2-2)$$

where  $\phi_a$  and  $\phi_b$  are the volume fractions of water and acetonitrile in the mixture, and  $P_a$  and  $P_b$  are the polarity values of the pure solvents.<sup>67</sup> Polarity values for pure solvents range from 0.0 - 10.0, with zero being the most nonpolar and ten being the most polar; the polarity of acetonitrile is 5.8 while that for water is 10.0. Table 2-1 shows the polarity values for the acetonitrile/water solvent mixtures used in this experiment. Solvent mixtures of acetonitrile and water were used instead of pure solvents because most of the solvents tested either ran off the surface of the matrigel or dissolved the matrigel tissue completely. All of the acetonitrile/water mixtures remained as intact droplets on top of the matrigel samples.

Before analyzing the matrigel samples, MALDI spectra were obtained for standard solutions of spiperone ( $2.5 \times 10^{-4}$  M) and ephedrine ( $6 \times 10^{-4}$  M) using each of the DHB solutions prepared in the five different solvent mixtures. The purpose of this experiment was to determine whether changing the solvent of the matrix solution had a significant effect on the crystallization process and therefore on the production of the  $(M+H)^+$  ion

Table 2-1. Composition and polarity values of the five matrix solvent mixtures used to optimize the MALDI process for spiperone and ephedrine in matrigel.

Solvent Mixture #	% Acetonitrile	% Water	Polarity Value (P')
1	100	-	5.8
2	70	30	7.1
3	50	50	8.0
4	30	70	8.9
5	-	100	10.0

signal, independently of the extraction process. Samples were prepared for MALDI by depositing equal amounts ( 1.0  $\mu\text{L}$  ) of the standard and matrix solutions on the sample plate and allowing the mixture to dry and crystallize. The crystallization process for each of the samples was observed under magnification. With the more volatile solvent mixtures (>50% acetonitrile) the crystallization process began immediately after adding the matrix solution. The resulting crystal layer that formed was composed of numerous needles which covered the entire surface of the sample plate. With the more polar solvent mixtures, however, the matrix droplet remained for several minutes before crystallizing. The resulting crystals were noticeably larger but still uniform. The average peak area of the  $(\text{M}+\text{H})^+$  ion after 100 laser shots for both spiperone and ephedrine using each of the solvent mixtures is shown in the top plot in Figures 2-7 and 2-8 respectively. The error bars represent the standard deviation. Mass assignment and peak area values were generated by the Lasermat software. The Lasermat has a rated mass accuracy of  $\pm 0.5$  Da below 5 kDa.<sup>64</sup> Prior to analysis, the instrument was mass calibrated using a standard solution of leucine enkephalin (M.W. 555) with DHB as the MALDI matrix. As can be seen from the plots for both standards, changing the solvent mixture did not have a significant effect on the production of  $(\text{M}+\text{H})^+$  ions.

For spiperone and ephedrine in matrigel, the production of the  $(\text{M}+\text{H})^+$  ion signal improved after increasing the polarity of the matrix solvent mixture (Figure 2-7 and Figure 2-8). One explanation for the trends observed is that adjusting the polarity of the solvent mixture to match that of the drug compounds achieved a more efficient extraction. This would explain the fact that ephedrine, a predominantly polar molecule, was more efficiently extracted from the matrigel using the two most polar solvent mixtures. With

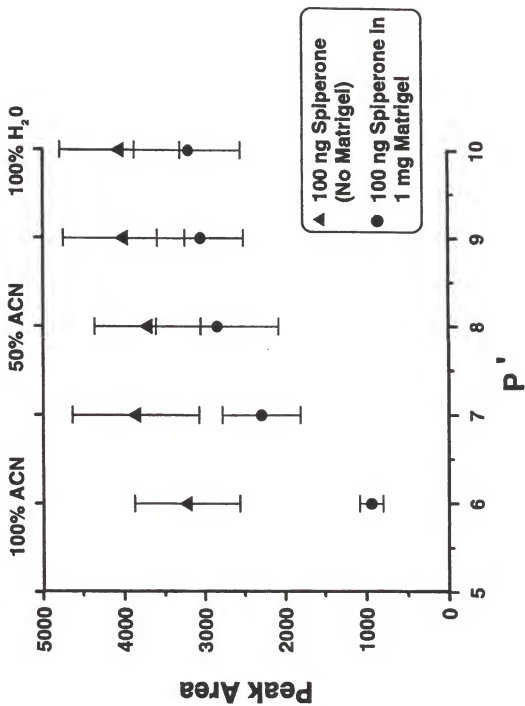


Figure 2-7. Plot of the average (M+H)<sup>+</sup> peak area for a spiperone standard (top) and for spiperone in matrigel (bottom) versus the DHB matrix solvent mixture polarity.

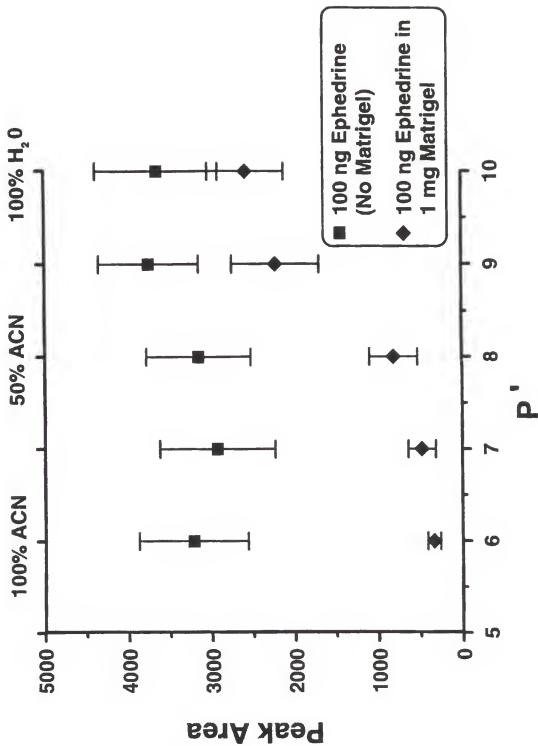


Figure 2-8. Plot of the average  $(M+H)^+$  peak area for an ephedrine standard (top) and for ephedrine in matrigel (bottom) versus the DHB matrix solvent mixture polarity.

spiperone on the other hand, a gradual increase in the  $(M+H)^+$  ion peak area was observed over the entire range of solvent mixtures because it has both polar and nonpolar parts. Upon repeating the experiments with matrigel under magnification, however, it was revealed that using the more polar, less volatile solvent mixtures allowed the matrix solution to soak on the surface of the matrigel for extended periods of time as was previously seen with the drug standards. Taking this into consideration, it is more likely that the trends observed for spiperone and ephedrine in matrigel are a function of both the extraction efficiency and the soak time of the matrix solution.

#### Optimization of the MALDI Matrix "Soak Time"

To determine the influence of the soak time of the matrix solution on the extraction efficiency of spiperone and ephedrine from matrigel a sample procedure was developed which allowed the crystallization of the MALDI matrix to be more precisely controlled. Previously, Cottrell and coworkers<sup>68</sup> described a procedure for controlling the crystallization of the matrix solution for peptides bound to nitrocellulose. In their work, a microscope slide was used to cover the sample on the Lasermat sample plate after the addition of the MALDI matrix droplet. By allowing the matrix solution to soak for a couple of minutes the elution of the peptides out of the nitrocellulose and into the matrix solvent was improved. Using this method, a two-fold increase in analyte ion signal was reported.

For the experiments with spiperone and ephedrine in matrigel, a Teflon disk approximately 0.5" in diameter was placed over the raised rim of the Lasermat sample plate immediately after the addition of the matrix solution. The samples were covered for

1 - 30 min. Figure 2-9 shows the plot of the average  $(M+H)^+$  peak area after 100 laser shots versus time using the DHB matrix solution prepared in 70% acetonitrile/30% water. Increasing the soak time from 1 - 10 min. resulted in the most significant increase in the  $(M+H)^+$  peak area for both compounds. At soak times beyond 15 min., no further increases were observed. This trend suggests that a partition equilibrium between the matrigel tissue and the matrix solvent was established. The soak experiments were repeated with each of the remaining four solvent mixtures. For all of the solvents tested, increasing the soak time increased the  $(M+H)^+$  ion signal of the respective drug compounds from matrigel. The best results were obtained using the most polar solvent mixtures at soak times of approximately 5 - 10 min.

#### Spatial Resolution Experiments with Spiperone in Matrigel

As outlined at the beginning of the chapter, one of the goals of this work was to evaluate the potential of MALDI for mapping drug compounds in biological tissues. From the work presented in the previous sections, it was determined that MALDI increased the sensitivity for detecting drug compounds in tissue by extracting the analyte molecules out of the tissue and into the matrix solvent. This has serious implications for applications involving mapping or imaging of compounds because as the analyte molecules are extracted out of the tissue, information about their original location in the tissue may be lost. Theoretically, once the analyte molecules are extracted into the matrix solvent they are free to migrate in the matrix solution until the solvent evaporates and they become encapsulated in the matrix crystals.<sup>67</sup> The loss of spatial information will be



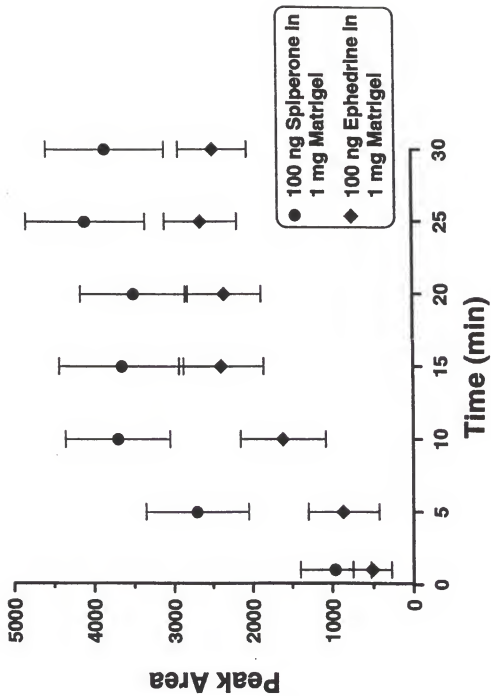


Figure 2-9. Plot of the average  $(M+H)^+$  peak area for siperone (top) and ephedrine (bottom) in matrigel versus the MALDI matrix soak time. The DHB matrix solution was prepared in 70% acetonitrile/ 30% water.

further compounded by the fact that at longer soak times, analyte molecules can migrate farther from their initial locations.

To address this issue, spatial resolution experiments were performed with spiperone in matrigel using the Lasermat instrument. The Lasermat software provides two aim positions on the sample plate target area 180° apart. The distance between the target spots was measured experimentally by coating the target area of the sample plate with a thin layer of Witeout correction fluid. After drying, the sample plate was inserted into the vacuum chamber of the Lasermat and 100 laser shots were taken at each laser aim position. Under magnification, two craters measuring approximately 0.1 mm in diameter were observed in the surface of the Witeout resulting from laser ablation. The distance between the centers of the craters at the two positions was measured to be approximately 0.3 mm.

Using a clean sample plate, spiperone mixed with matrigel was added to the left side of the sample plate (position 1) using a disposable pipet and allowed to dry completely. A parafilm mask was then laid flat over the entire sample area and cut to expose only the right side of the sample plate (position 2). This was done to prevent mixing of the matrigel samples from each position. Matrigel without any analyte was then deposited onto position 2 (Figure 2-10). After removing the parafilm mask, observation of the sample plate under magnification showed that two distinct sample regions had been prepared. To ensure that none of the spiperone from position 1 had migrated to position 2, thirty laser shots were taken at each of the two laser aim positions prior to the addition of the MALDI matrix solution (Figure 2-11). The spectrum from position 1 was dominated primarily by low molecular weight matrigel ions along with some spiperone

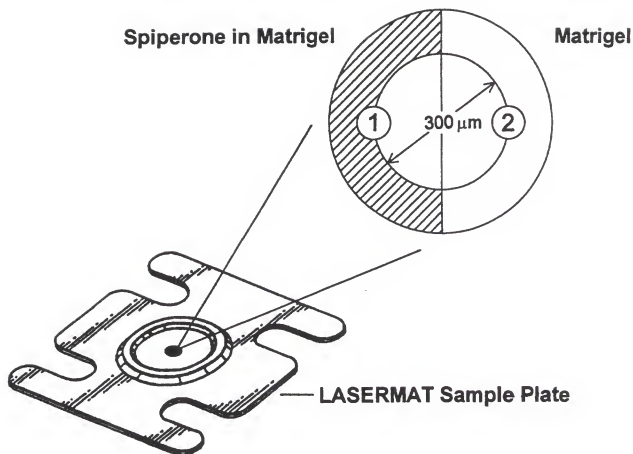


Figure 2-10. Diagram of the Lasermat sample plate showing the deposition procedure used for the spatial resolution experiments with spiperone in matrigel.

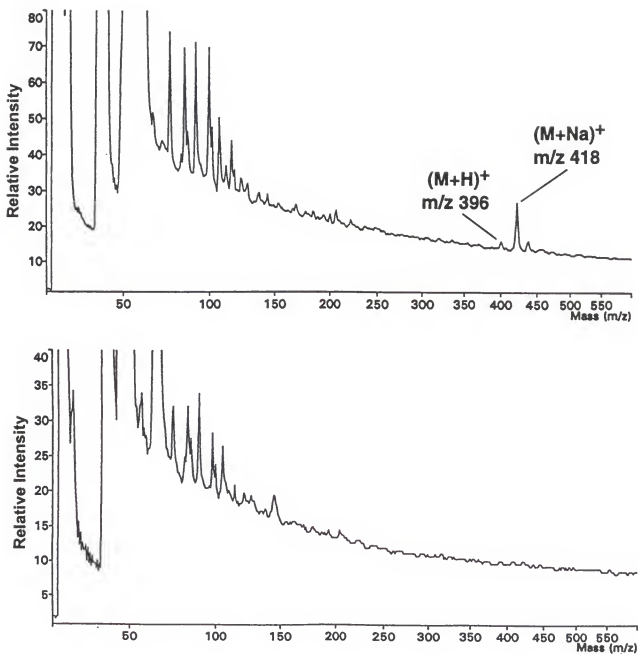


Figure 2-11. Comparison of the LDI spectra obtained from thirty laser shots at position 1 (top) and position 2 (bottom) on the Lasermat sample plate. Position 1 was loaded with 100 ppm of spiperone in matrigel. Position 2 contained only matrigel.

$(M+H)^+$  and  $(M+Na)^+$  ions. No spiperone ions were detected at position 2. For the MALDI experiment, 1.0  $\mu$ L of a 0.25 M DHB solution prepared in 30% acetonitrile/ 70% water was added over the entire target area of the sample plate. The matrix solution was allowed to soak on the sample by covering the target area with the teflon disk. After approximately five minutes the cover was removed and the matrix solution was allowed to crystallize, covering both positions 1 and 2. Once the crystals had completely dried, the sample plate was introduced into the ion source of the Lasermat. Thirty laser shots were again taken at each of the two laser aim positions. With the addition of the DHB matrix, spiperone was detected at both positions 1 and 2, suggesting that spiperone had in fact migrated during the soak time of the matrix solution (Figure 2-12). The ratio of spiperone detected at the two positions was determined from the average  $(M+H)^+$  peak areas to be approximately 2:1.

Taking into account the diameter of the target area and the distance of the laser spot at position 2 from the spiperone-matrigel boundary, the estimated migration distance for spiperone in matrigel after a five-minute soak time was calculated to be 0.15 - 1.25 mm. These results are significant given the fact that the boundaries between the various regions in complex tissues can be as small as 2 - 5  $\mu$ m.<sup>27</sup>

An alternative approach to performing MALDI of drug compounds in tissue is to spray the matrix on top of the tissue surface as a fine mist. The advantage of this approach is that the migration of the analyte molecules in the tissue can be reduced due to the rapid evaporation of the solvent and crystallization of the matrix solution. The electrospray apparatus used in this work consisted of a stainless steel syringe and needle (flat tip, 18 ga.) mounted vertically above a 0.25" thick stainless steel sample stage.

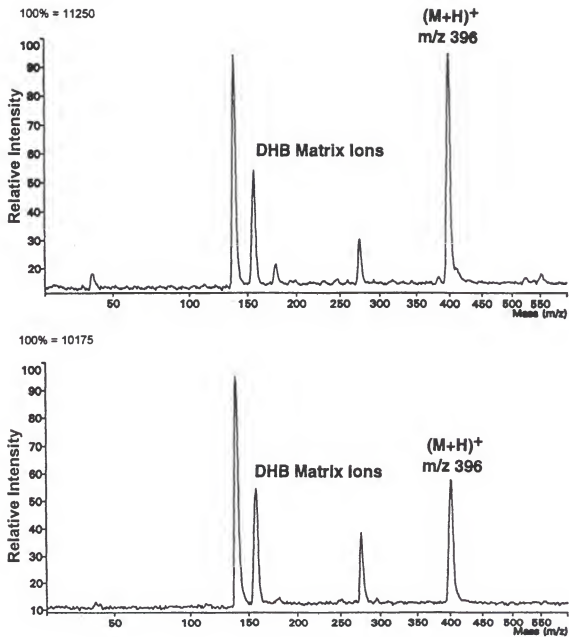


Figure 2-12. Comparison of the MALDI spectra obtained for spiperone (M.W. 395) from position 1 (top) and position 2 (bottom) on the Lasermat sample plate after addition of 1.0  $\mu$ L of 0.25 M DHB matrix solution.

The syringe was connected to a 20 kV power supply using a copper lead (Figure 2-13). The sample stage was connected to the power supply ground. The syringe and sample stage were housed inside of a Plexiglas chamber for safety concerns. Ceramic rods were attached to the sample stage to allow the stage to be positioned at variable distances from the tip of the needle during the spray deposition process.

Using the electrospray setup, the spatial resolution experiments with spiperone in matrigel were repeated. As before, spiperone mixed with matrigel was applied to the left side of the sample plate (position 1) while matrigel alone was deposited on the right side (position 2) using the parafilm mask to prevent mixing. The sample plate was then placed inside of the electrospray chamber and allowed to rest on the grounded sample stage. The matrix syringe was filled with 50  $\mu\text{L}$  of DHB matrix solution. At the onset of the first matrix droplet at the tip of the needle, a +5 kV potential was applied to the syringe. The voltage was increased to +10 kV at which point a fine, uniform, spray was formed which covered the entire sample plate. At potentials above +10 kV the needle began to vibrate, causing the matrix spray to miss the sample plate entirely. The distance of the sample stage from the syringe was also found to have a significant effect on the spray deposition process. A distance of 1 - 2" below the needle was found to give the most uniform deposition of the matrix. After about 30 s of spraying, a very thin, homogeneous crystal layer was formed on the surface of the matrigel sample. MALDI spectra were obtained for the sample at laser aim positions 1 and 2 as before. By electrospraying the DHB matrix solution, spiperone was only detected at position 1 (Figure 2-14). The area of the spiperone  $(\text{M}+\text{H})^+$  peak, however, was only one third of that obtained by applying the matrix solution as a drop, presumably because spiperone was not as effectively extracted

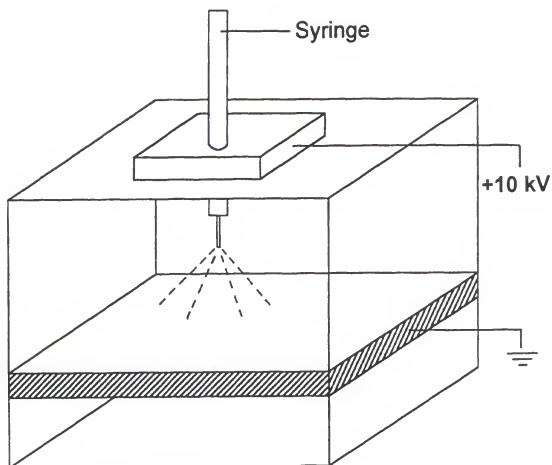


Figure 2-13. Schematic of the electro spray apparatus used to spray the MALDI matrix onto the surface of tissue samples.



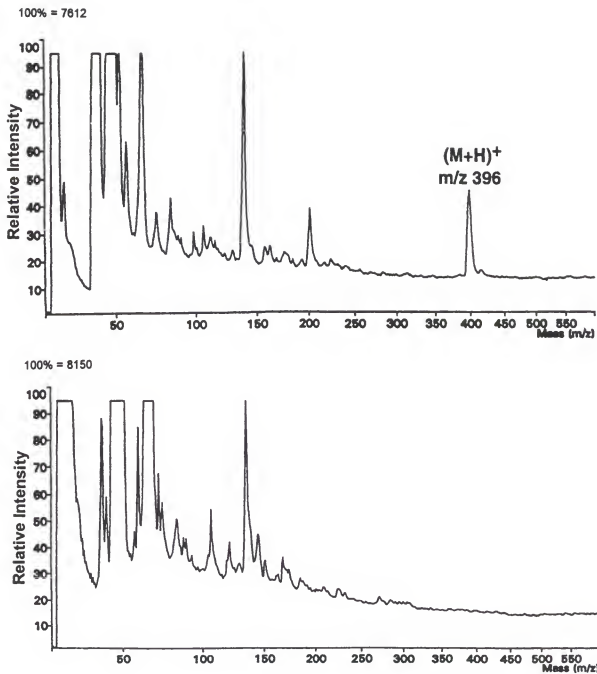


Figure 2-14. Comparison of the MALDI spectra obtained from position 1 (top) and position 2 (bottom) on the Lasermat sample plate after electrospray deposition of the DHB matrix solution.

from the matrigel. These results suggest that by electrospraying the matrix solution, migration of the analyte can be minimized when using MALDI. The migration of spiperone over shorter distances unfortunately could not be investigated due to the fixed laser aim of the Lasermat instrument.

### CHAPTER 3 DESIGN AND CONSTRUCTION OF A NOVEL LASER DESORPTION QUADRUPOLE ION TRAP MASS SPECTROMETER

After completion of the first MALDI experiments using the Lasermat; research efforts were focused on designing and constructing a new laser desorption instrument for MALDI, based on the quadrupole ion trap mass analyzer. While the Lasermat proved to be useful for detecting spiperone and ephedrine in matrigel, it lacked the mass resolution and MS/MS capabilities needed to detect trace levels of drug compounds from more complex biological tissues. This chapter introduces the quadrupole ion trap mass analyzer and provides a detailed description of the various components used to construct the new instrument. Included is a brief history of the development of the ion trap along with a description of its function and theory of operation. Also presented in this chapter is a review of previous laser desorption ion trap designs.

#### The Quadrupole Ion Trap Mass Spectrometer

##### Background History

The quadrupole ion trap was first described as a device for storing electrically charged particles, along with the quadrupole mass filter, by Paul and Steinwedel (University of Bonn, Germany) in a patent submitted in 1953.<sup>69</sup> In their patent, Paul and Steinwedel proposed using a combination of radio frequency (RF) and direct current (DC)

voltages to create a quadrupolar trapping field inside the volume of a solid ion trap consisting of two endcap electrodes and a central ring electrode (Figure 3-1). Initially, the ion trap was described as “still another electrode arrangement”. However since its introduction, the ion trap has developed into one of the most sensitive, selective, and versatile mass spectrometers to date.<sup>70</sup>

Initially, the ion trap was used primarily by physicist to study various physical and chemical properties of stored ions. In the first work by Paul and coworkers in the early 1950's, the energy absorption of stored ions was measured by applying an RF voltage across the endcap electrodes of the ion trap.<sup>71</sup> The energy absorbed was then related to the concentration of stored ions. Following this work, Wuerker et al.<sup>72</sup> demonstrated the storage of small charged particles of aluminum in the ion trap. Experiments were performed to measure the frequency of ion motion by applying a range of supplemental alternating current (AC) frequencies across the endcap electrodes. Photographs were also taken of the stored particle(s) showing their resonance in the trapping field. Building on this work, Dehmelt and Major<sup>73</sup> demonstrated the use of the ion trap for high resolution spectroscopic studies of ground state, metastable, atomic, and molecular ions.

In 1959, Fischer reported the first use of the ion trap for measuring the molecular weight of stored ions.<sup>74</sup> In his work, Fischer used the ion trap to measure the mass of a series of krypton isotopes at unit mass resolution using the original mass-selective detection technique.<sup>69</sup> With this technique, the motion of the stored ions was sensed by means of tuned circuits, such that a response was obtained for each  $m/z$  value in turn. The approach was similar to ion cyclotron resonance in that the ions were detected nondestructively, inside of the ion trap. In 1968, Dawson and Whetten<sup>75</sup> demonstrated the

June 7, 1960

W. PAUL ET AL  
APPARATUS FOR SEPARATING CHARGED PARTICLES  
OF DIFFERENT SPECIFIC CHARGES

2,939,952

Filed Dec. 21, 1954

4 Sheets-Sheet 4

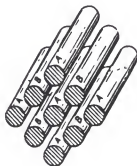


Fig. 10.

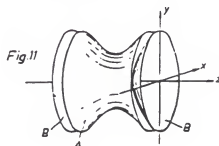


Fig. 11

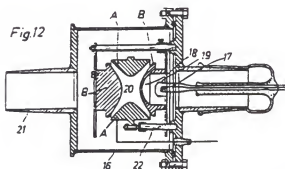


Fig. 12

INVENTORS  
WOLFGANG PAUL  
HELMUT STEINWEDL  
By *Dr. Paul H. ... J. Fisher*  
ATTORNEYS

Figure 3-1. Sketch of the original quadrupole ion trap taken from the U.S. patent 2,939,952 applied for by Wolfgang Paul and Helmut Steinwedel on December 24, 1953.<sup>69</sup>

first use of the ion trap as a true mass spectrometer by using a slightly different approach called mass-selective storage. In their experiment, different combinations of RF and DC voltages were applied to the ion trap such that only ions of a single  $m/z$  were stable at a given time. The ions were detected by ejecting them through small holes in one of the endcap electrodes using a short DC pulse, to an external detector. Satisfactory mass spectra were obtained using this operational mode, although over a limited mass range.

Almost sixteen years after Dawson and Whetten's work, the first commercially available ion trap mass spectrometer was introduced by Finnigan MAT in 1984. The Ion Trap Detector (ITD) 700 was designed as a low-cost benchtop detector for gas chromatography (GC). With this instrument, ions were formed within the volume of the ion trap by EI. Ions with  $m/z$  values up to 650 could be stored simultaneously inside of the ion trap by virtue of a 1.1 MHz RF potential applied to the ring electrode. Probably the most significant development leading to the commercialization of the ion trap was the mass-selective instability scan developed by Stafford et al. at Finnigan MAT.<sup>76</sup> In contrast to previous detection modes, the mass-selective instability scan involved ramping the RF amplitude applied to the ring electrode linearly with respect to time. As the RF potential was increased, ions of increasingly higher  $m/z$  developed unstable trajectories inside of the ion trap and were ejected through holes in one of the endcap electrodes to a detector (Figure 3-2). Mass spectra were obtained as a function of the RF potential needed to eject ions of various  $m/z$  values to the detector.

Since the introduction of the first commercial ion trap instrument, several advances in ion trap technology have been made to expand the range of applications of the ion trap to include the analysis of biomolecules. Of particular note was the advent of resonant

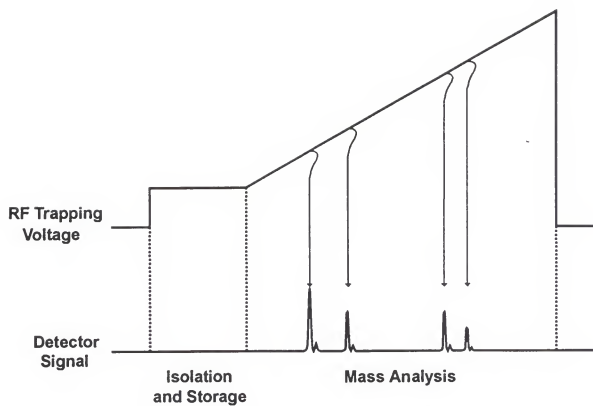


Figure 3-2. Diagram showing the generation of a mass spectrum using the mass-selective instability scan method.

ejection or axial modulation in 1988.<sup>77</sup> The technique of resonant ejection was originally developed to improve the resolution and dynamic range of the ITD. Variations on this technique have been developed to allow for the resonant excitation and subsequent fragmentation of ions inside of the ion trap for MS/MS.<sup>78</sup> Axial modulation has also been responsible for extending the mass range of the quadrupole ion trap to well beyond  $m/z$  50,000.<sup>79</sup> Advances have also been made in ion isolation with the advent of two-step,<sup>80</sup> apex,<sup>81</sup> and forward-reverse scan<sup>82</sup> isolation techniques. The application of these techniques will be discussed in detail in the following sections of this chapter.

The most significant advances in the past seven to eight years have been made in coupling external ionization sources to the ion trap. These sources allow ions to be formed outside of the confines of the ion trap. To date, almost every type of ionization source has been coupled to the ion trap including glow discharge (GD),<sup>83</sup> fast atom bombardment (FAB),<sup>84</sup> and electron and chemical ionization (EI/CI).<sup>85</sup> For the analysis of biomolecules the two most important ionization methods have been electrospray ionization (ESI)<sup>86</sup> and MALDI.<sup>20</sup>

### Ion Trap Theory

The quadrupole ion trap is the three-dimensional analogue of the more common quadrupole mass filter. However, instead of using four round or hyperbolic rods to create a quadrupolar trapping field, the ion trap makes use of three symmetrically cylindrical, hyperbolic electrodes. The central or ring electrode is toroidal in shape and is situated between two inverted, domed-shaped endcap electrodes (Figure 3-3). The following



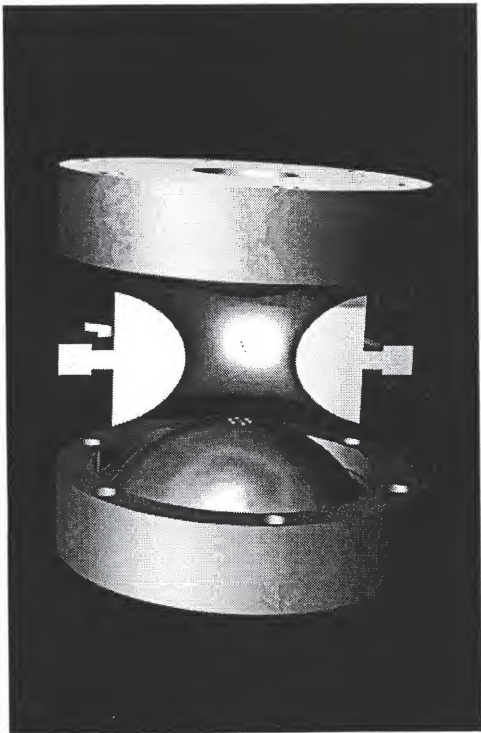


Figure 3-3. Computer representation of the quadrupole ion trap mass analyzer showing the exit endcap electrode (left), ring electrode (center), and entrance endcap electrode (right).

derivation was adapted from March and Todd.<sup>70</sup> The general equations defining the hyperbolic shape of the ring electrode and endcap electrodes are given by:

$$\frac{1}{r_0^2}(r^2 - 2z^2) = 1 \quad (3-1)$$

$$\frac{1}{2z_0^2}(r^2 - 2z^2) = -1 \quad (3-2)$$

where  $r_0$  is the inner radius of the ring electrode and  $z_0$  is the distance from the center of the ion trap to the endcap electrode. The simplest relationship between the ring electrode and the endcap electrodes which define a pure quadrupolar field is given by:

$$r_0^2 = 2z_0^2 \quad (3-3)$$

A quadrupolar trapping field is generated inside of the ion trap by applying an RF potential to the ring electrode. The field is uncoupled in the three coordinate directions (x,y,z). Therefore, the forces acting on an ion are independent of one another and also vary linearly with the ion's position from the center of the ion trap. The potential applied to the ring electrode can be represented mathematically by:

$$\Phi_0^R = U - V \cos \Omega t \quad (3-4)$$

where  $\Phi_0^R$  is the applied RF potential, U is the applied DC voltage, V is the zero-to-peak amplitude of the RF voltage,  $\Omega$  is the angular frequency of the RF trapping field applied to the ring electrode in rad/s, and t is the time variable. For an ion trap employing an ideal quadrupolar trapping field, the potential at any given point  $\Phi$ , can be represented by:

$$\Phi = \frac{\Phi_0^R - \Phi_0^E}{r_0^2 + 2z_0^2} [r^2 - 2z^2] + \frac{2z_0^2 \Phi_0^R + r_0^2 \Phi_0^E}{r_0^2 + 2z_0^2} \quad (3-5)$$

where  $\Phi_0^E$  is the potential applied to the endcap electrodes. Equation 3-5 is identical to the general expression for the potential inside of a quadrupole ion trap given by Knight.<sup>87</sup> Substituting equation 3-3 into equation 3-5 and assuming that both endcap electrodes are grounded (normal operational mode) gives the more common expression:

$$\Phi = \frac{\Phi_0^R}{2r_0^2} [r^2 - 2z^2] + \frac{\Phi_0^R}{2} \quad (3-6)$$

The differential equation of motion for a singly charged positive ion subject to the potential of equation 3-6 can be obtained from the following:

$$\frac{d^2 \vec{r}}{dt^2} = -\frac{e}{m} \nabla \Phi \quad (3-7)$$

where  $m$  is the mass of the ion and  $e$  is the electronic charge. By inserting equation 3-4 into equation 3-6, setting the field strength at the center of the ion trap to zero (in order to satisfy Laplace's equation), and differentiating; the motion of the ion in the radial ( $r$ ) and axial ( $z$ ) directions can be written as:

$$\frac{d^2 r}{dt^2} + \frac{2e}{2mr_0^2} (U - V \cos \Omega t) r = 0 \quad (3-8)$$

$$\frac{d^2 z}{dt^2} + \frac{4e}{2mr_0^2} (U - V \cos \Omega t) z = 0 \quad (3-9)$$

These equations are examples of the Mathieu equations developed 150 years ago to explain the motion of vibrating membranes.<sup>88</sup> The general form of the Mathieu equation can be expressed as:

$$\frac{d^2 u}{d\xi^2} + (a_u - 2q_u \cos 2\xi)u = 0 \quad (3-10)$$

where  $u$  represents  $r$  or  $z$ , and  $\xi = \Omega t/2$ . The stability parameters  $a_u$  and  $q_u$  determine whether an ion's motion will be stable or unstable in the quadrupolar field. By performing a series of operations and substitutions, the stability parameters can be expressed in terms of the RF and DC potentials applied to the ring electrode and to the  $m/z$  of the ion of interest as follows:

$$a_u = a_z = -2a_r = \frac{-8eU}{m(r_0^2 + 2z_0^2)\Omega^2} \quad (3-11)$$

$$q_u = q_z = -2q_r = \frac{-4eV}{m(r_0^2 + 2z_0^2)\Omega^2} \quad (3-12)$$

A graphical representation of stable solutions of the Mathieu equation can be generated by using the dimensionless parameters  $a_z$  and  $q_z$  as the ordinate and abscissa respectively. Figure 3-4 shows the regions in  $(a_z, q_z)$  space where the radial and axial components of the ion trajectory are stable. The overlap region near the origin represents the range of  $a_z$  and  $q_z$  values that give rise to stable ion trajectories in both the radial and axial directions simultaneously. This region is more commonly referred to as the Mathieu stability region (Figure 3-5). When an ion has values of  $a_z$  and  $q_z$  which fall within the Mathieu stability region, its motion is stable within the volume of the ion trap.

The lines drawn down and across the stability diagram shown in Figure 3-5 are called iso- $\beta$  lines, and describe the detailed trajectories of ions at that particular point. The form of an ion trajectory in the  $r, z$  plane has the general appearance of a Lissajous curve composed of two fundamental frequency components  $\omega_{r,0}$  and  $\omega_{z,0}$  of the secular motion,

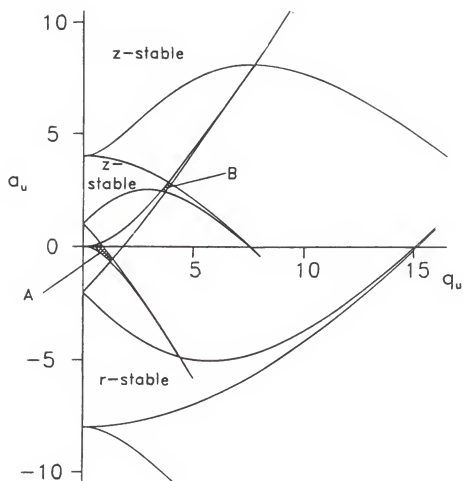


Figure 3-4. Diagram showing the regions of stable ion trajectories in both the radial ( $r$ ) and axial ( $z$ ) directions for the quadrupole ion trap. Regions of simultaneous overlap are denoted A and B.<sup>70</sup>

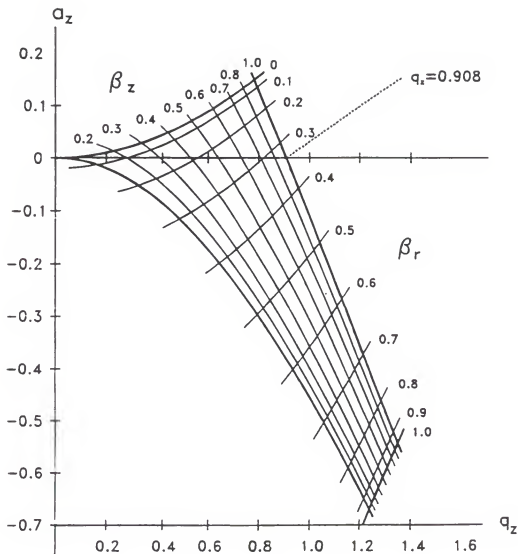


Figure 3-5. Mathieu stability diagram plotted in  $(a_z, q_z)$  space. Ions with  $a_z$  and  $q_z$  values within this region are stable within the ion trap and can be stored. The lines running down and across the stability region are iso- $\beta$  lines used to define the frequency of oscillation of stored ions.<sup>70</sup>

with a superimposed micromotion of frequency  $\Omega \pm \omega$  Hz (Figure 3-6). The relationship between ion frequency and the parameter  $\beta$  is given by:

$$\omega_{n,u} = \left( n + \frac{1}{2} \beta_u \right) \Omega \quad (3-13)$$

where  $0 \leq \beta_u \leq 1$  and  $n = \pm 1, \pm 2, \dots$ . When  $n = 0$ , the fundamental frequency of ion motion reduces to  $\omega_{n,u} = \frac{1}{2} \beta_u \Omega$ .

The values of  $a_z$  and  $q_z$  as defined by equations 3-11 and 3-12, respectively, correspond to a single ion isolated in an ideal quadrupole ion trap for which the electrodes extend to infinity. In order to produce a functional ion trap, however, the electrodes must be truncated. Truncation of the electrodes introduces higher-order multipole components to the potential which causes non-linear resonances in ion motion.<sup>89</sup> To compensate for these phenomenon, the ion trap is “stretched” axially by assembling the ion trap in such a way that the distance between the endcap electrodes is increased by 10.6% ( $z_0 = 0.783$  cm).<sup>90</sup> Despite the stretch in geometry, the stability diagram is changed only slightly.<sup>91</sup>

### Operation of the Ion Trap

In the normal mode of operation, ions formed inside of the ion trap by EI are trapped and stored by applying an RF potential to the ring electrode while holding the two endcap electrodes at ground. The applied RF has a frequency of 1.0485 MHz and an amplitude of 0-7500 V<sub>o-p</sub>. In the instrument constructed for this work, ions were generated externally by MALDI then directed into the ion trap using a series of focusing lenses and a DC quadrupole deflector. A -5 V DC offset potential was also applied to the

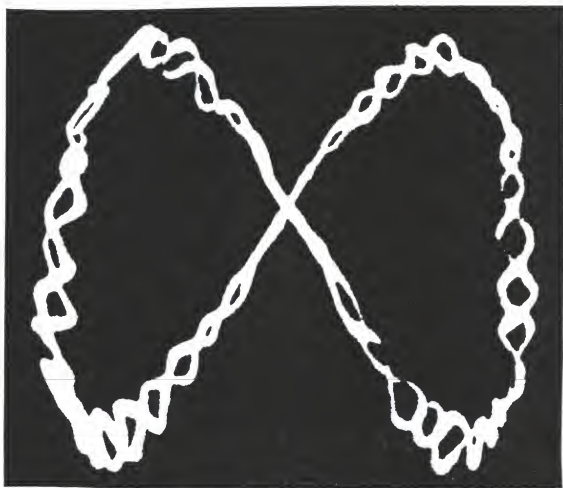


Figure 3-6. Photograph of the ion trajectories for aluminum particles stored inside the ion trap. The trajectories have a fundamental frequency of motion and a superimposed micromotion having the form of a Lissajous curve.<sup>72</sup>



ring and endcap electrodes to control the kinetic energy of the ions as they entered the trap. Typically, the RF amplitude applied to the ring electrode is set low ( $q_z=0.100$  for  $m/z$  100) during the initial ionization event to allow ions over a range of  $m/z$  values to be successfully trapped and stored in the ion trap. For MALDI, however, relatively high RF amplitudes ( $q_z=0.400$ ) were required due to the high kinetic energy (3-5 eV) of the ions. A buffer gas of helium ( $10^{-3}$  torr) was also introduced directly into the ion trap. The purpose of the buffer gas was to increase the trapping efficiency of the ions and to collisionally cool the ions to the center of the trap where their motion becomes more stable in the quadrupolar field.

### Ion isolation

Ions over a range of  $m/z$  values or ions of a single  $m/z$  value can be isolated in the ion trap using a variety of methods including apex,<sup>81</sup> two-step,<sup>80</sup> random noise,<sup>92</sup> stored-waveform inverse Fourier transform (SWIFT),<sup>93</sup> and filtered noise.<sup>92</sup> The two most commonly used methods are apex and two-step isolation. In apex isolation (Figure 3-7), the RF potential applied to the ring electrode is first increased to place the ion of interest at a  $q_z=0.78$  (B). A negative DC potential is then applied to the ring electrode to move the ion to a point ( $a_z=0.15$ ) just inside the apex of the stability region (C). At the apex, all ions of  $m/z$  greater than the ion of interest are ejected radially from the ion trap, while those ions with lower  $m/z$  values are ejected axially. After isolation, the DC potential is turned off and the RF amplitude is lowered to position the isolated ion at a more stable  $q_z=0.30$  (A). In two-step isolation (Figure 3-8), ions of  $m/z$  greater than that of the selected ion of interest are ejected from the ion trap across the  $\beta_z=0$  boundary by applying a

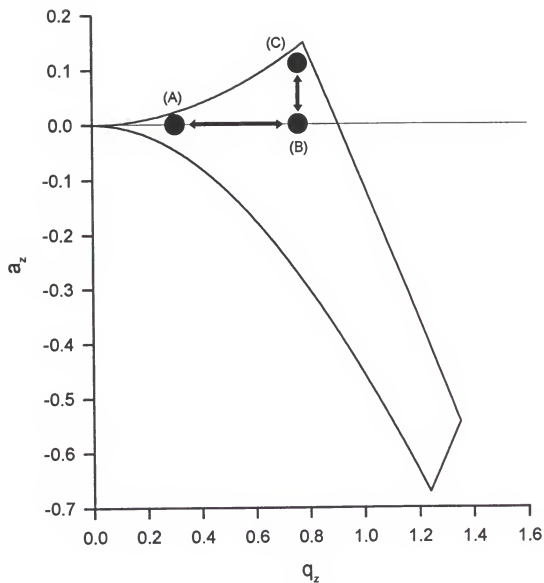


Figure 3-7. Mathieu stability diagram showing the changes in RF and DC voltage levels, plotted as  $q_z$  and  $a_z$  respectively, for apex-isolation. Ions of lower and higher  $m/z$  values are ejected simultaneously at the apex (C).

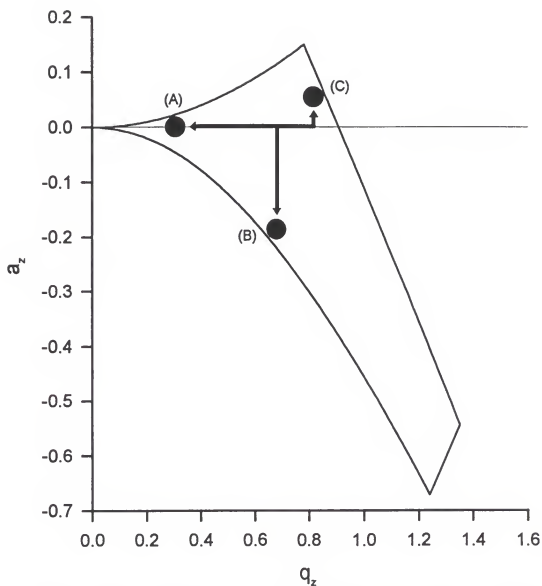


Figure 3-8. Mathieu stability diagram showing the changes in RF and DC voltage levels, plotted as  $q_z$  and  $a_z$  respectively, for two-step isolation. Higher  $m/z$  ions are ejected across the  $\beta_z=0$  line at position (B). Lower  $m/z$  ions are ejected across the  $\beta_z=1$  line at position (C).

positive DC potential to the ring electrode (B). After ejecting the higher masses, the RF amplitude is increased so that the ion of interest is placed at a  $q=0.85$ . A negative DC potential is then applied to the ring electrode causing all those ions with  $m/z$  values lower than the ion of interest to be ejected across the  $\beta_z=1$  boundary (C).

The major drawback of the apex and two-step isolation methods is the fact that they can only be used to isolate ions up to approximately  $m/z$  600 because of the high DC voltages required. The molecular weights of the drug compounds studied in this work ranged from 165 - 1206 Da. In order to isolate the higher mass ions ( $>m/z$  600) an alternative method known as forward-and-reverse scanning<sup>82</sup> was used (Figure 3-9). In forward-and-reverse scanning an auxiliary AC voltage (typically 219 kHz, 3 - 6  $V_{o-p}$ ) is applied 180° out of phase across the endcap electrodes (A). The main RF is then ramped up until the frequency of the ion of interest is just below the auxiliary frequency (B). During the RF ramp (forward scan), ions of  $m/z$  lower than the ion of interest sequentially come into resonance with the supplementary field and are ejected from the trap. After ejecting the low mass ions, the auxiliary field is turned off and the RF amplitude is set to the maximum value (C). The auxiliary field is then turned back on (D) and the RF amplitude is ramped down (reverse scan); this time until the frequency of the ion of interest is just above the auxiliary frequency (E). In this way, those ions with  $m/z$  values greater than the ion of interest are resonantly ejected leaving only the ion of interest in the ion trap (F).

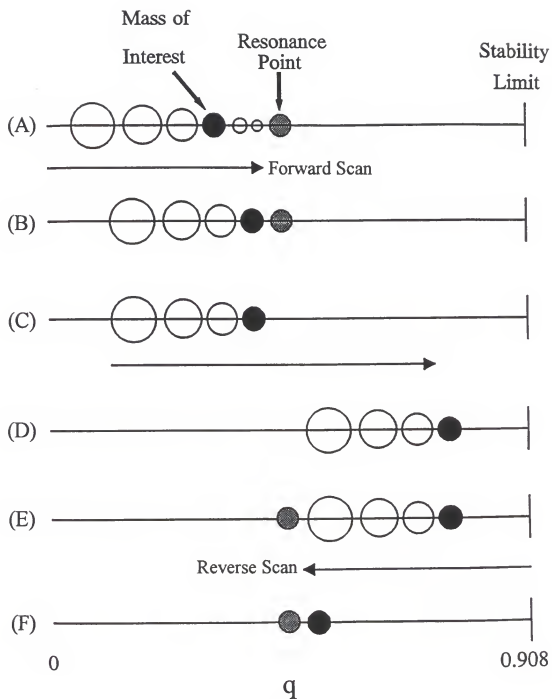


Figure 3-9. Ion isolation using the forward-and-reverse scan method. Higher and lower  $m/z$  ions are ejected from the ion trap by coming into resonance with a supplementary AC frequency applied to the endcap electrodes.<sup>94</sup>

### Tandem mass spectrometry (MS/MS)

After isolation, the remaining parent ions can be fragmented inside of the ion trap to produce daughter ions. These daughter ions, being products of the isolated parent ions only, can then be used for structure elucidation. This process is known as tandem mass spectrometry or MS/MS. MS/MS is performed by first setting the RF potential on the ring electrode to correspond to a  $q_z=0.30$  for the parent ion of interest. An auxiliary AC or “tickle” frequency (6-8  $V_{o-p}$ ) is then applied across the endcap electrodes and tuned to the frequency of the ions (118 kHz) (Figure 3-10). When the auxiliary frequency matches the secular frequency of the ions, they become resonantly excited and undergo collisions with the constant pressure of helium buffer gas in the ion trap. These collisions deposit energy into the ions which cause them to fragment. This process is termed collision-induced dissociation (CID).<sup>78</sup> By repeating the process of isolating, fragmenting, and storing the ions; several stages of mass spectrometry or MS<sup>n</sup> can be carried out inside of the ion trap.

### Ion detection

Ions stored in the ion trap are detected using the mass-selective instability scan<sup>76</sup> where the RF amplitude applied to the ring electrode is increased linearly with respect to time. Typically, the RF voltage is ramped from 100 - 7500  $V_{o-p}$  in 110 ms. In this way, ions of increasingly higher  $m/z$  are made to approach the edge of the stability region ( $q_z=0.908$ ). Once the ions reach the stability edge, they take on axially unstable trajectories and are ejected from the ion trap to an electron multiplier situated directly

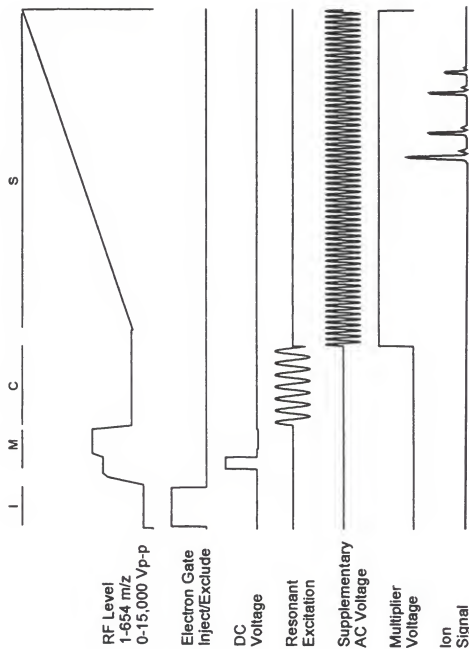


Figure 3-10. Typical scan function for MS/MS showing the different voltages applied to ring and endcap electrodes during the ionization (I), mass isolation (M), CID (C), and analytical scan (S) stages.

behind the exit endcap electrode. One of the problems associated with this method is that during the RF ramp, the higher  $m/z$  ions still inside of the ion trap contribute a significant space charge potential which ultimately degrades the resolution of the resulting mass spectrum.<sup>70</sup> This can be overcome by applying an auxiliary frequency (typically 3-6  $V_{o-p}$  at 485 kHz) to the endcap electrodes during the analytical scan. As the RF amplitude is increased, the ions secular motion enters into resonance with the supplementary field causing the ions to be ejected in a tightly focused packet. This method is known as resonance ejection or axial modulation.<sup>85</sup>

### Mass range extension

The maximum  $m/z$  ion that can be detected in the normal operational mode of the ion trap using the mass-selective instability scan with an axially modulation frequency of 485 kHz is 650.<sup>70</sup> This upper limit is determined by rearrangement of equation (3-12) to give:

$$(m/z)_{\max} = \frac{8eV_{\max}}{q_{\text{eject}}(r_0^2 + z_0^2)\Omega^2} \quad (3-14)$$

where  $V_{\max} = 15000 V_{p-p}$ ,  $r_0 = 1$  cm,  $z_0 = 0.792$  cm,  $\Omega/2\pi = 1.0485$  MHz, and  $q_{\text{eject}} = 0.908$  are the operating parameters for the Finnigan ITS40 mass spectrometer used in the new instrument. While the ion trap can be made to trap and store ions of  $m/z$  greater than 650; the RF voltage levels needed to successfully eject these ions can not be reached during the normal mass selective-instability scan. The obvious solution would be to increase the



maximum RF voltage applied to the ring electrode. However this would result in severe arcing between the ring and endcap electrodes.

Several alternative approaches have been proposed to increase the mass range of the ion trap.<sup>95</sup> In general, these methods involve either reducing the size of the ion trap ( $r_0, z_0$ ), reducing the drive frequency ( $\Omega$ ), or lowering the  $q_{\text{eject}}$  at which ions are ejected from the ion trap. For all of the high mass analysis performed with the new laser desorption instrument, the last method was used. In this method, an auxiliary AC frequency (6 - 8  $V_{\text{op}}$ ) is applied to the endcap electrodes during the mass-selective instability scan. However, instead of setting the axial modulation frequency to 485 kHz, as is normally done for resonance ejection, the frequency is lowered so that ions are made to come into resonance with the auxiliary field earlier in the RF ramp. As a result, the ions are ejected from the ion trap at lower  $q_{\text{eject}}$  values (Figure 3-11). By ramping the RF voltage to its maximum value of 7500  $V_{\text{op}}$ , a much higher maximum mass can be ejected and therefore detected. The plot of the maximum mass detectable for a given axial modulation frequency is shown in Figure 3-12. One of the consequences of ejecting ions at lower  $q_{\text{eject}}$  values, however, is that the assigned mass is lower than the actual mass of the ion. This is because the ion is ejected at a much lower RF voltage level. To compensate for this, the assigned mass must be corrected using the following equation:<sup>70</sup>

$$(m/z)_{\text{new}} = (m/z)_{\text{old}} * \left( \frac{q_{\text{eject new}}}{q_{\text{eject old}}} \right) \quad (3-15)$$

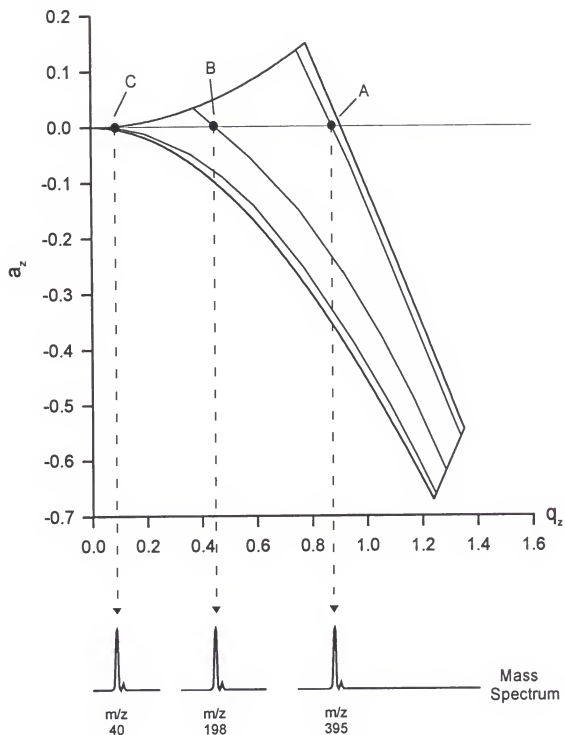


Figure 3-11. Mathieu stability diagram showing resonance ejection of spiperone at three different axial modulation frequencies: (A)  $q_{\text{eject}}=0.906$ , (B)  $q_{\text{eject}}=0.454$ , and (C)  $q_{\text{eject}}=0.0908$ . Notice that as the  $q_{\text{eject}}$  is lowered, the mass assignment for spiperone is also shifted lower.

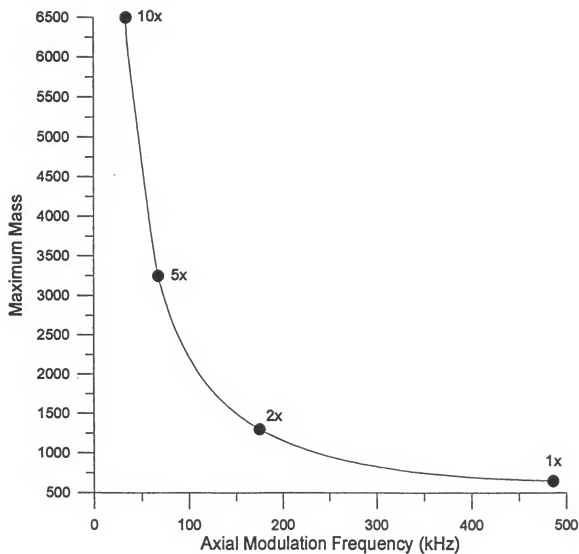


Figure 3-12. Plot of the maximum mass detectable using the mass-selective instability scan for a given axial modulation frequency.

## Coupling LDI to the Ion Trap

### MALDI Inside the Ion Trap

The early interest in coupling laser desorption ion sources to the ion trap was driven by the need for improved resolution and by the potential of sequencing high mass peptides, proteins, and oligonucleotides using the MS<sup>n</sup> capabilities of the ion trap. Laser desorption on the quadrupole ion trap was first reported by Cotter and coworkers in 1989.<sup>96</sup> In this work, the vacuum housing of a Finnigan ITD 700 was modified to allow for the insertion of a stainless steel sample probe (Figure 3-13). A flange fitted with a ZnSe lens was added to the chamber for the introduction of the desorption laser beam. Modifications were also made to the ion trap as well. Two 0.15" diameter holes were drilled in opposite sides of the ring electrode. Using this configuration, laser desorbed ions were produced inside of the ion trap volume for several biomolecules including sucrose and leucine enkephalin. Fragment spectra were also obtained by gating a beam of energetic electrons into the trap during the laser desorption event. Building on this work, Glish et al.<sup>97</sup> demonstrated MS/MS of internally generated laser desorbed ions by CID.

In 1992, Vargas<sup>98</sup> used a modified Finnigan ITMS instrument to study the phase dependency of laser desorbed ions generated inside of the ion trap. In this work, a stainless steel probe fitted with a graphite tip was positioned at the ring electrode surface. An RF phase synchronous triggering circuit was then used to trigger the desorption laser (N<sub>2</sub>, 337 nm) at phase delay increments of 20°. Using this setup, the trapping efficiency of C<sub>3</sub><sup>+</sup> graphite ions was found to follow a cyclical pattern comparable to the RF sine wave.

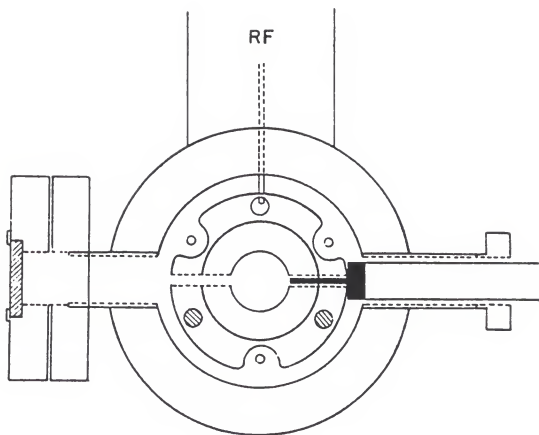


Figure 3-13. Cross section of the ring electrode showing the modifications made to perform laser desorption inside of the ion trap.<sup>96</sup>

The first report of MALDI inside of the ion trap was made by Cotter using the modified ITD instrument used for the first LDI experiments.<sup>99</sup> For MALDI, a sample mixture of matrix and analyte was deposited onto the tip of a 0.09" diameter probe and inserted into one of the holes in the ring electrode (Figure 3-14). The sample surface was positioned flush with the inner surface of the ring electrode. To prevent shorting of the ring electrode, the probe tip was connected to the grounded probe shaft through a Teflon spacer. Light from a Q-switched Nd:YAG laser (266 nm) was then focused through the second hole in the ring electrode and made to strike the sample surface using a series of externally mounted UV quartz lenses. The laser was triggered using the electron gate-pulse used in the normal operational mode of the ITD to gate electrons into the ion trap for electron ionization. A second trigger pulse, derived from the RF synchronization pulses available on the ITD RF board, was input into a delay pulse generator to allow firing of the laser at preset phase angles of the RF voltage applied to the ring electrode. Control of the system was provided by the Finnigan ITD software. Using this instrument, MALDI spectra were obtained in the extended mass range mode (resonant ejection at lower  $q_{\text{eject}}$ ) for several biomolecules including angiotensin I (M.W. 1296),  $\alpha$ -endorphin (M.W. 1746), and parathyroid hormone (M.W. 3286).

Vargas also reported MALDI inside of the ion trap for several biomolecules including the drug compound spiperone.<sup>100</sup> MALDI was performed by depositing 2.0  $\mu\text{L}$  of a 0.1  $\mu\text{g}/\mu\text{L}$  spiperone solution onto a probe tip followed by an equal volume of 100 mM nicotinic acid matrix solution. MALDI MS and MS/MS spectra were acquired for spiperone and compared with the corresponding spectra obtained by LDI. Samples of

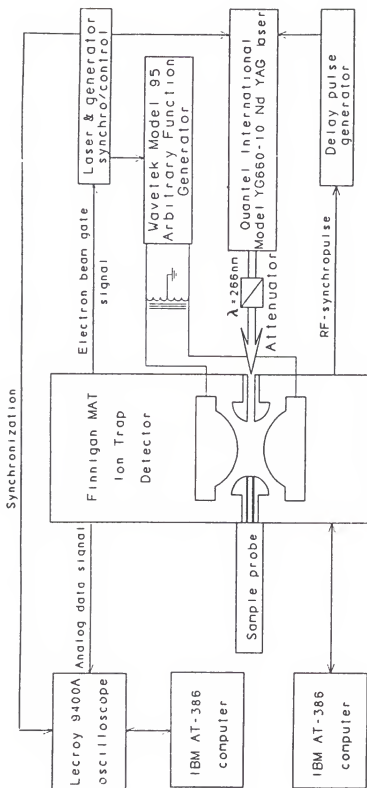


Figure 3-14. Block diagram of the ITD 700 system modified for MALDI.<sup>99</sup>

spiperone in matrigel were also analyzed by MALDI using DHB matrix with 0.1% trifluoroacetic acid (TFA).

One of the major drawbacks to performing MALDI inside of the ion trap is that there is an upper mass limit determined by the kinetic energy of the ions. Beavis and Chait<sup>101</sup> showed that for MALDI generated ions, the initial kinetic energy increases linearly with mass (Figure 3-15). Therefore for high mass MALDI ions, the initial kinetic energy of the ions becomes greater than the pseudopotential well-depth of the quadrupolar trapping field. Glish calculated a high mass limit of  $m/z$  9830 for MALDI inside of the ion trap.<sup>102</sup> Above this limit, the high kinetic energy of the ions causes them to shoot across the internal volume of the ion trap and strike the opposite side of the ring electrode without being trapped. Another problem associated with using the internal MALDI configuration is that late desorbing neutrals from the sample can undergo ion-molecule reactions with MALDI ions already stored in the ion trap.<sup>62</sup> In performing LDI/MS/MS of trimethylphenylammonium chloride, Glish et al. observed desorption of neutrals tens of milliseconds after the initial laser pulse.<sup>97</sup> Ion-molecule reactions can interfere with the MS/MS process, degrade resolution, and can complicate the resulting mass spectrum with extraneous peaks.

The most significant limitation of the internal configuration for analyzing intact biological tissues, however, is the fact that the sample is completely enclosed inside the volume of the ion trap. This is particularly important because in order to perform microscopy, the microscope objective needed to focus the laser and to view the sample under magnification must be placed close to the sample surface. For imaging drug compounds in tissue it is also important that the sample be able to move freely to allow



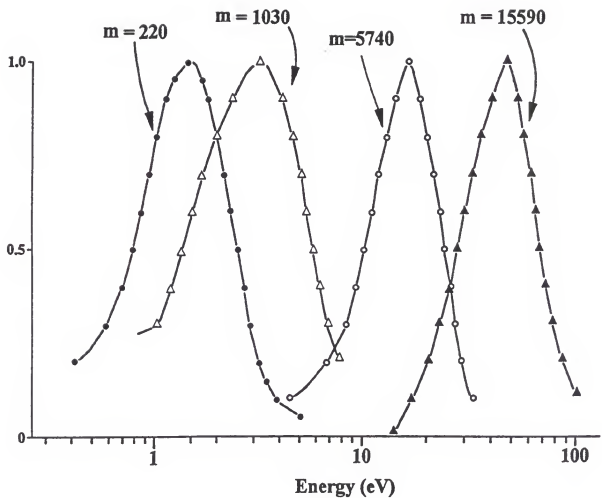


Figure 3-15. Initial translational kinetic energy distributions for a series of polypeptide ions formed by MALDI.<sup>101</sup>

specific regions of the tissue to be targeted for analysis. Neither requirement can be easily met with the sample positioned inside the ion trap volume.

### MALDI Using an External Source Configuration

The first laser desorption work utilizing an external ion source was reported by Louris and coworkers in 1990.<sup>103</sup> The setup employed a fiber optic to introduce laser light into an external ion source located just outside of the entrance endcap electrode. Metal ions were produced externally by laser desorption then injected with an Einzel lens into the ion trap where they were allowed to react with neutral benzene molecules.

Following this preliminary work, Bier et al.<sup>20</sup> at Finnigan developed the first MALDI ion trap instrument utilizing an external ion source (Figure 3-16). The instrument was constructed from an existing commercial Finnigan MAT TSQ 700 triple quadrupole mass spectrometer. The ion trap was placed in the differentially pumped analyzer region of the vacuum manifold, replacing the three sets of quadrupole rods. A 3 kV lens was positioned behind the exit endcap electrode and used to focus ions to a 20 kV conversion dynode/electron multiplier assembly. The ion source used was the standard TSQ 700 EI/CI source, modified for MALDI by drilling the aperture of the first two extraction lenses to a diameter of 0.150" to afford a wider angle of acceptance into the optical path. Two additional holes were drilled through these lenses to allow light from a nitrogen laser to be introduced into the source through a 200  $\mu\text{m}$  core fiber optic. The fiber optic was positioned so that the transmitted radiation impinged upon the sample at a 45° angle. Observation of the sample was made possible by mounting a vacuum flange fitted with a magnifying glass to the outside of the vacuum chamber just above the ion source. The

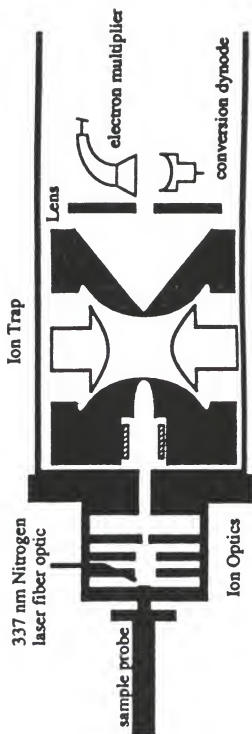


Figure 3-16. Schematic of the MALDI ion trap instrument developed by Bier et al. utilizing an external ion source configuration. The ion source was modified for MALDI from an existing Finnigan TSQ 700 EI/CI designed for GC.<sup>20</sup>

laser was triggered using the normal ionization gate trigger pulse. Additional circuitry was used to phase-lock the triggering of the laser with the RF voltage.

For MALDI, samples were deposited onto a stainless steel probe and positioned approximately 0.100" from the first extraction lens in the ion source. The sample probe was electrically isolated from the ion source block with a Vespel sleeve. Ions desorbed from the sample surface were extracted by the three-element lens system and transmitted axially into the ion trap. The lens system and ion trap were operated at relatively high voltages: -159 V, -188 V, -505 V, and -15 V respectively. A small tube lens positioned inside of the entrance endcap electrode was used to gate ions into the ion trap. The lens potential was varied between +36 V (gate closed) and -186 V (gate open). Using this design, intact  $(M+H)^+$  ions were obtained for several peptides and proteins up to  $m/z$  43,300 (egg albumin). Results of this work also showed that higher RF voltage levels were needed during ion injection to trap the higher mass MALDI ions.

Using an external source configuration similar to Bier's original design, Vargas constructed the first generation MALDI ion trap instrument at the University of Florida.<sup>62</sup> In this instrument, the ion trap was situated in the differentially pumped analyzer region of a cradle-type vacuum chamber fitted with a quartz window flange to allow for the introduction of the desorption laser beam. The EI/CI ion source used in the instrument was adapted from a Finnigan 4500 single quadrupole GC/MS instrument.

Samples for MALDI were introduced into the ion source on a stainless steel probe having a 45° angle tip. Light from a nitrogen laser (337 nm) was focused into the ion source through a 0.100" diameter hole in the side of the source block (Figure 3-17). The hole was originally installed as a GC transfer port. Using this design, Vargas obtained

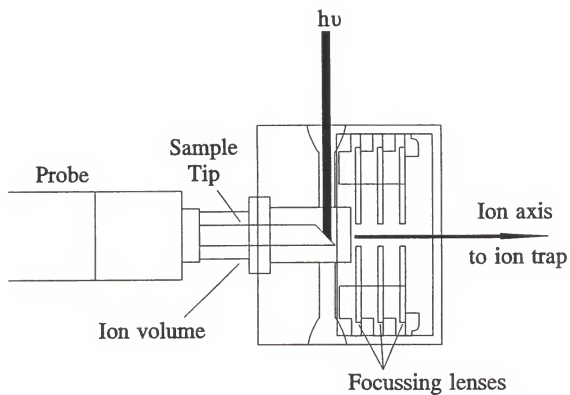


Figure 3-17. External ion source configuration used in the first generation MALDI ion trap instrument developed at the University of Florida. Samples were introduced into the ion source on a sample probe having a 45° angle tip.<sup>62</sup>

MALDI MS and MS/MS spectra for spiperone using DHB.<sup>104</sup> MALDI was also attempted for spiperone mixed with matrigel (Figure 3-18). Peaks were observed for protonated spiperone at  $m/z$  396 and for the sodium adduct at  $m/z$  418. MS/MS could not be performed for spiperone from matrigel, however, due to the low parent ion signal intensity. The poor ion signal was believed to result from having the sample situated at a 45° angle with respect to the ion source extraction lenses.

The second generation MALDI ion trap instrument constructed at the University of Florida by Booth<sup>66</sup> utilized an external ion source from a commercial Vestec MALDI-TOF instrument (Figure 3-19). The ion source incorporated three high voltage focusing lenses (rated at  $\pm 35$  kV) designed specifically for performing MALDI of high mass biomolecules. The open configuration of the lens system also allowed samples to be easily viewed through a large quartz window mounted above the source region. To maximize the ion transmission efficiency, both the ion source and ion trap were situated in the source region of the Vestec vacuum chamber. For MALDI, light from a pulsed nitrogen laser was focused through a small hole in the second focusing lens and directed onto samples deposited onto the tip of a stainless steel probe inserted into the face of the first extraction lens. Using this design, MALDI spectra were obtained for several peptides up to M.W. 2847.5 (melittin). Sequence information was also obtained for the octapeptide angiotensin II (M.W. 1046.2) by performing MS/MS with helium buffer gas.

The instrument constructed by Booth was also used to analyze tissue samples prepared for the work presented in this dissertation. Of particular note was the MS<sup>6</sup> analysis of spiperone in matrigel and the MS/MS analysis of the anticancer drug taxol (M.W. 853) from rat liver tissue.<sup>105</sup> A more detailed discussion of the pharmaceutical

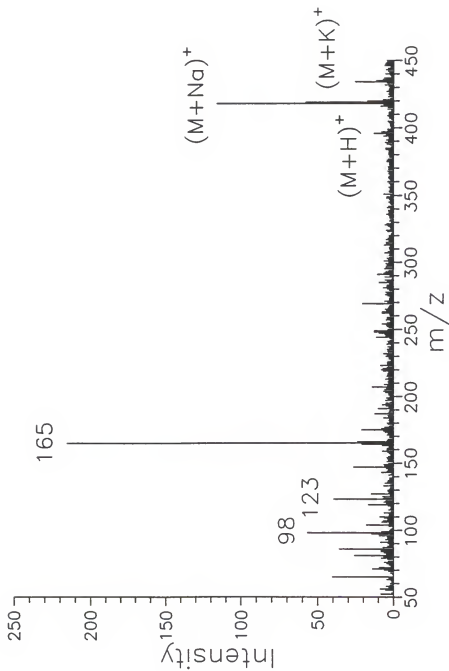


Figure 3-18. MALDI/MS spectrum of spiperone in matrigel (100 ppm) using DHB.<sup>62</sup>

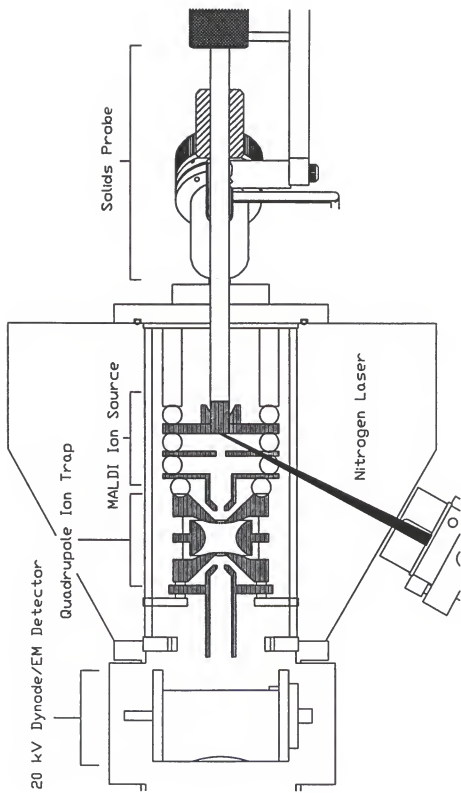


Figure 3-19. Schematic of a MALDI ion trap instrument modified from a commercial Vestec MALDI-TOF mass spectrometer.<sup>66</sup>



drug compounds studied will be given in chapter 4. Liver tissue was obtained from a male Sprague-Dawley rat and immediately frozen for storage. A thin section approximately 2.0 mg in weight was cut and incubated in a 1.0 mL solution containing 100 ng of taxol (Bristol-Myers Squibb). After a 1 hr incubation period, the section was removed from solution, washed with deionized water, and placed onto the tip of the MALDI probe. One microliter of DHB matrix solution was then pipetted on top of the dried liver section and allowed to dry and crystallize. The MALDI MS and MS/MS spectra for taxol from the incubated liver tissue is shown in Figure 3-20. With only one stage of mass spectrometry, the peaks in the spectrum corresponding to taxol were not distinguishable from the intense background signal from the liver tissue. Using the MS/MS capabilities of the ion trap, the taxol  $(M+K)^+$  ion at  $m/z$  892 was resonantly excited and fragmented (after mass isolating the region between  $m/z$  882 - 902), producing the characteristic taxol daughter ions at  $m/z$   $(509+K)^+$ ,  $(569+K)^+$ , and  $(794+K)^+$ . Comparing the MS/MS spectrum from Figure 3-20 with the daughter ion spectrum from a taxol standard, the presence of taxol in the incubated liver tissue was confirmed (Figure 3-21). The amount of taxol detected was calculated to be approximately 360 fg based on the amount of taxol absorbed during the incubation period and the amount of tissue ablated by the laser.

While the second generation MALDI instrument was capable of detecting drug compounds from tissues, the limited space in the source region made it impossible to implement a microscopy system for imaging experiments. The open configuration of the ion source lens system also ruled out the possibility of performing laser desorption/chemical ionization (LD/CI) of drug compounds in tissue.

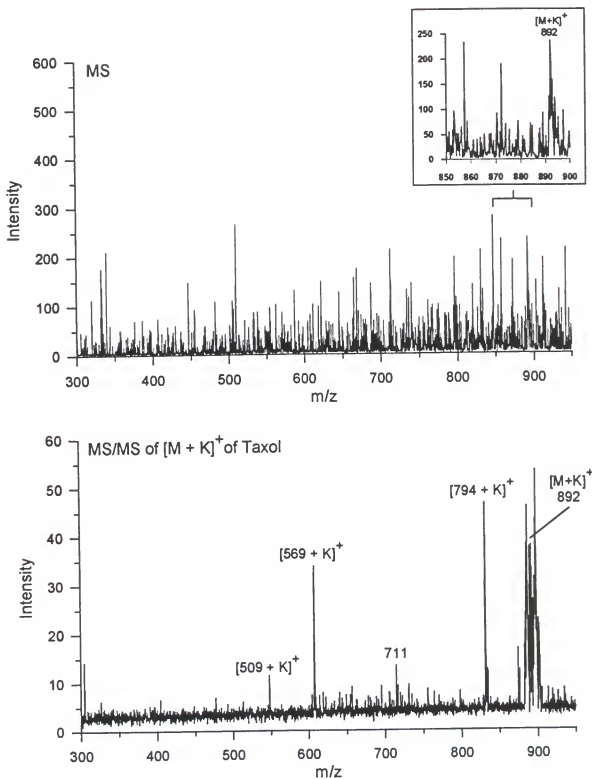


Figure 3-20. MALDI MS (top) and MS/MS (bottom) spectra for taxol from rat liver tissue incubated in a taxol solution (100 ng) for 1 hr.<sup>66</sup>

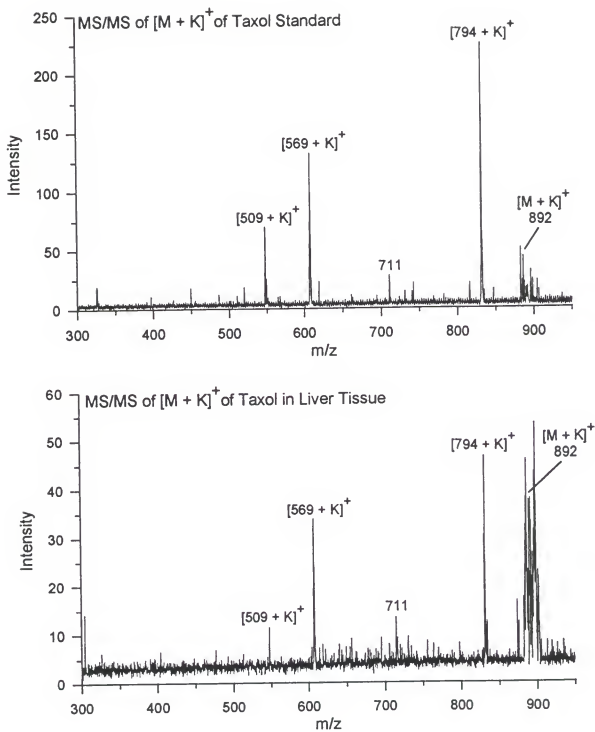


Figure 3-21. Comparison of the MALDI MS/MS spectra for a taxol standard (top) and for taxol from incubated rat liver tissue (bottom).<sup>66</sup>

### Instrument Design

In contrast to the MALDI ion trap instruments discussed so far, the instrument constructed for this work was designed specifically for the analysis of drug compounds from intact biological tissues. The instrument consisted of a Finnigan 4500 EI/CI ion source and a Finnigan ITS40 ion trap mass analyzer housed inside of a differentially pumped, cradle-type vacuum chamber (Figure 3-22). The ion source was situated 90° off-axis with respect to the ion trap to allow the desorption laser beam to be directed onto the sample surface at a 90° angle. With this configuration, either the sample probe or the laser beam can be manipulated for applications involving imaging of drug compounds in tissue. The off-axis design was also incorporated to make it easier to position a microscope objective close to the sample without interfering with the ion trap.

In order to transmit ions formed in the ion source 90° into the ion trap for mass analysis, a DC quadrupole deflector was used. The ion source and the ion trap were mounted directly to the DC quadrupole deflector assembly to increase ion transmission efficiency. After mass analysis, the ions were detected using an electron multiplier positioned behind the exit endcap electrode of the ion trap. The following sections discuss in detail the design considerations for the various parts of the instrument.

#### Vacuum Manifold and Pumping System

The vacuum manifold used to house the working components of the instrument (ion source, ion trap, DC quadrupole deflector, and detector) was obtained from Finnigan MAT (San Jose, CA). The design of the manifold was cradle-type and measured 30.0" x

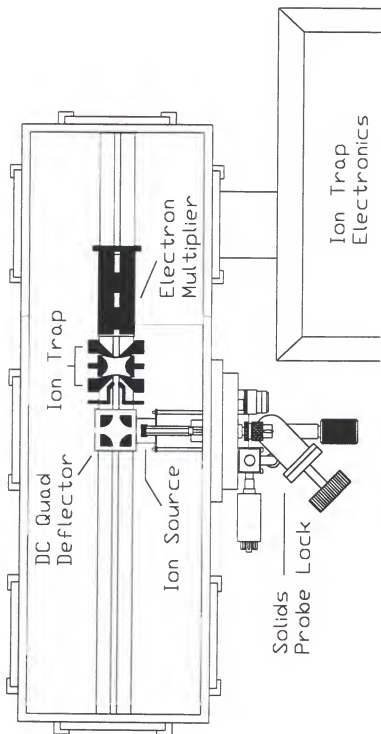


Figure 3-22. Autocad drawing of the vacuum chamber used for the laser desorption instrument showing the setup of the ion source, DC quadrupole deflector, ion trap, and detector.

10.0" x 10.0". The walls of the manifold were constructed of 0.5" stainless steel plate. Ten 4.0" diameter holes were machined in the walls and base of the manifold to serve as connection ports for the source, RF feedthrough, ion gauge, laser window, turbo pumps, and various other electrical feedthroughs. All port connections were made to fit 5.25" O-ring vacuum flanges. The top of the manifold was fitted with a 0.125" O-ring groove and sealed with two 1.0" thick glass plates. Inside of the manifold a stainless steel optical rail was positioned along the floor of the chamber to support the DC quadrupole deflector assembly and the multiplier. Aluminum brackets were also mounted to the base of the chamber to support a series of quartz heaters used to heat the vacuum chamber. The quartz heaters were powered with an external Variac power controller. To allow for differential pumping, a baffle wall was constructed out of 0.258" thick aluminum plate. The vacuum manifold was supported on a table constructed from two Finnigan 4500 frames. The original table tops were replaced with two 1.65" thick aluminum plates measuring 25.5" x 22.0". Two square slots were cut into each plate to accommodate the turbomolecular pumps.

The pumping system for the vacuum chamber consisted of a TPH 270 L/s turbomolecular pump (source region) and a TPH 330 L/s turbomolecular pump (analyzer region), both from Balzers (Hudson, NH). The turbo pumps were mounted directly to the bottom of the manifold through two 4.0" connection ports. Power was supplied independently to each of the turbo pumps by two Balzers TCP 300 turbo controllers. Both turbo pumps were backed by a single 300 L/min mechanical pump (Alcatel Corporation, Hingham, MA). The pressure in the source and analyzer regions was monitored using separate Bayard-Alpert type ion gauges (Granville-Phillips, Boulder,

CO). The ion gauge used to monitor the source pressure was connected to a Granville-Phillips model 280 gauge controller equipped with digital readout. The analyzer ion gauge was connected directly to a Finnigan 4500 vacuum control module. The vacuum controller was also used to distribute power to both turbo pumps and the mechanical pump. A vacuum protect mode was supplied with the vacuum controller which cut power to the pumping system when the base pressure of the manifold exceeded  $10^{-4}$  torr. Using this pumping system a working base pressure of  $1.2(10)^{-7}$  torr was achieved after approximately three days.

### Ion Source

The Finnigan 4500 EI/CI ion source consisted of a stainless steel source block containing three electrostatic lenses: two flat, stainless steel focusing lenses and a third exit tube lens 0.270" in length. The ion source was fitted with a removable, high pressure ion volume for performing CI. Situated normal to the lens stack was a rhenium filament and collector cup used to produce the electron beam for EI/CI. Also located in the source block were four cartridge heaters. The 4500 source was originally designed as an EI/CI source for gas chromatography. Normally, the GC transfer line was inserted into a small hole in the side of the source block. Another hole was provided just below the GC port hole to introduce a calibration gas into the source. Both port holes lead directly to the central ionization region inside of the source block. In order to perform LD/CI, the calibration gas line was replaced with a methane reagent gas line. To prevent methane from leaking out of the source, the GC port was tapped and sealed with a small flathead screw. A new calibration gas line was positioned in the source block opposite the

methane gas line. No other modifications were made to the source block in order to perform MALDI.

The source block was supported by four 4.0" rods mounted to the inside surface of a 6.0" Conflat vacuum flange (Figure 3-23). In addition to providing support for the source block, the source flange was also fitted with a solids probe lock for introducing the sample probe. The flange was equipped with feedthroughs for the lens system, filament, collector, and source heaters. Power and control of the filament and the lens voltages was provided by a Finnigan 4500 lens control module. The voltage range for each of the lenses is listed in Table 3-1. A gate circuit was used to vary the potential of the exit tube lens between +170 V (gate closed) and a typical setting of - 24 V (gate open).

One of the reasons for the poor ion transmission efficiency in the first generation MALDI ion trap instrument was the fact that the ion source block was not directly mounted to the ion trap assembly. After repeated insertion of the sample probe into the ion source, the source block eventually became misaligned with the entrance endcap electrode. To stabilize the ion source in the new instrument, a source adapter was designed and mounted directly to the two entrance rods of the DC quadrupole deflector (Figure 3-24). The adapter was machined out of high temperature Macor ceramic to electrically isolate the source from the rods of the DC deflector. The adapter was machined to lock into the end of the source block upon insertion of the source assembly into the vacuum chamber. A 0.5" hole was machined through the center of the adapter to allow the exit tube lens to pass through easily.



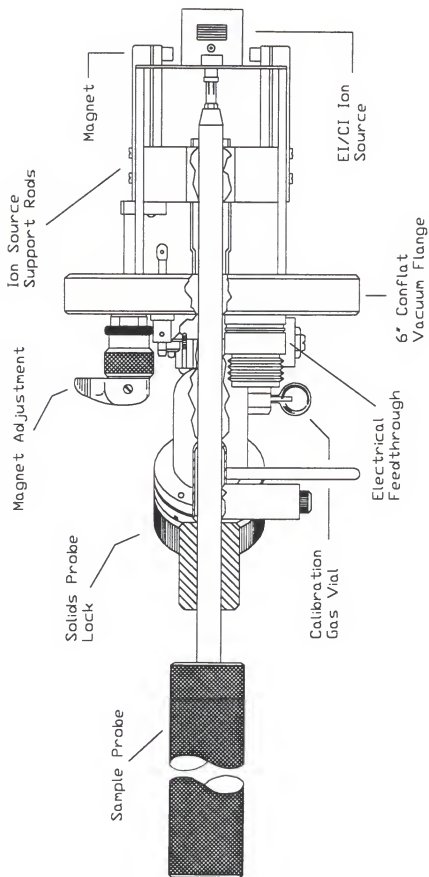
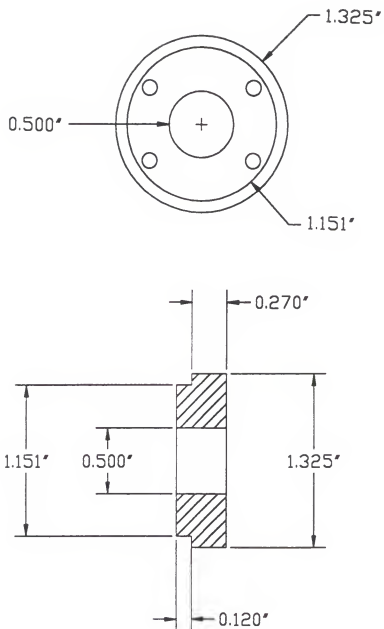


Figure 3-23. Schematic of the Finnigan 4500 ion source assembly.

Table 3-1. Ion source lens voltages supplied by the Finnigan 4500 lens control module operated in the positive ion mode.

<b>Ion Source Parameter</b>	<b>Value</b>
Extraction Lens (L1)	-1 to -45 V
Focusing Lens (L2)	-1 to -95 V
Tube Lens (Quad Entrance)	-5 to -25 V



Material: Macor Ceramic

Figure 3-24. Ceramic adapter for interfacing the ion source block to the DC quadrupole deflector assembly.

### DC Quadrupole Deflector Assembly

The use of a DC quadrupole as a 90° deflector was first described by Zeman for use with a laser-ion coaxial beam spectrometer.<sup>106</sup> In 1988, Russell et al.<sup>107</sup> reported a preliminary design for a time-of-flight Fourier transform mass spectrometer (TOF-FTMS) employing a DC quadrupole deflector for beam steering. Pedder and Yost in 1989 described the use of a DC quadrupole deflector to transmit ions formed by EI/CI into the body of a quadrupole ion trap.<sup>108</sup> For the new laser desorption instrument, the DC quadrupole deflector was chosen over other varieties of beam steering devices because it did not distort the ion beam appreciably after it had been turned 90° and because the gap between the quadrupole rods allowed the desorption laser beam to pass through easily. The DC quadrupole deflector was constructed from four quarter round, stainless steel rods of radius 0.50" and length 3.25". For added stability, the rods were bolted to the inside surface of two anodized aluminum caps. The rods were secured to the caps with Teflon screws to prevent grounding. Opposing rods were electrically connected using copper wire. A stainless steel tube lens was also mounted to the two quadrupole rods situated normal to the ion source adapter to help focus the ions into the ion trap. Special washers and sleeves were machined out of Torlon, a high temperature ceramic, to provide support and electrical isolation for the tube lens. To assure proper alignment of the tube lens with the ion trap the end of the tube lens was machined to fit inside the entrance endcap electrode of the ion trap. The ion trap was held in place using a mounting plate supported by two aluminum rods attached to the anodized aluminum mounting blocks of the DC quadrupole assembly (Figure 3-25). The entire DC quadrupole deflector assembly

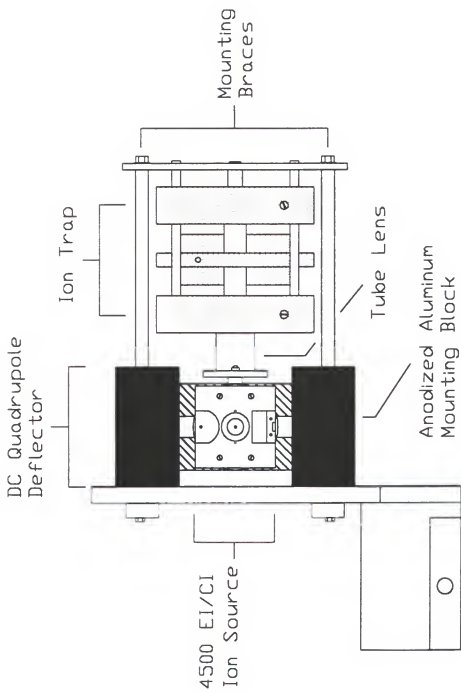


Figure 3-25. Schematic of the DC quadrupole deflector assembly. For increased ion transmission efficiency, the ion source and ion trap were mounted directly to the quadrupole rods.

including the attached ion trap was then mounted to an aluminum support plate which allowed the assembly to be vertically aligned with the ion source. Power and control of the DC quadrupole deflector assembly was provided by a Finnigan 4500 Quadrupole Electronics Module (QEM). The voltages supplied by the QEM are listed in Table 3-2.

The DC quadrupole was operated by aligning the quadrupole rods vertically and applying different combinations of voltages to the two sets of opposing rods. In this way, a quadrupolar field was defined in the x,y plane, perpendicular to the rods. Ions entering between the first two adjacent rods were turned  $90^\circ$  around one of the quadrupole rods and focused into the ion trap through the tube lens. One of the drawbacks of the DC quadrupole deflector is that there is no focusing of the ion packet in the z-direction (parallel to the rods).<sup>109</sup> To compensate for this, relatively high voltages were applied to the tube lens in order to refocus the ion beam after it had been turned  $90^\circ$ . In addition to functioning as a beam steering device, the quadrupole deflector also acts as an energy analyzer. In previous work, Pedder<sup>109</sup> showed by simulation that ions of virtually any energy could be transmitted with 60-70% efficiency by properly adjusting the voltages applied to the quadrupole rods. However, for a given set of voltages the energy window was found to be rather narrow. A full characterization of the DC quadrupole deflector has been given by Zeman and more recently by Pedder.<sup>106,109</sup>

### Laser Setup

The laser employed in the new instrument was a Laser Science Inc. (Cambridge, MA) model VSL-337ND pulsed nitrogen laser operating at a wavelength of 337.1 nm with a spectral bandwidth of 0.2 nm. The laser had a 3 ns pulse width (FWHM) with an

Table 3-2. DC quadrupole assembly voltages supplied by the Finnigan 4500 QEM.

<b>Instrument Parameter</b>	<b>Value</b>
Quad Pair 1	0 to -10 V
Quad Pair 2 (Turning Quads)	0 to -97 V
Tube Lens	0 to -130 V
Trap Offset	+30 to -30 V

average jitter of  $\pm 10$  ns, and a repetition rate  $< 20$  Hz. The laser energy was  $> 250$   $\mu\text{J}/\text{pulse}$  with a peak power of 85 kW. Pulse-to-pulse stability was given as  $\pm 4\%$  at 10 Hz repetition rate. The laser was near-diffraction limited which allowed the laser beam to be more easily focused to a small spot. The beam cross section was  $40 \text{ mm}^2$ . The laser setup is shown in Figure 3-26. The laser was placed on an aluminum table taken from the Vestec MALDI-TOF instrument and positioned parallel to the vacuum chamber. The laser table was fitted with adjustable feet to allow the height of the laser to be varied. The laser beam was deflected using a right angle prism and directed through a low distortion quart window mounted in the side of the vacuum chamber opposite the ion source. Before entering the vacuum manifold the laser beam was focused down to a spot size of approximately  $0.13 \text{ mm}^2$  (as measured on the sample surface under magnification) using a single focusing lens (Melles-Griot). The focal length of the lens was 25.4 cm. The beam intensity was adjusted between  $10^6 - 10^7 \text{ W}/\text{cm}^2$  using a wheel attenuator (Newport Corp.) situated between the laser and the prism. Alignment of the laser was accomplished by observing the fluorescence from a drop of Witeout correction fluid deposited and dried on the sample probe tip. The position of the laser spot on the sample probe was controlled manually using an x,y,z-micromanipulator attached to the prism (Newport Corp.). Rough positioning was also accomplished by simply rotating the sample probe. The laser was triggered externally using the rising edge of a TTL pulse provided by the Finnigan ITS40 electronics. A 3 ms delay was added to the laser trigger pulse using a Wavetek model 275 function generator (Indianapolis, IN). This was necessary to ensure that ions were being formed after the tube lens in the ion source had been gated open. No attempt was made to phase-lock the triggering of the laser with the main RF applied to the ring electrode.



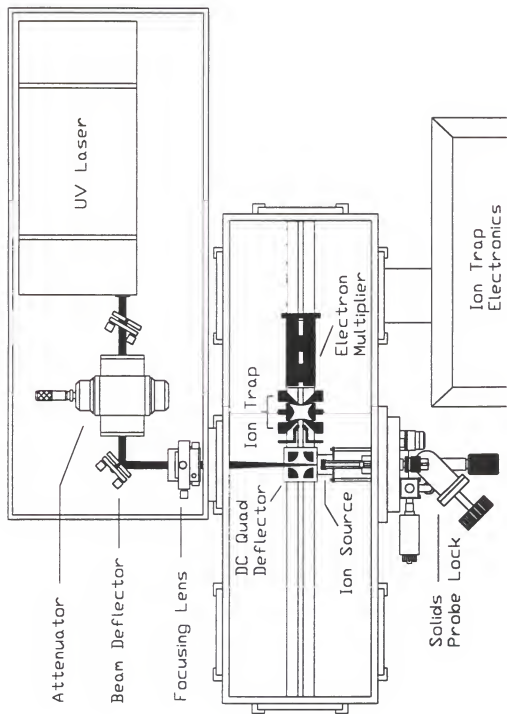


Figure 3-26. Autocad drawing of the new instrument including the laser setup.

### Software Control

The electronics used to control the operation of the ion trap were obtained from a Finnigan ITS40 GC/MS instrument. The ITS40 electronics module has a 80186 microprocessor located on the scan and acquisition (SAP) board which controls the RF amplitude and frequency and the DC voltages applied to the ring and endcap electrodes during all stages of ion trap operation (Figure 3-27). In addition, the SAP also processes data acquired from the detector and downloads it to the PC where it can be displayed as a mass spectrum. The software used to control the SAP (Gatorware) was written by Tim Griffin and Nathan Yates at the University of Florida.<sup>110,111</sup> Gatorware allows the user to control the operation of the ion trap through lists of instructions known as scan tables (Figure 3-28). Each scan table tells the SAP what voltages to apply to the ion trap for a specified amount of time. The Gatorware software also provided computer control over the auxiliary board used to set the axial modulation frequency and amplitude for performing mass range extension and CID.

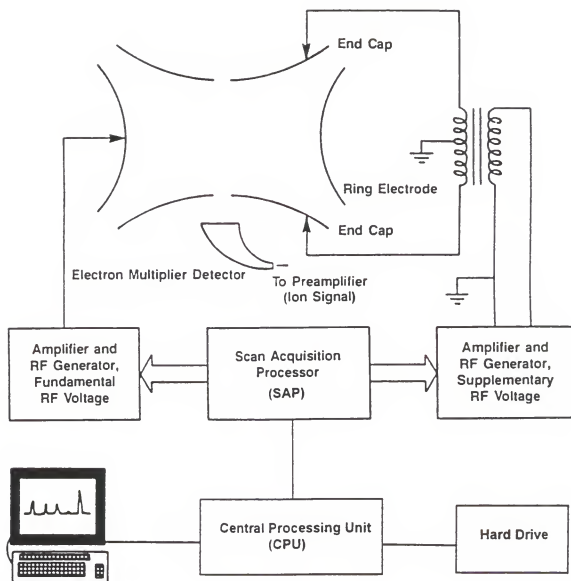


Figure 3-27. Block diagram depicting the interconnections between the ion trap, the SAP board of the ITS40 electronics module, and a personal computer.

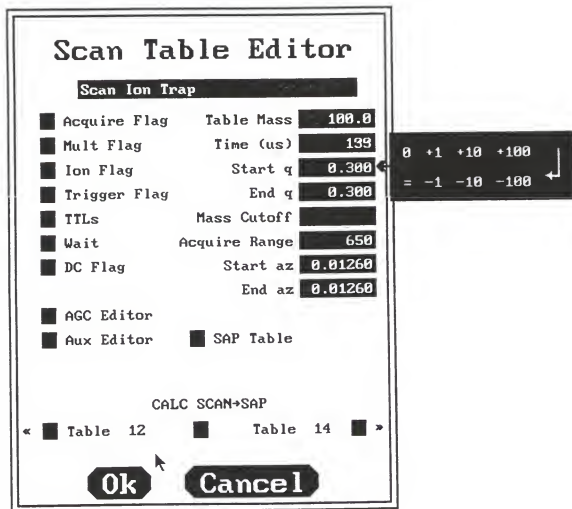


Figure 3-28. Example of a scan table provided by the Gatorware software.

## CHAPTER 4

### MALDI OF DRUG COMPOUNDS IN TISSUE USING A QUADRUPOLE ION TRAP MASS SPECTROMETER

In the final stage of this project, applications of the new laser desorption instrument were made for the analysis of three significant pharmaceutical drug compounds spiperone, taxol, and polymyxin B<sub>1</sub>. The goal of this work was to demonstrate the usefulness of MALDI coupled with the MS/MS capabilities of the ion trap for detecting trace levels of these drug compounds from complex biological tissues. This chapter begins with a brief review of the initial experiments performed to tune and calibrate the new instrument. Following this section are the experimental results for spiperone in rat cerebral tissue, taxol in mouse ovarian tumor tissue, and polymyxin B<sub>1</sub> in human plasma. Also included with the results are introductions to each of the drug compounds studied, along with a detailed description of their pharmacological use and mechanism of action. The chapter concludes with the results for the initial laser desorption/chemical ionization experiments with trimethylphenylammonium bromide.

#### Instrument Calibration & Optimization

##### EI of Perfluorotributylamine Calibration Gas

Before performing MALDI of drug compounds in tissue, the new laser desorption instrument was calibrated using perfluorotributylamine (PFTBA M.W. 670.96), a common

calibration compound used in many commercial mass spectrometers. PFTBA is particularly useful for mass calibration because it produces fragment ions spanning the normal mass range of the ion trap. The calibration gas was introduced into the ion source using the standard 4500 needle valve inlet mounted to the outside face of the ion source flange. The pressure inside the source region of the vacuum manifold was measured at  $6 \times 10^{-6}$  torr (uncorrected) using a Bayard-Alpert ion gauge. Helium buffer gas was also introduced into the analyzer region at an indicated pressure of  $8 \times 10^{-6}$  torr. EI was performed with a 70 eV electron beam from the rhenium filament situated in the ion source block. The EI spectrum obtained for PFTBA is shown in Figure 4-1. The corresponding EI scan function parameters used to acquire this spectrum are listed in Table 4-1. Mass calibration was performed using the Gatorware software. PFTBA was also used to tune the voltages for the ion source lenses, DC quadrupole rods, and the ion trap offset by observing the intensity of the fragment peaks as a function of the various voltage level settings. The optimized voltages for EI are listed in Table 4-2.

After tuning and mass calibrating the instrument with PFTBA, MALDI was attempted using a standard solution of spiperone in methanol. A small volume of the standard was mixed with a solution of DHB matrix and deposited on the tip of the sample probe. After allowing the sample to dry and crystallize, the sample probe was inserted into the vacuum manifold through the solids probe lock and positioned in front of the first extraction lens in the ion source. The EI scan function used to obtain the spectrum for PFTBA was modified for MALDI by adding six laser trigger tables (Table 4-3). A 50 ms cool table was also added after each laser trigger table to allow the laser to recharge between fires. The RF level during injection was increased to  $q = 0.400$  for a table mass

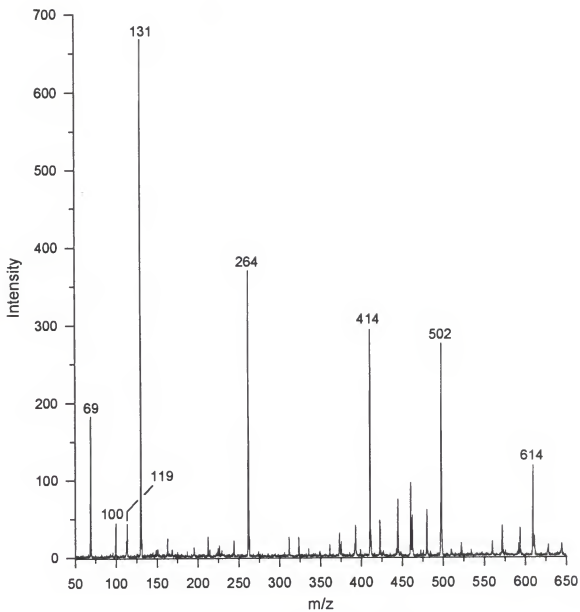


Figure 4-1. EI spectrum of perfluorotributylamine (PFTBA) calibration gas.

Table 4-1. EI scan function parameters used for the analysis of PFTBA.

#	Scan Table	Table Mass	(RF Volt.)		(DC Volt.)		(Axial Modulation)		Time (ms)
			Start q	End q	Start a*	End a	Freq. (kHz)	Amp. (V)	
1	Reset	100	0.000	0.000	0.0189	0.0189	—	—	1
2	Preionize	100	0.180	0.180	0.0189	0.0189	—	—	0.5
3	Ionize	100	0.180	0.180	0.0189	0.0189	—	—	30
4	Cool	100	0.180	0.180	0.0189	0.0189	—	—	1
5	Prescan	100	0.180	0.180	0.0189	0.0189	485	0	0.5
6	Scan	100	0.180	0.890	0.0189	0.0189	485	4	110
7	Empty Trap	100	0.000	0.000	0.0189	0.0189	—	—	1

\* corresponds to a trap offset of - 12V.



Table 4-2. Optimized instrument parameters for EI.

<b>Instrument Parameter</b>	<b>Voltage Level</b>
Extractor Lens (L1)	-11.7 V
Focusing Lens (L2)	-52.6 V
Tube Lens (Quad Entrance)	-18.2 V
Quad Pair 1	0 V
Quad Pair 2	-53 V
Tube Lens (Trap Entrance)	-64 V
Trap Offset	-12 V

Table 4-3. MALDI scan function parameters used for the analysis of spiperone.

#	<u>Scan Table</u>	Table	(RF Volt.)		(DC Volt.)		(Axial Modulation)		Time (ms)
			<u>Mass</u>	<u>Start q</u>	<u>End q</u>	<u>Start a*</u>	<u>End a</u>	<u>Freq. (kHz)</u>	
1	Reset	100	0.000	0.000	0.0042	0.0042	-	-	1
2	Preionize	100	0.400	0.400	0.0042	0.0042	-	-	0.5
3	Trig Laser 1	100	0.400	0.400	0.0042	0.0042	-	-	10
4	Cool	100	0.400	0.400	0.0042	0.0042	-	-	50
5	Trig Laser 2	100	0.400	0.400	0.0042	0.0042	-	-	10
6	Cool	100	0.400	0.400	0.0042	0.0042	-	-	50
7	Trig Laser 3	100	0.400	0.400	0.0042	0.0042	-	-	10
8	Cool	100	0.400	0.400	0.0042	0.0042	-	-	50
9	Trig Laser 4	100	0.400	0.400	0.0042	0.0042	-	-	10
10	Cool	100	0.400	0.400	0.0042	0.0042	-	-	50
11	Trig Laser 5	100	0.400	0.400	0.0042	0.0042	-	-	10
12	Cool	100	0.400	0.400	0.0042	0.0042	-	-	50
13	Trig Laser 6	100	0.400	0.400	0.0042	0.0042	-	-	10
14	Cool	100	0.400	0.360	0.0042	0.0042	-	-	50
14	Prescan	100	0.360	0.360	0.0042	0.0042	485	0	0.5
15	Scan	100	0.360	0.890	0.0042	0.0042	485	4	110
16	Empty Trap	100	0.000	0.000	0.0042	0.0042	-	-	1

\* corresponds to a trap offset of - 5V.

of 100. The voltage settings for the source lenses, the DC quadrupole deflector, and the ion trap offset were unchanged. No peaks were observed for spiperone or DHB using the optimized EI voltage settings.

#### Instrument Simulation using SIMION V6.0s

In order to tune the instrument for MALDI, a computer simulation program, SIMION V6.0s, was employed. SIMION V6.0s (Idaho National Engineering Laboratory, ID) is a C-based program designed to model electrostatic ion optics elements via 2D and 3D potential arrays. The potential arrays are sized, oriented, and positioned as instances within an ion optics workspace. Ions are then allowed to move within the workspace to determine how the fields generated by the potential arrays impact the ions' trajectories. Visualization features in SIMION V6.0s allow the user to cut into any component to more closely inspect ion trajectories and potential energy surfaces. Another important feature of SIMION V6.0s is that it allows the various potentials assigned to each array to be adjusted quickly and independently of one another.

For the simulation experiments, 2D potential arrays were generated for the ion source, the DC quadrupole deflector assembly (including the tube lens), and the entrance endcap electrode of the ion trap (Figure 4-2). The tip of the sample probe was also included for the MALDI simulations. The entire ion trap was not modeled to save memory space and to cut down on the time needed to refine the individual arrays. The grid spacing for the arrays was set to 0.1 mm/grid. In the first simulation, a packet of ten ions was started in the ion source with an initial kinetic energy of 0.05 eV (typical K.E.

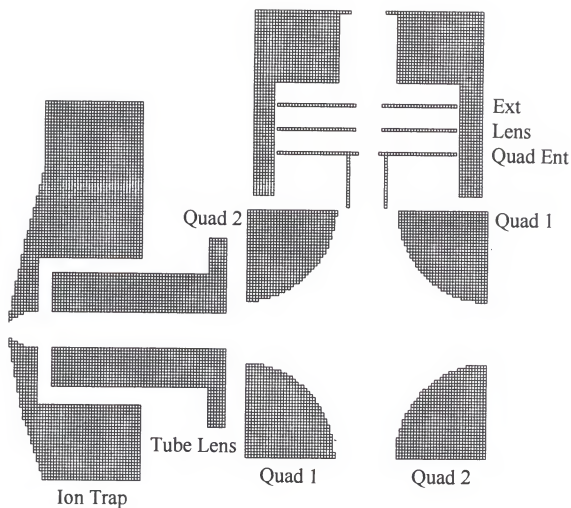
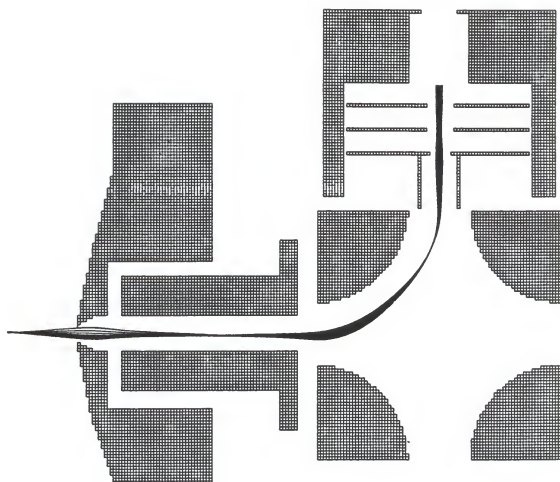


Figure 4-2. SIMION V6.0s potential arrays for the ion source lenses (Ext, Lens, Quad Ent), DC quadrupole deflector (Quad 1, Quad 2), tube lens, and the ion trap entrance endcap electrode of the new laser desorption instrument.

for EI generated ions). The  $m/z$  of the ions was set to 396 to simulate the trajectories for spiperone ions. The potentials of the various arrays were set to correspond to the experimentally optimized EI voltage settings. Using these voltages the ions were successfully focused into the DC quadrupole deflector, turned  $90^\circ$  around Quad 2, and injected through the entrance endcap aperture (Figure 4-3).

For the second simulation experiment the same potential arrays and voltage settings were used, but the initial kinetic energy of the ions was increased to 2.5 eV to simulate the trajectories for spiperone ions generated by MALDI. Beavis and Chait determined that MALDI produced ions above  $m/z$  1000 have similar velocity distributions and travel at an average velocity of 750 m/s.<sup>101</sup> Lower mass ions, however, are not cooled to the same degree in the expanded supersonic jet, and therefore travel at velocities approaching 2000 m/s. From interpolation, the velocity of spiperone ions formed by MALDI was estimated to be approximately 1150 m/s. The simulated trajectories for the MALDI-generated spiperone ions using the EI voltage settings is shown in Figure 4-4. With the higher initial kinetic energy, the ions were not sufficiently turned by the quadrupole rods and ended up hitting the tube lens before making it into the ion trap. These results explain the inability to acquire MALDI spectra for spiperone experimentally using the EI voltage settings. To compensate for the increased kinetic energy of the MALDI ions, the voltages for Quad 2 and the tube lens were increased to -68V and -81V, respectively. Using these optimized SIMION voltages, the first experimental MALDI spectrum for spiperone was obtained (Figure 4-5).

**EI**

Ion Mass: 396 Da

Kinetic Energy: 0.05 eV

Number of Ions: 10

Ext: -11.7 V

Lens: -52.6 V

Quad Ent: -18.2 V

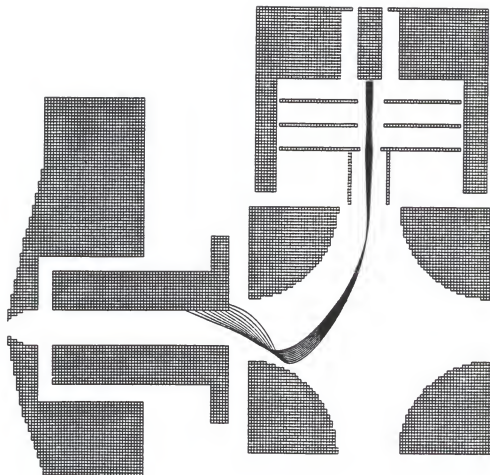
Quad 1: 0 V

Quad 2: -53 V

Tube Lens: -64 V

Trap Offset: -12 V

Figure 4-3. Simulated trajectories for EI generated spiperone ions (0.05 eV) using the experimentally optimized EI voltage settings.



MALDI

Ion Mass: 396 Da

Kinetic Energy: 2.5 eV

Number of Ions: 10

Ext: -11.7 V

Lens: -52.6 V

Quad Ent: -18.2 V

Quad 1: 0 V

Quad 2: -53 V

Tube Lens: -64 V

Trap Offset: -12 V

Figure 4-4. Simulated trajectories for MALDI generated spiperone ions (2.5 eV) using the experimentally optimized EI voltage settings.

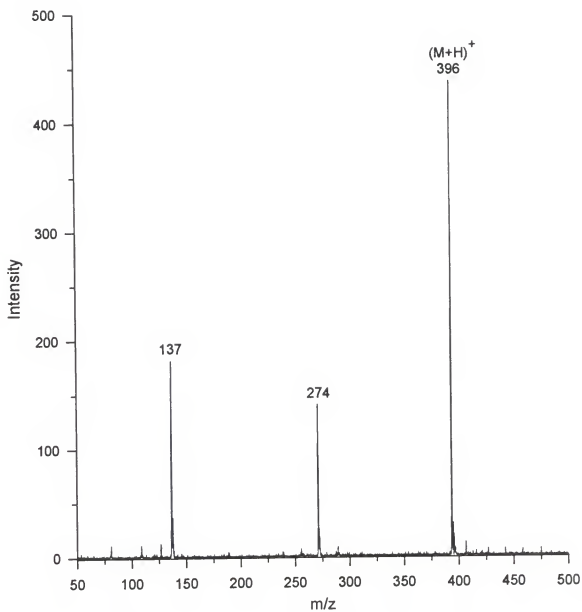


Figure 4-5. MALDI MS spectrum of spiperone (M.W. 395) using DHB matrix.



The dependence of the voltage settings for the quadrupole rods and the tube lens on the initial kinetic energy of the ions was further investigated by simulating the trajectories for ions of increasing  $m/z$  up to  $m/z$  3000 (10 eV). Although the average velocity of MALDI ions above  $m/z$  1000 remains constant at 750 m/s, their kinetic energy increases linearly with mass.<sup>101</sup> From the simulations, it was found that as the kinetic energy of the ions increased, higher voltages were required on Quad 2 and the tube lens to turn and focus the ions into the ion trap. For ions above  $m/z$  1000, a small positive potential (2 - 5V) was also needed on Quad 1.

#### High Mass Calibration using a Peptide Mixture

Normally, the ion trap is calibrated using the Gatorware software at a resonant ejection frequency of 485 kHz ( $q_{\text{eject}} = 0.906$ ). For all of the high mass experiments ( $>m/z$  650) presented in this chapter, the resonant ejection frequency was set to 130 kHz. As discussed previously in chapter 3, one of the consequences of extending the mass range by using lower resonant ejection frequencies is that the ions are ejected at lower RF voltages. Because the Gatorware software sets the mass calibration curve according to a  $q_{\text{eject}} = 0.906$ , the assigned masses for ions using the lower resonant ejection frequency were significantly lower. To calibrate the instrument for the extended mass range ( $\sim 2000$  Da), MALDI was performed using a mixture of three peptide standards: methionine-arginine-phenylalanine-alanine (MRFA M.W. 523.6), methionine enkephalin-arginine-glycine-leucine (M.W. 900.4), and angiotensin II (M.W. 1046.2). Working standards for these peptides were prepared at  $2 \times 10^{-5}$  M in deionized water. Equal amounts (50  $\mu\text{L}$ ) of each standard solution was then mixed in a 0.5 mL vial. For MALDI, 10  $\mu\text{L}$  of the peptide

mixture was mixed with an equal volume of a 0.5 M DHB matrix solution prepared in 50% acetonitrile/50% water. One microliter of the mixture was deposited on the tip of the sample probe. Using the optimized SIMION voltages and the MALDI scan function parameters for spiperone (using an axial modulation frequency of 130 kHz), the MALDI spectrum shown in Figure 4-6 was obtained. Slightly higher voltages were needed on Quad 2 and the tube lens to obtain a satisfactory signal for the higher mass angiotensin II ions. The major peaks in the spectrum at  $m/z$  525, 901, and 1047, corresponded to the  $(M+H)^+$  ions for MRFA, methionine enkephalin-arginine-glycine-leucine, and angiotensin II, respectively. Significant sodium adduct peaks were also observed for MRFA ( $m/z$  547) and angiotensin II ( $m/z$  1069). The low intensity peaks below  $m/z$  300 corresponded to ions from the DHB matrix. The calibration curve for the extended mass range ( $y = 2.63944x + 1.89841$ , where  $y$  = corrected  $m/z$  and  $x$  =  $m/z$  at 485 kHz) was generated by plotting the actual mass of the ions versus the observed mass assigned by the Gatorware software.

#### Analysis of Spiperone from Rat Cerebral Tissue

Spiperone was developed by Bristol-Myers Squibb as an antipsychotic drug for the treatment of various neurological diseases including schizophrenia. Currently, schizophrenia affects 1 in every 100 people worldwide between the ages of 16 and 30.<sup>112</sup> Schizophrenia is caused by an imbalance in the levels of neurotransmitters, the substances that allow communication between nerve cells, in the brain.<sup>113</sup> The symptoms associated with schizophrenia are varied, but generally include severe thought and speech disturbances, hallucinations, delusions, anxiety, and uncontrollable behavior.

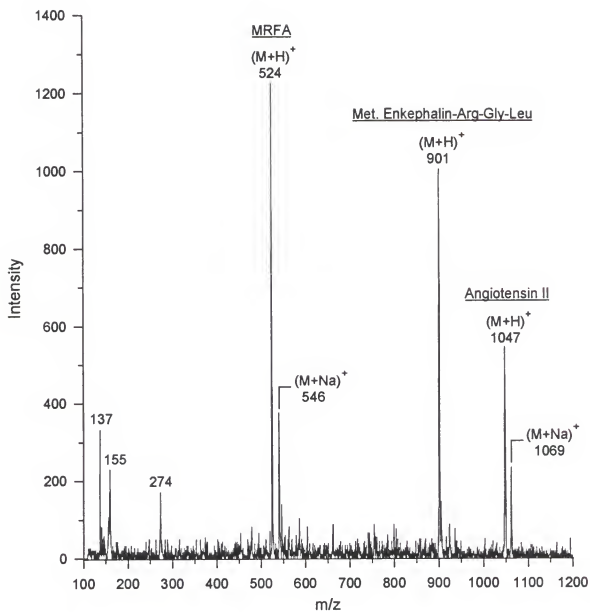


Figure 4-6. MALDI MS spectrum of a peptide mixture of MRFA (M.W. 523.6), methionine enkephalin-arginine-glycine-leucine (M.W. 900.4), and angiotensin II (M.W. 1046.2).

Of particular importance in neurological disorders such as schizophrenia is the role of the neurotransmitter serotonin (5-hydroxytryptamine). Serotonin, or 5-HT, is synthesized in brain neurons from the amino acid tryptophan and is stored in vesicles in the synaptic terminal.<sup>63</sup> Upon a nerve impulse, serotonin is released into the synaptic cleft and binds to specific receptor sites on the adjacent neuron. Current research has identified at least four populations of receptors for serotonin, 5-HT<sub>1</sub>, 5-HT<sub>2</sub>, 5-HT<sub>3</sub>, and 5-HT<sub>4</sub>, each having various subtypes.<sup>114</sup> The 5-HT<sub>1A</sub> receptors are located primarily in the central nervous system and are associated with depression, anxiety, and other psychiatric disorders. The onset of severe depression occurs when the neural pathways in the brain are understimulated due to the lack of serotonin release into the synaptic junction. Conversely, when the release of serotonin is too great, the synaptic junction becomes flooded, causing overstimulation of the neurons. People with schizophrenia show unusually high levels of activity in specific regions of the brain during hallucinations and periods of anxiety.<sup>113</sup> The actions of serotonin can be modulated by drugs that either block its storage, stimulate or inhibit its release, or mimic or inhibit its action at various postsynaptic receptors.

Sipiperone belongs to a class of compounds known as azipirones which are similar in structure to serotonin. These compounds bind to 5-HT<sub>1A</sub> receptors in the central nervous system and inhibit the firing of the 5-HT neurons.<sup>115</sup> In this way, the number of sympathetic nerve discharges (SNDs) is reduced. The problem with sipiperone as an antipsychotic drug, however, is that it does not selectively bind to 5-HT<sub>1A</sub> receptors. Instead, sipiperone also has high affinity for 5-HT<sub>2</sub> and dopamine D<sub>2</sub> receptors which can stimulate SNDs.<sup>115</sup> Because these receptors are present at different densities throughout

the brain, there is great interest in studying the selectivity of spiperone by determining its concentration in various cerebral regions. As a first step towards potentially mapping spiperone and other psychotropic drug compounds in the brain, experiments were performed on rat cerebral tissue incubated in spiperone.

#### MALDI MS and MS/MS of Standard Spiperone

In order to confirm the presence of spiperone from rat cerebral tissue, reference MS and MS/MS spectra were first obtained for a spiperone standard. A stock solution of spiperone was prepared by dissolving 0.01 g of the solid material in 25 mL of methanol. A 1:10 dilution of this stock solution was used to make the final  $10^{-4}$  M standard solution. One microliter of the standard solution was mixed with 1.0  $\mu\text{L}$  of DHB matrix solution (0.1 M) on the tip of the sample probe to give a molar ratio of 1:1,000. The MALDI spectrum acquired for spiperone was dominated primarily by the  $(\text{M}+\text{H})^+$  peak at  $m/z$  396 and lower  $m/z$  ions corresponding to the DHB matrix.

After obtaining a steady signal for spiperone, MS/MS was performed by first isolating the  $(\text{M}+\text{H})^+$  ion using the forward-and-reverse scan method. After isolation, the  $(\text{M}+\text{H})^+$  ion was resonantly excited and fragmented by CID (115 kHz, 8 V, 20 ms) using a constant indicated pressure of helium buffer gas in the analyzer region of  $1 \times 10^{-5}$  torr. The MS/MS spectrum for spiperone, including the proposed fragmentation pathways is shown in Figure 4-7. The major daughter ions observed for spiperone were  $m/z$  290,  $m/z$  265,  $m/z$  230, and  $m/z$  165. The MALDI MS/MS scan function parameters are listed in Table 4-4.

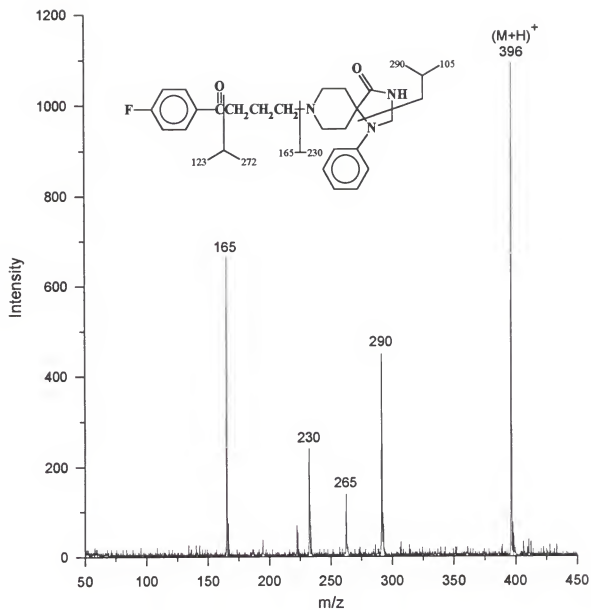


Figure 4-7. MALDI MS/MS spectrum of a spiperone standard.

Table 4-4. MALDI MS/MS scan function parameters used for the analysis of spiperone.

#	Scan Table	Table	(Axial Modulation)							Time (ms)
			Mass	(RF Start q	(RF End q	(DC Start a	(DC End a	Freq. (kHz)	Amp. (V)	
1	Reset	100	0.000	0.000	0.0042	0.0042	—	—	1	
2	Preionize	100	0.400	0.400	0.0042	0.0042	—	—	0.5	
3	Trig Laser 1	100	0.400	0.400	0.0042	0.0042	—	—	10	
4	Cool	100	0.400	0.400	0.0042	0.0042	—	—	50	
5	Trig Laser 2	100	0.400	0.400	0.0042	0.0042	—	—	10	
6	Cool	100	0.400	0.400	0.0042	0.0042	—	—	50	
7	Trig Laser 3	100	0.400	0.400	0.0042	0.0042	—	—	10	
8	Cool	100	0.400	0.400	0.0042	0.0042	—	—	50	
9	Trig Laser 4	100	0.400	0.400	0.0042	0.0042	—	—	10	
10	Cool	100	0.400	0.400	0.0042	0.0042	—	—	50	
11	Trig Laser 5	100	0.400	0.400	0.0042	0.0042	—	—	10	
12	Cool	100	0.400	0.400	0.0042	0.0042	—	—	50	
13	Trig Laser 6	100	0.400	0.400	0.0042	0.0042	—	—	10	
14	Cool	100	0.400	0.400	0.0042	0.0042	—	—	50	
15	Eject Low Masses	396	0.101	0.860	-0.017	-0.017	485	5	0.5	
16	Eject High Masses	396	0.860	0.310	-0.017	-0.017	115	5	0.5	
17	Cool	396	0.310	0.300	-0.017	-0.017	—	—	1	
18	CID	396	0.300	0.300	-0.017	-0.017	115	8	20	
19	Cool	396	0.300	0.091	-0.017	-0.017	—	—	1	
20	Prescan	100	0.360	0.360	0.0042	0.0042	485	0	0.5	
21	Scan	100	0.360	0.890	0.0042	0.0042	485	4	110	
22	Empty Trap	100	0.000	0.000	0.0042	0.0042	—	—	1	

### Preparation of the Cerebral Tissue

For the tissue experiments with spiperone, whole brain was obtained from a male Sprague-Dawley rat immediately after the animal was sacrificed. The brain was washed with several aliquots of HEPES buffer solution and frozen ( $-20^{\circ}\text{C}$ ) for storage in a small plastic container. While the brain was still frozen, it was sectioned into two halves between the right and left parietal lobes. A thin slice approximately 0.5 mm thick was cut from the inner portion of the left cerebral hemisphere using a disposable scalpel. The section was cut to include portions of the cerebral cortex, hippocampus, corpus callosum, occipital cortex, and cerebellum. Before incubation, the tissue was trimmed to fit the diameter of the sample probe tip (5.0 mm) and weighed on a sheet of weighing paper. The weight of the tissue section was measured to be 2.0 mg. After weighing, the cerebral tissue was transferred to a small glass vial containing 1.0 mL of a  $10^{-4}$  M solution of spiperone in methanol. After an incubation period of 1 hr. the section was removed from the vial, taking special care not to fold or tear the tissue. The tissue was gently shaken then washed with several drops of water to remove any excess spiperone solution remaining on the tissue surface. The weight of the tissue after incubation was 9.2 mg. Under microscopic observation the tissue appeared swollen with narrow, evenly spaced ridges on the surface. No differentiation between the various regions of the brain was noted.



### MALDI Analysis of Cerebral Tissue

For MALDI, the tissue section was first positioned on the tip of the stainless steel sample probe then flattened using the end of a spatula. 1 - 2  $\mu\text{L}$  of 0.1 M DHB matrix solution was then pipetted onto the surface of the tissue and allowed to soak for several minutes. After approximately 10 minutes the matrix solution had completely dried and crystallized, covering the entire surface of the tissue. The addition of the DHB matrix was also found to help adhere the tissue to the sample probe. For analysis, the sample probe was inserted into the ion source and the laser was fired at various positions on the sample.

In contrast to the earlier experiments with spiperone in matrigel, the shot-to-shot reproducibility of the ion signal from the cerebral tissue was rather poor. This was caused by the formation of several pockets in the tissue surface upon further drying of the sample in the vacuum chamber. Once a satisfactory signal was obtained for spiperone; MS/MS was performed using the same scan function parameters used for the spiperone standard. The MALDI MS/MS spectrum for spiperone from the rat cerebral tissue is compared with the MS/MS spectrum for the spiperone standard in Figure 4-8. The spectrum was acquired from the sum of eighteen laser shots at a single spot on the cerebral tissue. After analysis, the tissue sample was observed under the microscope. Several small laser holes were observed in the tissue in addition to the pockets mentioned earlier. However, the exact location of the laser spot corresponding to the MS/MS spectrum shown in Figure 4-8 could not be determined. Based on the thickness of the tissue section (0.5 mm), the volume of tissue sampled by the laser ( $8.5 \times 10^{-3} \text{ mm}^3$ ), and the calculated amount of

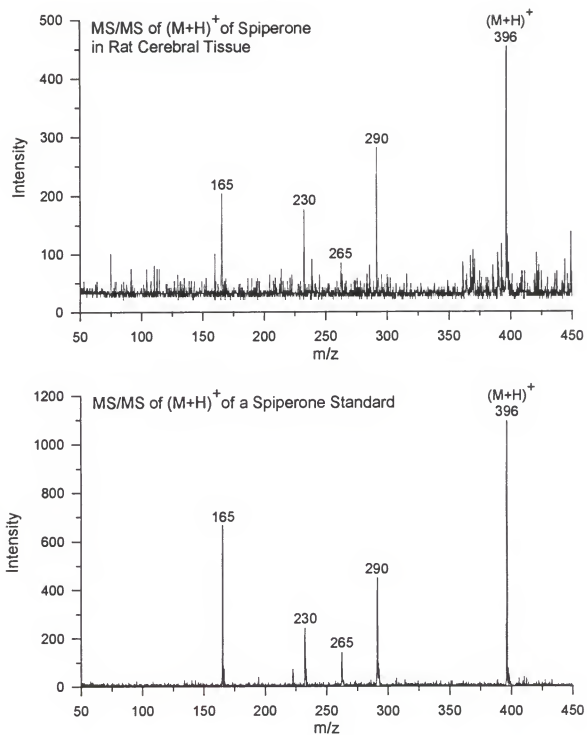


Figure 4-8 Comparison of the MALDI MS/MS spectrum for spiperone from rat cerebral tissue (top), with the corresponding spectrum for a spiperone standard (bottom).

spiperone solution absorbed by the tissue after incubation (7.2 mg); the amount of spiperone sampled was determined to be approximately 311 pg.

#### Analysis of Taxol from Mouse Ovarian Tumor Tissue

The second drug compound studied was the anticancer agent taxol. Taxol is the trade name for paclitaxel, a member of the Taxus alkaloid family of natural products found in the bark of the Pacific yew tree.<sup>116</sup> Since its approval by the U.S. Food and Drug Administration in 1992, taxol has been shown in clinical trials to be an effective treatment for a number of cancers including breast, lung, and especially ovarian.<sup>117</sup> In fact in a recent study, women suffering from advanced ovarian cancer who were given taxol in combination with other anticancer medications lived an average of fourteen months longer than patients who received other therapies.<sup>118</sup> Currently, researchers are pursuing the challenge of creating whole families of synthetic taxol analogues which exhibit even better therapeutic properties and can be used to treat a wider range of cancers.<sup>119</sup> Because of its early success and future potential, taxol is considered one of the most promising treatments for cancer.

The mechanism of how taxol functions in the human body was uncovered by Horwitz and Schiff in 1978.<sup>120</sup> In their research, they found that taxol binds to tubulin, a protein used to make structures in the cell known as microtubules. Microtubules serve as part of the cell's internal skeleton and also play a crucial role in a number of vital functions including cell division (mitosis). For a cell to divide, the microtubule skeleton must first disassemble, then reform into spindle fibers which help to line up and separate the duplicate sets of chromosomes. Once the DNA material is separated, the microtubules

must disassemble once more and reform into the skeletal systems for the two new cells. The more traditional anticancer drugs such as vinca alkaloids and colchicine work by tearing apart a spindle's microtubules so that the cancer cell cannot divide.<sup>121</sup> When taxol attaches to tubulin, however, the protein loses its flexibility and the microtubules become extremely stable and static. In this way, the microtubules can no longer disassemble and the cancer cell is destroyed as it divides.<sup>120</sup> Because cancer cells divide more frequently than healthy cells, taxol primarily attacks tumors which exhibit runaway cell division.

While the mechanism for taxol at the cellular level is well understood, there is still a great deal of interest in how taxol actually reaches the cancer site and attacks the tumor as a whole. One of the leading theories suggests that taxol concentrates in the vascular network surrounding the tumor and attacks the outer shell of the tumor first.<sup>122</sup> As the tumor recedes, the vascular region also contracts allowing taxol to attack the next layer of the tumor. This process is repeated until the tumor is destroyed. Other theories propose a combination of processes in which taxol attacks the tumor from the outer and inner regions simultaneously.<sup>122</sup> In an attempt to investigate these processes, MALDI was performed on samples of ovarian tumor tissue from mice treated with taxol. The goals of this experiment were twofold: first, to see if MALDI could be used to detect trace levels of taxol from the complicated tumor tissue, and second to see if there was a preferential location of taxol in the tumor.

#### MALDI MS and MS/MS of Standard Taxol

Pure taxol (M.W. 853) was obtained from Bristol-Myers Squibb. A standard  $10^{-4}$  M solution was prepared by dissolving 0.01 g of the material in 25 mL of methanol then

making a 2.5:10 dilution. For MALDI, 1.0  $\mu\text{L}$  of the standard solution was deposited onto the sample probe and mixed with an equal volume of DHB matrix solution. After drying, the sample was inserted into the ion source and the laser was fired at several places on the sample until a satisfactory spectrum was obtained. Because the molecular weight of taxol is greater than 650 Da, the mass range of the ion trap was extended by resonantly ejecting the ions at a frequency of 130 kHz ( $q_{\text{eject}} = 0.295$ ). The MALDI MS spectrum acquired for taxol after thirty laser shots is shown in Figure 4-9. Although the laser power was adjusted to just above the threshold irradiance level, fragment ions were still observed in the spectrum. This type of fragmentation is common with large, thermally labile biomolecules, and generally results from metastable decay or collisions with the helium buffer gas upon injection into the ion trap.<sup>20</sup> To perform MS/MS on taxol, the  $(\text{M}+\text{H})^+$  ion at  $m/z$  854 was isolated using the forward-and-reverse scan method, then fragmented by CID at  $q = 0.300$  using an axial modulation frequency of 115 kHz. The scan function parameters used to obtain the MALDI MS/MS spectrum for taxol are listed in Table 4-5. As can be seen in the MS/MS spectrum shown in Figure 4-10, abundant daughter ions were produced from cleavage of the central ester linkage followed by successive losses of acetic acid and benzoic acid groups.

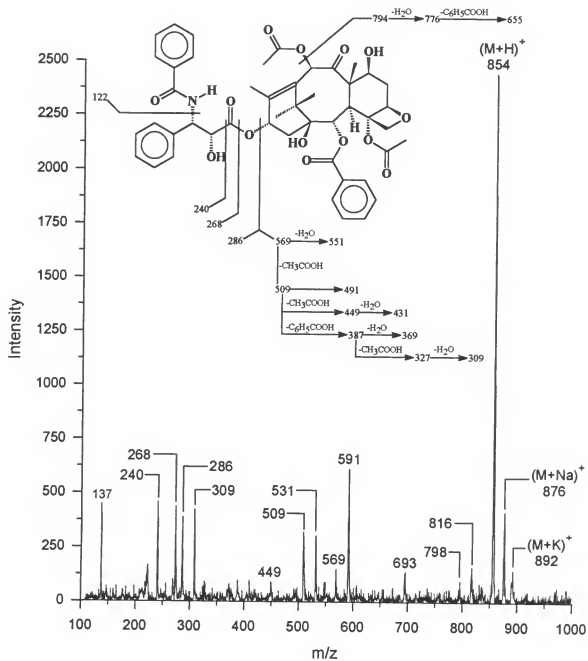


Figure 4-9. MALDI MS spectrum of taxol (M.W. 853) using DHB matrix.

Table 4-5. MALDI MS/MS scan function parameters used for the analysis of taxol.

#	Scan Table	Table	(Axial Modulation)							Time (ms)
			(RF Start q)	(RF End q)	(DC Start a)	(DC End a)	Freq. (kHz)	Amp. (V)		
1	Reset	100	0.000	0.000	0.0042	0.0042	—	—	1	
2	Preionize	100	0.400	0.400	0.0042	0.0042	—	—	0.5	
3	Trig Laser 1	100	0.400	0.400	0.0042	0.0042	—	—	10	
4	Cool	100	0.400	0.400	0.0042	0.0042	—	—	50	
5	Trig Laser 2	100	0.400	0.400	0.0042	0.0042	—	—	10	
6	Cool	100	0.400	0.400	0.0042	0.0042	—	—	50	
7	Trig Laser 3	100	0.400	0.400	0.0042	0.0042	—	—	10	
8	Cool	100	0.400	0.400	0.0042	0.0042	—	—	50	
9	Trig Laser 4	100	0.400	0.400	0.0042	0.0042	—	—	10	
10	Cool	100	0.400	0.400	0.0042	0.0042	—	—	50	
11	Trig Laser 5	100	0.400	0.400	0.0042	0.0042	—	—	10	
12	Cool	100	0.400	0.400	0.0042	0.0042	—	—	50	
13	Trig Laser 6	100	0.400	0.400	0.0042	0.0042	—	—	10	
14	Cool	100	0.400	0.400	0.0042	0.0042	—	—	50	
15	Eject Low Masses	332*	0.101	0.860	-.0014	-.0014	485	5	0.5	
16	Eject High Masses	332	0.860	0.310	-.0014	-.0014	115	5	0.5	
17	Cool	332	0.310	0.300	-.0014	-.0014	—	—	1	
18	CID	332	0.300	0.300	-.0014	-.0014	115	10	10	
19	Cool	332	0.300	0.091	-.0014	-.0014	—	—	1	
20	Prescan	100	0.360	0.360	0.0042	0.0042	130	0	0.5	
21	Scan	100	0.360	0.890	0.0042	0.0042	130	8	110	
22	Empty Trap	100	0.000	0.000	0.0042	0.0042	—	—	1	

\* uncalibrated mass for taxol displayed on the monitor

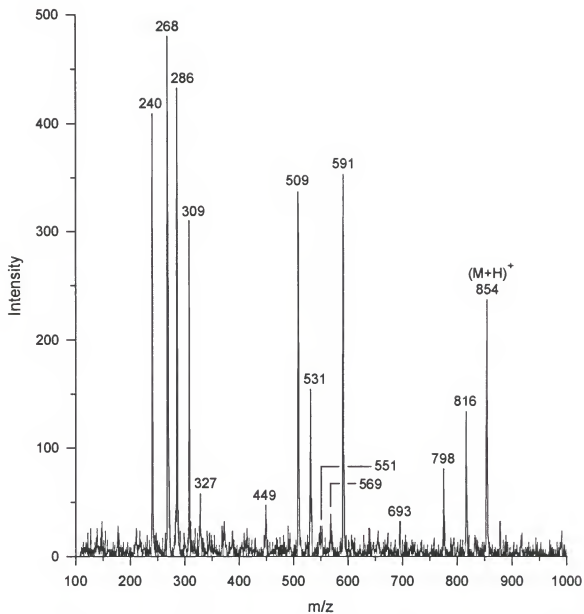


Figure 4-10. MALDI MS/MS spectrum of a taxol standard after mass isolation and CID of the  $(M+H)^+$  ion at  $m/z$  854.



### Preparation of the Ovarian Tumor Tissue

Three ovarian tumors approximately 10 mm in diameter were obtained from the Bristol-Myers Squibb Oncology Division (Princeton, NJ). The tumors were human in origin, but had been implanted subcutaneously as fragments into immunodeficient, nude mice. Taxol was dissolved in a vehicle consisting of 10% cremphor, 10% ethanol, and 80% saline and administered to the mice intravenously. After approximately 1 hr. the animals were sacrificed and the tumors were surgically excised using standard procedures. Each of the tumors was then snap frozen, placed in a small plastic vial, and packed on dry ice for shipment. Upon receipt at the University of Florida, the tumors were placed in cold storage at  $-70^{\circ}$  C. The concentration of taxol in the tumors was reported to be 10 - 50  $\mu\text{g/g}$  of tumor.

In preparation for analysis one of the frozen tumors was cut in half, then sectioned into thin slices approximately 0.5 mm thick using a disposable scalpel. Special care was taken to ensure that both the inner and outer regions of the tumor were sampled in each slice. Under microscopic observation, a reddish vascular region could be seen surrounding the more whitish interior of the tumor. In contrast to the rat cerebral tissue studied in the first application experiment, the surface of the tumor tissue was relatively smooth.

### MALDI Analysis of Ovarian Tumor Tissue

For the MALDI experiment, a thin section of tissue was cut down the center of the tumor and placed onto the surface of the sample probe. The weight of the section was

previously measured to be 6.5 mg. After positioning the tissue on the probe tip, 5.0  $\mu\text{L}$  of a 0.1 M DHB matrix solution in methanol was deposited dropwise onto the surface of the tissue using an Eppendorf pipette. In our previous experiments with the rat cerebral tissue, the matrix solution remained on the surface of the tissue for several minutes before crystallizing. This was most likely due to the fact that the tissue had become saturated during the incubation period. With the ovarian tumor, however, the majority of the matrix solution was absorbed directly into the tissue. The sample was allowed to dry and crystallize at room temperature. Observation of the sample under the microscope revealed that matrix crystals had formed inside of the tissue as well as on the tissue surface. No pockets or other inhomogenities in the tissue surface were noted.

The top spectrum in Figure 4-11 shows the MALDI MS spectrum obtained for taxol after isolating a 50 Da window around the  $(\text{M}+\text{H})^+$  ion at  $m/z$  854 using the forward-and-reverse scan method. Using the instrumental and scan function variables for the taxol standard, the isolated  $(\text{M}+\text{H})^+$  was resonantly excited and fragmented producing the MS/MS spectrum shown at the bottom of Figure 4-11. Because of the relatively wide isolation window used, the  $(\text{M}+\text{Na})^+$  peak at  $m/z$  876 was present in both the MS and MS/MS spectra. Each spectrum was acquired after thirty laser shots at an irradiance of approximately  $10^7$   $\text{W}/\text{cm}^2$ . Comparison of the taxol daughter ion spectrum from the ovarian tumor with the corresponding spectrum from the taxol standard showed good agreement (Figure 4-12). After analysis, the tissue was removed from the ion source and observed under the microscope. Inspection of the sample revealed that the laser had burned completely through the tissue in several spots. The holes formed by the laser were measured to be approximately 0.1 mm in diameter. Based on the thickness of the section

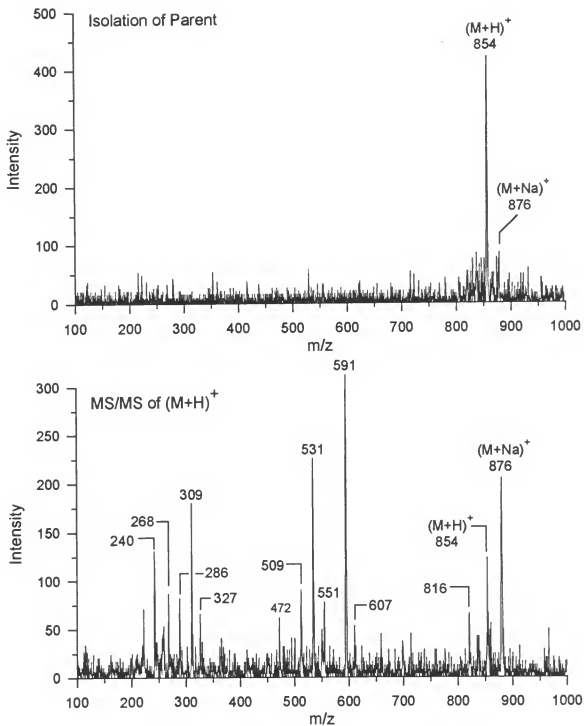


Figure 4-11. MALDI MS (top) and MS/MS (bottom) spectra for taxol from a thin section of ovarian tumor tissue obtained from a mouse treated with taxol intravenously.

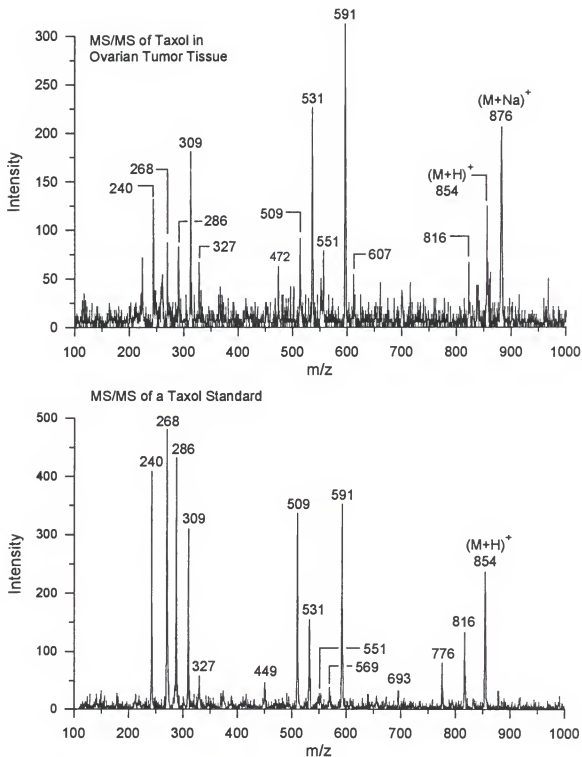


Figure 4-12. Comparison of the MALDI MS/MS spectrum for taxol in ovarian tumor tissue (top) with the corresponding spectrum for a taxol standard (bottom).

(0.5 mm) the amount of tissue sampled was determined to be approximately 0.09%. Assuming the maximum loading of the original tumor (50  $\mu\text{g/g}$ ), the spectra shown in Figure 4-11 correspond to approximately 280 pg of taxol.

As was the case in the previous experiment with the cerebral tissue, the thick layer of matrix crystals on top of the tissue prevented any correlation of the acquired spectra with a specific region of the tissue. The lack of a microscopic viewing system in the instrument compounded the problem. Experiments were repeated with laser desorption alone (no matrix). However, no signal for taxol was observed. Finally, attempts were made to analyze the different regions of the tumor separately by microdissecting the tumor prior to adding the matrix solution. This too was unsuccessful due to the small size of the tumor.

#### Analysis of Polymyxin B<sub>1</sub> from Human Plasma

In the final application experiment, MALDI was used to analyze the antibiotic drug compound Polymyxin B<sub>1</sub>. Polymyxins are cyclic amphipathic peptides containing free amino acid groups and a fatty acid tail. Polymyxins are produced from *Bacillus polymyxa* and are commonly used to treat a variety of bacterial diseases including pneumonia, meningitis, and gonorrhea.<sup>63</sup> Polymyxins work by binding to the cell membranes of Gram-negative bacteria and disrupting their structure and permeability properties.<sup>123</sup> Recently there has been a great deal of interest in developing liquid chromatography/tandem mass spectrometric methods (LC/MS/MS) to quantitate polymyxin B<sub>1</sub> in human plasma. While these methods have been shown to produce adequate detection limits and accuracies, they require lengthy extraction and separation procedures prior to analysis.<sup>8</sup> The goal of this

final experiment was to evaluate the use of MALDI as a quick screening method for polymyxin B<sub>1</sub> and potentially other drug compounds from human plasma.

#### MALDI MS and MS/MS of Standard Polymyxin B<sub>1</sub>

Polymyxin B<sub>1</sub> (M.W. 1203) was obtained from Sandoz Research Institute (East Hanover, NJ). A standard solution was prepared by dissolving 1.0 mg of pure polymyxin B<sub>1</sub> in 10.0 mL of 50/50 methanol/water to give a final concentration of  $8.3 \times 10^{-5}$  M. For analysis, 2.0  $\mu$ L of the standard solution was first applied to the sample probe and allowed to dry. Four microliters of a 1.0 M DHB matrix solution prepared in methanol was then pipetted on top of the standard. The matrix solution dissolved the dried polymyxin B<sub>1</sub>, then crystallized upon evaporation of the solvent. The sample was further dried under a stream of warm air for an extended period up to 30 min. The MALDI MS/MS spectrum for polymyxin B<sub>1</sub> (Figure 4-13) was acquired using the instrumental and scan function parameters used previously for taxol. The only modifications involved changing the table mass of the isolation and MS/MS scan tables to correspond to the (M+H)<sup>+</sup> ion of polymyxin B<sub>1</sub>. MS/MS of the isolated (M+H)<sup>+</sup> ion of polymyxin B<sub>1</sub> at m/z 1204 resulted in the production of several low intensity daughter ions. The major daughter ions at m/z 1186, 1168, and 1150 resulted from successive losses of water. The daughter ion at m/z 1103 resulted from cleavage of the terminal acyl chain beta to the amide linkage. Cleavage of the first and third amide bonds along the peptide tail resulted in the two daughter ions at m/z 762 and m/z 963, respectively. A small peak at m/z 744 was also produced from loss of water from the m/z 762 ion.

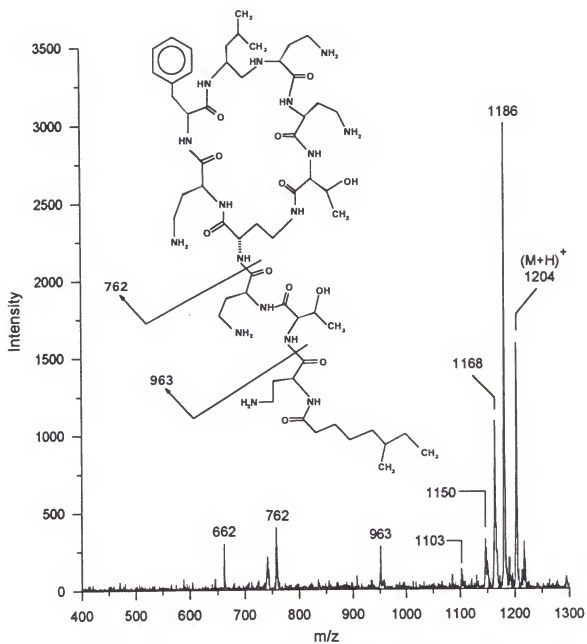


Figure 4-13. MALDI MS/MS spectrum of standard polymyxin B<sub>1</sub> using DHB matrix.

### MALDI Analysis of Human Plasma

Human blood was obtained from the University of Florida Infirmery and centrifuged to obtain whole plasma. Immediately following, 1.0 mL of the plasma was spiked with 1.0 mg of polymyxin B<sub>1</sub> and vortexed for approximately 10 min. For MALDI, 1.0  $\mu$ L of the drug/plasma mixture was spread over the tip of the sample probe. One microliter of DHB matrix solution prepared in methanol was then added on top of the plasma mixture. The matrix solution dissolved some of the plasma sample resulting in a gelatinous material on the probe tip. Irregular shaped matrix crystals were also observed in the plasma as well as around the edges of the sample. The MALDI MS and MS/MS spectra obtained for polymyxin B<sub>1</sub> from the plasma sample after thirty laser shots is shown in Figure 4-14. The entire analysis time from sample preparation to acquisition of the spectrum took approximately 8 min. The LC/MS/MS method by Boue<sup>8</sup> was reported to take close to an hour, including sample preparation. By comparing the MS/MS spectrum from the plasma sample with the daughter ion spectrum obtained for the polymyxin B<sub>1</sub> standard (Figure 4-15), the presence of polymyxin B<sub>1</sub> in the plasma was confirmed.

The shot-to-shot reproducibility and signal-to-noise (S/N) ratio for polymyxin from the plasma were rather poor. Attempts were made to adjust the polarity of the matrix solvent to extract more of the polymyxin out of the plasma. Since polymyxins contain both hydrophilic and hydrophobic parts, the choice of solvent was challenging. In the LC/MS/MS analysis of polymyxin B<sub>1</sub>, solid phase extraction (SPE) cartridges were used to extract polymyxin B<sub>1</sub> from spiked plasma samples.<sup>8</sup> In that work, the plasma



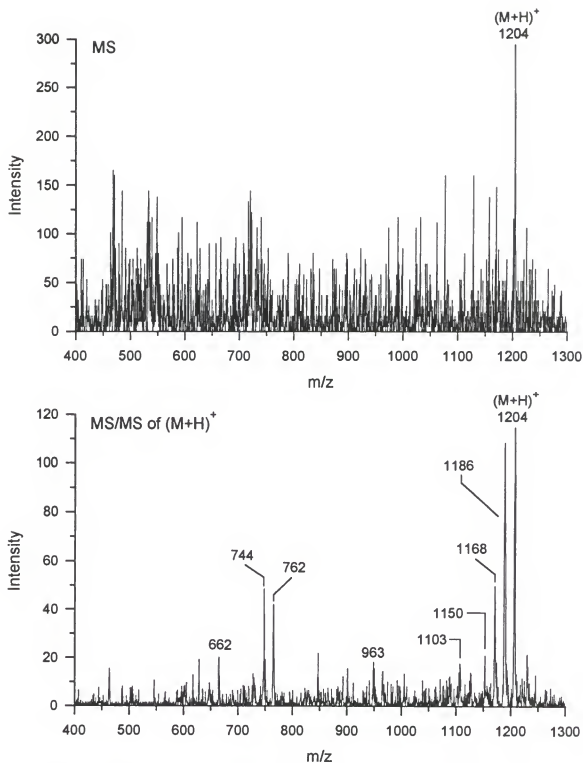


Figure 4-14. MALDI MS (top) and MS/MS (bottom) spectra of polymyxin B<sub>1</sub> from a 1.0  $\mu$ L sample of human plasma spiked with polymyxin B<sub>1</sub> (1 mg/mL).

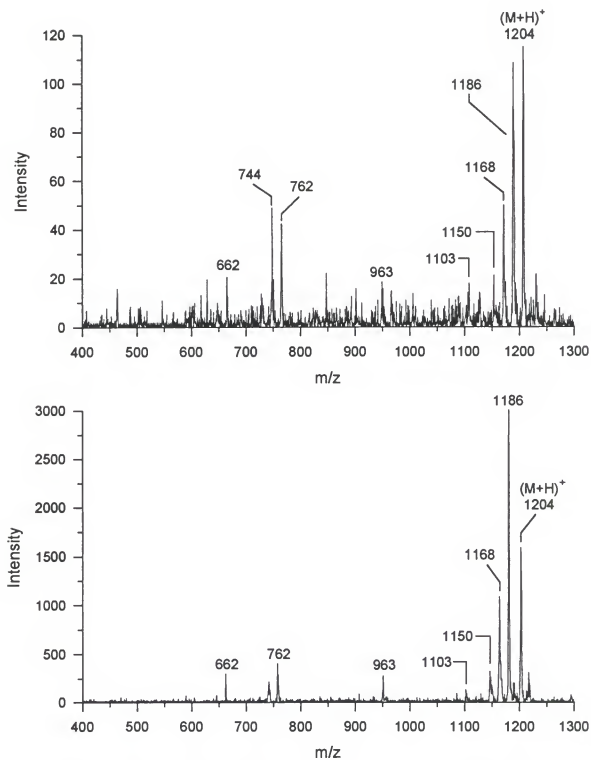


Figure 4-15. Comparison of the MS/MS spectra for polymyxin B<sub>1</sub> mixed with human plasma (top) and a polymyxin B<sub>1</sub> standard (bottom).

samples were first loaded onto SPE cartridges. Polymyxin was then eluted from the cartridges using a series of solvents. The best recovery rates (60-67%) were obtained using a 95% acetonitrile solution with 0.5% trifluoroacetic acid (TFA).

MALDI was repeated on a new 1.0  $\mu\text{L}$  sample of spiked plasma using a concentrated DHB matrix solution prepared in 95% acetonitrile with 0.5% TFA. As was the case in the previous MALDI experiment, it was difficult to obtain a reproducible ion signal for polymyxin B<sub>1</sub> from the plasma, presumably due to the incomplete drying of the plasma samples prior to analysis and the irregular matrix crystals that formed. In future experiments, a better approach to analyzing plasma samples by MALDI may be to completely dissolve the analyte/plasma mixture first, then add in the matrix solution in a similar solvent system prior to depositing the sample on the probe tip. Using this method, the sample surface and the matrix crystal layer should be more uniform. While MALDI may not be as quantitative an assay as LC/MS/MS, these initial results suggest that MALDI does have potential as a fast screening method for drug compounds in plasma.

#### LD/CI as an Alternative to MALDI

From the results presented in this chapter, MALDI using a quadrupole ion trap mass spectrometer was shown to be a viable technique for detecting trace levels of drug compounds from biological matrices. However, these same results revealed several drawbacks to MALDI which may limit its potential for imaging drug compounds in tissue. The first problem, discussed in chapter 2, is that the MALDI matrix solution can cause migration of the analyte molecules from their original location in the tissue. Second, from the experiments performed in this chapter with actual tissue from test animals, it was

learned that the matrix crystals can also make correlating the mass spectrum obtained from the tissue with the actual spot sampled by the laser difficult at best.

An ideal alternative to MALDI for imaging compounds in tissue may be laser desorption/chemical ionization (LD/CI). In LD/CI, the desorption laser is used to vaporize the analyte into the gas phase as intact neutrals. Ionization of the analyte occurs separately through ion molecule reactions (including charge exchange, proton-transfer, and proton-abstraction) between the desorbed neutrals and an excess of ionized reagent gas introduced into the ion source.<sup>124</sup> Typical reagent gas pressures for CI are between 0.1 - 1.0 torr to ensure that there is a 1000-fold or greater excess of reagent gas in the ion source.<sup>125</sup> LD/CI was first introduced by Cotter<sup>126</sup> in 1980 in experiments with a sector instrument. In this work, reagent ions formed from isobutane reagent gas were used to ionize a series of glucuronide steroid neutrals formed by laser desorption. To date, most of the applications of LD/CI have been for the analysis of low molecular weight peptides deposited onto solid substrates.<sup>127</sup> The analytical appeal of post-chemical ionization is that the degree of fragmentation of the analyte can be controlled by the choice of reagent ion.<sup>127</sup> Also, since the yield of desorbed neutrals produced from laser desorption is typically much greater than the yield of desorbed ions,<sup>128</sup> post-chemical ionization offers the potential of enhancing the sensitivity significantly. The advantage of using LD/CI over MALDI for imaging drug compounds in tissue is that there is no matrix solution added to the sample which can cause the analytes to migrate.

The first application of LD/CI to the analysis of biological tissues was reported by Perchalski at the University of Florida in 1985 using a Finnigan TSQ triple quadrupole mass spectrometer.<sup>129</sup> The instrument was modified by machining the side flange of the

ion source to fit a fused silica lens used to introduce the desorption laser beam. The laser used was a coaxial flashlamp-pumped dye laser operated with Rhodamine 6G. The pulsewidth of the laser was 2.0  $\mu\text{s}$  with a pulse energy of 1.49 J. The EI/CI ion source of the TSQ was pressurized with methane reagent gas (0.9 torr) and heated to 160° C. Using this setup, LD/CI spectra were acquired for the antiepileptic drug phenytoin from fixed sections of rat liver tissue (Figure 4-16). The tissue was obtained from a test animal that had been given a loading of phenytoin (150 mg/kg) prior to sacrifice. In this work, postchemical ionization was used to prolong the phenytoin ion signal lifetime up to 400 ms in order to compensate for the slow scan speed of the quadrupole mass filter.

More recently in our laboratory, Vargas<sup>62</sup> attempted LD/CI of spiperone mixed with matrigel using an external LDI source on a quadrupole ion trap instrument. The goal of this experiment was to increase the sensitivity for detecting spiperone from matrigel by taking advantage of the excess of neutrals formed during the laser desorption process. Samples were deposited onto the tip of a stainless steel probe and inserted into the enclosed region of a high pressure ion volume situated in a Finnigan 4500 EI/CI ion source. The laser beam from a pulsed nitrogen laser was focused onto the sample surface through a 0.125" diameter hole machined in the side of the ion volume. Using this setup, however, no increase in ion signal was obtained for spiperone from matrigel, presumably due to the inability to achieve high enough reagent gas pressures in the ion volume to perform efficient CI.

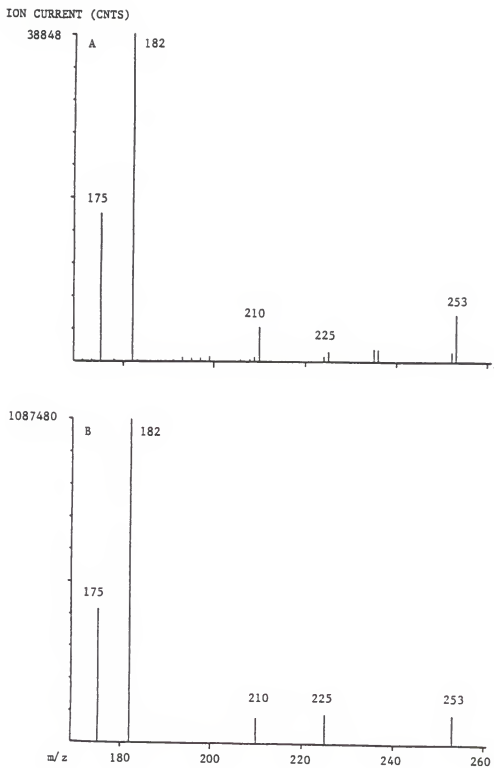


Figure 4-16. Comparison of the LD/CI daughter ion spectra of  $m/z$  253 for phenytoin from rat liver tissue (top), and for phenytoin deposited onto a copper grid (bottom).<sup>129</sup>

### Initial LD/CI Experiments with Trimethylphenylammonium Bromide

Before attempting LD/CI on analytes in tissue using the new laser desorption instrument, experiments were first performed with a test compound, trimethylphenylammonium bromide (TMPA). This compound was chosen to optimize the laser desorption instrument for LD/CI because it absorbed strongly at the wavelength of the desorption laser (337 nm) and therefore produced abundant ions and neutrals without the need for MALDI. A concentrated solution (0.1 M) was prepared by dissolving solid TMPA in methanol. For analysis, 1.0  $\mu\text{L}$  of the standard solution was deposited onto the surface of a stainless steel ion volume back. After drying, the CI ion volume cover was placed over the sample and secured to the ion volume back with the small wire clip (Figure 4-17). The entire ion volume assembly was then inserted into the ion source and locked into place in front of the first extraction lens.

In the first experiment, laser desorption was performed on TMPA without the presence of any reagent gas in the ion source. The laser beam was focused onto the sample surface through the exit hole in the ion volume cover. LD spectra were acquired using a modified version (lower  $q_{\text{inject}} = 0.180$ ) of the original MALDI scan function for sipiperone. With laser desorption alone, the spectrum acquired for TMPA contained only fragment ions (Figure 4-18). The peak at  $m/z$  121 corresponded to loss of a methyl group from the TMPA ion; loss of a hydrogen from the  $m/z$  121 ion gave the fragment peak at  $m/z$  120. A peak at  $m/z$  59 was also seen in the spectrum resulting from the loss of the phenyl group from the TMPA ion.

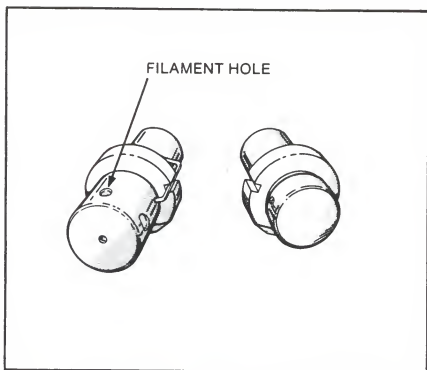


Figure 4-17. Diagram of the CI ion volume assembly (left) used for the LD/CI experiments. Samples were deposited onto the flat surface of the ion volume back (right).<sup>130</sup>



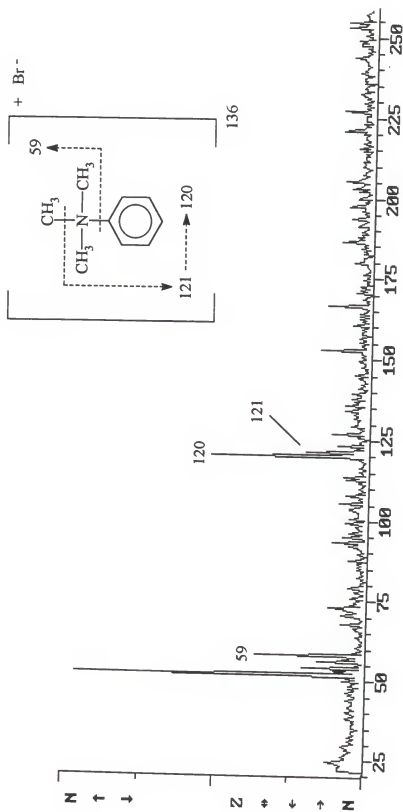


Figure 4-18. Laser desorption spectrum of trimethylphenylammonium bromide (TMPA), showing the fragment ions at  $m/z$  121, 120, and 59.

In the second experiment, methane reagent gas was introduced directly into the ion volume through a piece of 0.125" o.d. polyethylene tubing inserted through the GC transfer port in the source block. Prior to triggering the laser, the rhenium filament in the source was turned on to continuously ionize the reagent gas. The energy of the electron beam was set to 70 eV by varying the potential difference between the filament and the grounded source block. With the filament still on, the laser was fired at various spots on the sample probe. Because ions formed by CI have significantly less initial kinetic energy than MALDI generated ions, the voltage level on the source lenses had to be increased to successfully extract and focus the ions from the source into the DC quadrupole deflector. The voltages on the DC quadrupole rods were changed only slightly. Initially, the spectra acquired for TMPA were dominated by the fragment ions at  $m/z$  121, 120, and 59. However, by increasing the reagent gas pressure, the production of the molecular ion at  $m/z$  136 was improved significantly, as can be seen in Figure 4-19. The optimum pressure in the ion source region of the vacuum chamber was measured at  $6 \times 10^{-4}$  torr from the readout of the Bayard-Alpert ion gauge. The pressure inside the ion volume was measured at 0.2 torr using a capacitance manometer. The increase in the molecular ion signal for TMPA was due to a combination of collisional stabilization of the desorbed analyte ions and charge exchange or proton transfer reactions between the desorbed neutrals and the excess of methane reagent ions.

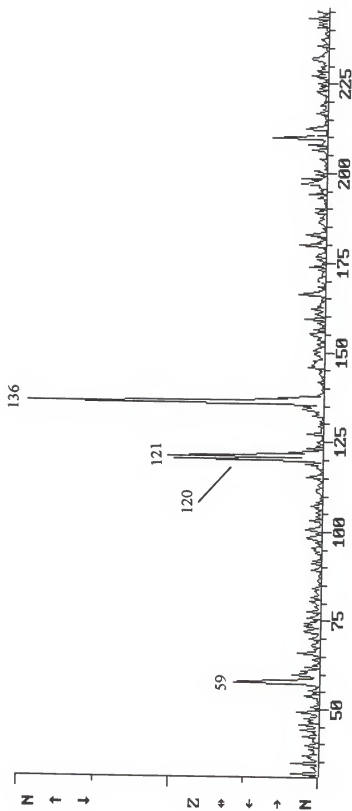


Figure 4-19. LD/CI spectrum of TMPA showing the increase in the parent ion at  $m/z$  136 using 0.2 torr of methane reagent gas in the ion source.

### LD/CI of Spiperone in Rat Cerebral Tissue

Following the initial optimization experiments with TMPA, LD/CI was attempted on a thin section of rat cerebral tissue that had been incubated in a solution of spiperone. The sample preparation procedure followed was the same as that used previously for the MALDI experiment, with the exception that no matrix solution was added to the tissue prior to analysis. Also, instead of using the MALDI probe to introduce the sample into the instrument, the tissue section was placed inside the enclosed ion volume. After inserting the ion volume into the ion source, laser desorption was performed on the tissue section. Without the addition of the MALDI matrix, no peaks were observed for spiperone or for the tissue itself. Following this experiment, methane reagent gas was introduced into the ion source at an initial pressure of 0.2 torr. The laser was again fired at several spots on the tissue. LD/CI was attempted for the tissue sample using reagent gas pressures up to 0.9 torr. As was the case in the first experiment, however, no signal was recorded for spiperone.

After analysis, the tissue sample was removed from the ion source and observed under the microscope. In contrast to the tissue samples analyzed by MALDI, there were no laser holes in the tissue. The observations and results from these initial LD/CI experiments suggest that without the addition of the UV matrix, the absorbance of the tissue is not strong enough to allow the laser to probe through the tissue and desorb analyte molecules embedded below the surface. This is not surprising given the relatively low energy per pulse of the nitrogen laser (250  $\mu\text{J}/\text{pulse}$ ). To overcome this problem in the future, a laser with significantly higher energy (1-2 J/pulse) will be needed.

## CHAPTER 5 CONCLUSIONS AND FUTURE WORK

The goals of this project were to determine if MALDI could be used to detect pharmaceutical drug compounds from intact biological tissues, and to evaluate the potential of MALDI on a quadrupole ion trap mass spectrometer for future microprobe analysis of drug compounds from complex biological matrices. In the first work with the Lasermat instrument, MALDI was used successfully to increase the production of the  $(M+H)^+$  ion for spiperone and ephedrine from matrigel. The MALDI mechanism for drug compounds in tissue was found to involve two sequential steps. In the first step, the embedded analyte molecules were extracted from the tissue and into the matrix solution applied on top of the tissue. In the second step, the extracted analyte molecules became encapsulated in the matrix crystal layer which formed upon evaporation of the matrix solvent.

Three parameters were found to be important in increasing the amount of analyte detected using MALDI. Adjusting the polarity of the matrix solvent to match that of the embedded drug compound was found to cause more of the analyte to partition out of the tissue and into the matrix solution. In addition, the crystallization speed of the matrix solution was found to have a significant effect on the production of analyte ion signal from matrigel. It was observed that when the matrix droplet was allowed to soak on top of the tissue for several minutes before crystallizing, a more efficient extraction of the drug compounds from the matrigel was achieved. This in turn resulted in an increase in the

peak area of the analyte  $(M+H)^+$  ion signal. The final parameter studied was the concentration of the matrix solution. Addition of a small volume of DHB matrix solution at concentrations of 0.01 M, 0.15 M, and 0.25 M resulted in the production of  $(M+H)^+$  ion signals for both spiperone and ephedrine in matrigel. With the most concentrated matrix solution, sevenfold and ninefold increases in the peak area of the  $(M+H)^+$  ions of ephedrine and spiperone were observed, respectively.

While the results of the experiments with matrigel clearly showed that optimizing the MALDI process can increase the sensitivity for detecting drug compounds in tissue, it is not suggested that lengthy optimization procedures be conducted for every potential compound analyzed. Instead, future experiments should focus on developing MALDI protocols for whole classes of compounds. For example, in this work three different drug compounds (spiperone, taxol, and polymyxin B<sub>1</sub>) were detected from biological matrices using the same DHB matrix in methanol. The MALDI protocols should include the choice of matrix compound, solvent mixture, and matrix solution concentration that work best for a group of compounds. While DHB proved to be useful in all of the applications presented here, it is likely that other MALDI matrices will perform better for different classes of compounds. The use of co-matrices has been shown to increase the reproducibility of MALDI signals and should therefore be investigated for analysis of tissues.<sup>55</sup> The advantage of developing MALDI protocols for whole classes of compounds rather than individual compounds is that the analysis time would be significantly reduced. These protocols would also be useful in cases where the tissue sample being analyzed contains an unknown compound.

In the second part of this project, an external laser desorption ion source was coupled to an ion trap mass spectrometer using a DC quadrupole deflector. The operation of the ion injection system was optimized for MALDI using the ion optics simulation program SIMION V6.0s. Experiments were performed to simulate the trajectories for ten ions formed by EI and MALDI, respectively. The results of the simulations confirmed that the DC quadrupole deflector functions as an energy analyzer. As the initial kinetic energy of the ions increased, higher voltage levels were required on the quadrupole rods of the deflector to successfully turn and focus the ions into the ion trap. While simulations were performed to investigate the trajectories for MALDI ions up to  $m/z$  3000 (10 eV), a full characterization of the DC quadrupole deflector system was not performed in this work. Future simulation experiments should focus on determining the maximum  $m/z$  MALDI ions that can be successfully turned and focused by the DC quadrupole deflector using the current instrumental power supplies. Simulations should also be used to further optimize the transmission efficiency of the ion injection system using greater numbers of ions with the goal of increasing the overall sensitivity of the instrument.

To evaluate the potential of the new instrument for future microprobe analysis, three pharmaceutical drug compounds (spiperone, taxol, and polymyxin B<sub>1</sub>) were analyzed in tissues obtained directly from test species. In these experiments, the addition of the MALDI matrix solution produced significant background ions from the tissue which complicated the spectra. To overcome this problem, the  $(M+H)^+$  ion for the respective analytes was isolated inside of the ion trap, then fragmented by CID to produce daughter ions. The presence of the drug compounds in the various tissues was confirmed by comparing the resulting daughter ion spectra with the corresponding daughter ion spectra

for standards of each drug compound. The lowest level of drug compound detected was 280 pg for spiperone from rat cerebral tissue. The results of these experiments showed that the MS/MS capabilities of the ion trap are necessary for detecting trace levels of drug compounds from complex biological matrices.

While MALDI was shown to be a useful technique for detecting drug compounds in tissue, it may prove less useful for applications involving imaging of analytes in tissue. In the experiments with spiperone in matrigel, addition of the matrix solution caused the analyte to migrate from its original location in the tissue. Electrospray deposition of the matrix solution was performed and found to reduce the migration of spiperone in matrigel. However, the sensitivity for detecting spiperone was significantly reduced because of the rapid evaporation and crystallization of the matrix solution. Electrospray deposition was not performed on any of the actual tissue samples from test animals prepared in this work. Future experiments should be performed to determine whether electrospray deposition can be used to detect trace levels of drug compounds from complex tissues. Another problem encountered with MALDI was the fact that the thick matrix crystal layer that formed on top of the tissue samples prevented specific regions of the tissue from being identified and targeted for analysis. For tissue samples in which the location of the analyte of interest is previously known, this problem can be overcome by cutting out the region of tissue containing the analyte and analyzing it separately from the rest of the tissue. However, in applications where the location of the drug is not known, it is necessary to be able to observe the tissue surface in order to determine which regions of the tissue were sampled by the desorption laser.



One possible solution is to apply the matrix solution to the sample probe first, then place a thin tissue section on top of the dried matrix crystals. This technique is known as substrate-assisted laser desorption ionization (SALDI). To perform SALDI of tissue samples it is likely that a laser with at least a millijoule to possibly a joule of energy per pulse will be needed to burn through the tissue to desorb both the embedded analyte molecules and the matrix crystals underneath. Another possible alternative is to freeze the tissue samples and use the ice crystals that form within the tissue as the absorbing matrix. The difficulty in doing this, however, is that the sample must be kept frozen inside of the vacuum chamber during the analysis. This can be achieved by introducing a liquid nitrogen cold finger into the vacuum chamber in such a way that it makes contact with the sample probe in the ion source. MALDI in this way would require an IR laser to match the absorbance of the ice crystals.

One of the most promising alternatives for detecting drug compounds from tissue without the use of a matrix solution is laser desorption/chemical ionization. In this work, preliminary LD/CI experiments were performed with TMPA using methane reagent gas. By introducing an excess of reagent gas ions into the ion source during the laser desorption event, the production of the intact molecular ion for TMPA was increased. LD/CI experiments were also performed on samples of spiperone in rat cerebral tissue. Without the addition of the UV-absorbing matrix, however, the laser beam was not able to probe deeply enough into the tissue to desorb and ionize the embedded analyte molecules. While the results of these initial experiments were inconclusive, they demonstrated that the design of the new instrument was adequate for performing LD/CI. Future work with LD/CI should focus first on understanding the LD/CI process itself. To date, most of the

applications of post-chemical ionization have been made for thermally desorbed neutrals from solids probes. Pressure studies and experiments with various reagent gases should be conducted to optimize the CI process for laser desorbed neutrals. For LD/CI of tissues, a more powerful laser (in the mJ-J/pulse range) should be employed to ensure that the maximum number of analyte neutrals are desorbed from the tissue to increase the sensitivity.

In order for the new laser desorption instrument to be used for microprobe applications, instrumental improvements must be made to allow the sample to be viewed under magnification inside of the vacuum chamber and to allow specific regions of tissue samples to be targeted with high spatial resolution. With the off-axis design of the ion source, samples can easily be viewed by positioning a microscope objective in front of the ion source block. To secure the objective, a holder can be mounted directly to the DC quadrupole deflector assembly. It is suggested that a reflecting microscope objective be used since it incorporates special optics which can withstand the high irradiance levels of the laser beam. These objectives are also ideal because they can provide magnification up to 40x at focal lengths of greater than two inches. To view the image of the sample a CCD camera and monitor can be positioned outside of the vacuum chamber. There are two possible ways to pinpoint specific locations on samples which can be implemented on the new laser desorption instrument. The first method involves rastering the laser beam across the surface of the sample while holding the sample probe in position in the ion source. This can be done by using a motor driven mirror positioned outside of the vacuum chamber to focus the laser beam into the ion source. Motorized mirror systems use a computer-controlled x,y,z micromanipulator to direct the laser beam with spatial

resolution as low as 0.1  $\mu\text{m}$ . The advantage of this approach is that it requires no modifications of the existing instrumental hardware. However, since the diameters of the holes in the ion source lenses used to introduce the laser beam onto the sample are much less than the diameter of the sample probe, the outer edges of tissues samples would not be interrogated by the laser beam. The second approach involves moving the sample probe while keeping the laser beam fixed. This can be accomplished by adding an x,y,z manipulator between the solids probe lock and the vacuum flange of the ion source. This approach requires modifications to the source flange, but would allow the entire area of the sample to be analyzed.

In addition to moving towards imaging of drug compounds in tissue, future applications of the laser desorption instrument should also focus on developing quantitative assays for drug compounds in various biological matrices. One approach to doing this is to use internal standards mixed with the matrix solution. Other potential experiments include monitoring drug metabolites and possibly naturally occurring biomolecules such as neurotransmitters directly from biological tissues.

In conclusion, from the results presented in this dissertation MALDI was shown to be an ideal technique for detecting drug compounds directly from intact biological tissues. It is also clear from this work that the MS/MS capabilities of the ion trap are needed for detecting trace levels of compounds from very complex tissues. With the addition of both a microscopic viewing system and a sample manipulation system, the new laser desorption quadrupole ion trap instrument has the potential for a true molecular microprobe.

## LIST OF REFERENCES

1. Kahn, P. *Science*. **1995**, 270, 368-370.
2. Umesh, V.; Welling, P. *The Drug Development Process*. Marcel Dekker Press: New York, **1996**, 447.
3. Nicholas, T.; Gardner, G; Gordon, D. *Tetrahedron*. **1995**, 51, 8135-8173.
4. Thayer, A.M. *Chem. Eng. News*. **1996**, 74, 7, 57-73.
5. Stahl, E. *Drug Analysis by Chromatography and Microscopy*. Ann Arbor Press: Ann Arbor, **1973**, 57-81.
6. Perun, T.J.; Propst, C.L. *Nucleic Acid Targeted Drug Design*. Marcel Dekker Press: New York, **1992**, 619-720.
7. Betzig, E.; Trautman, J.K. *Science*. **1992**, 257, 189-195.
8. Boue, S. Ph.D. Dissertation. *The Analysis of Antibiotics using Electrospray Quadrupole Ion Trap Mass Spectrometry: IRMPD and LC/MS*. University of Florida, **1997**.
9. Nowack, R. *Science*. **1995**, 270, 369-371.
10. Williams, M.; Malick, J. *Drug Discovery and Development*. Humana Press: Clifton, NJ, **1987**, 447-458.
11. Hercules, D.M.; Novak, F.P.; Viswanadham, S.K.; Wilk, Z.A. *Anal. Chem. Acta*. **1987**, 193, 61-71.
12. Kelland, D.; Wallach, E.R. *Anal. Chem. Acta*. **1987**, 195, 89-96.
13. Lee, M.S.; Yost, R.A. *Biomed. Environ. Mass Spectrom*. **1988**, 15, 193-205.
14. O'Shea, D.C.; Callen, W.R.; Rhodes, W.T. *Introduction to Lasers and their Applications*. Addison Wesley: Menlo Park, **1978**.
15. Honig, R.E.; Woolston, J.R. *Appl. Phys. Lett*. **1963**, 2, 138-139.

16. Conzemius, R.J.; Svec, H.J. *Anal. Chem.* **1978**, *50*, 1854-1861.
17. Bingham, R.A.; Salter, P.L. *Anal. Chem.* **1976**, *48*, 1735-1739.
18. Perchalski, R.J.; Wilder, B.J.; Yost, R.A. *Anal. Chem.* **1983**, *55*, 2002-2005.
19. Spengler, B.; Cotter, R.J. *Anal. Chem.* **1990**, *62*, 793-799.
20. Schwartz, J.C.; Bier, M.E. *Rapid Commun. Mass Spectrom.* **1993**, *7*, 27-32.
21. Verbukun, A.H.; Bruynseels, F.J.; Van Grieken, R.E. *Biomed. Mass Spectrom.* **1985**, *12*, 438-462.
22. Heinen, H.J.; Wechsung, R.; Vogt, H.; Hillenkamp, F.; Kaufmann, R. *Biotechn. Umschau* **1984**, *2*, 346-351.
23. Wechsung, R.; Hillenkamp, R.; Kaufmann, R.; Nitsche, R.; Vogt, H. *Scanning Electron Microsc.* **1978**, *I*, 611-615.
24. Kaufmann, R.; Hillenkamp, F.; Wechsung, R.; Heinen, H.J.; Schurmann, M. *Scanning Electron Microsc.* **1979**, *II*, 279-282.
25. Kaufmann, R.; Hillenkamp, F.; Wechsung, R. *Med. Progr. Technol.* **1979**, *6*, 109-115.
26. Vandeputte, D.; Savory, J. *Biomed. Environ. Mass Spectrom.* **1989**, *18*, 598-602.
27. *Laser Microprobe Mass Analyzer Brochure*. Leybold-Heraeus: Export, PA, **1982**.
28. Verbukueken, A.H.; Van Grieken, R.E. *Anal. Chem. Acta.* **1987**, *195*, 62-70.
29. Cotter, R.J.; Tabet, J. *Amer. Lab.* **1984**, April, 86-99
30. Karas, M.; Bahr, U.; Giebmann, U. *Mass Spectrom. Rev.* **1991**, *10*, 335-357.
31. McCrery, D.A.; Gross, M.L. *Anal. Chem. Acta.* **1985**, *178*, 105-115.
32. Van Vaeck, L.; Claereboudt, J.; De Waele, J. *Anal. Chem.* **1985**, *57*, 2944-2951.
33. Hillenkamp, F.; Karas, M.; Bachmann, D. *Anal. Chem.* **1985**, *57*, 2935-2939.
34. Karas, M.; Hillenkamp, F. *Anal. Chem.* **1988**, *60*, 2299-2301.

35. Vertes, A.; Gijbels, R. *Laser Ionization Mass Analysis*. John Wiley & Sons: New York, 1993, 127-149.
36. Karas, M.; Bahr, U.; Ingendoh, A.; Hillenkamp, F. *Angew. Chem. Int. Ed. Engl.* 1989, 28, 760-761.
37. Wu, K.J.; Steding, A.; Becker, C.H. *Rapid Commun. Mass Spectrom.* 1991, 5, 319-324.
38. Stahl, B.; Steup, M.; Karas, M.; Hillenkamp, F. *Anal. Chem.* 1991, 63, 1463-1472.
39. Hercules, D.M.; Kubis, A.J.; Somayajula, K.V.; Sharkey, A.G. *Anal. Chem.* 1989, 61, 2516-2523.
40. Henzel, W.J.; Billeci, T.M.; Stults, J.T.; Wong, S.C.; Grimley, C.; Watanabe, C. *Proc. Natl. Acad. Sci. U.S.A.* 1993, 90, 5011-5015.
41. Karas, M.; Bahr, U.; Ingendoh, A.I.; Nordhoff, E.; Stahl, B.; Hillenkamp, F. *Anal. Chim. Acta.* 1990, 241, 175-185.
42. Mock, K.K.; Sutton, C.W.; Cottrell, J.S. *Rapid Commun. Mass Spectrom.* 1992, 6, 233-238.
43. Eckerskorn, C.; Strupat, K.; Karas, M.; Hillenkamp, F.; Lottspeich, F. *Electrophoresis* 1992, 13, 664-665.
44. Aebersold, R.M.; Teplow, D.B.; Hood, L.E.; Kent, S.B. *J. Biol. Chem.* 1986, 261, 4229-4238.
45. Fenselau, C.; Vestling, M.M. *Anal. Chem.* 1994, 66, 471-477.
46. Strupat, K.; Karas, M.; Hillenkamp, F. *Anal. Chem.* 1994, 66, 464-470.
47. Beavis, R. *Org. Mass Spectrom.* 1992, 27, 864-868.
48. Vertes, A.; Gijbels, R.; Irinyi, G. *Anal. Chem.* 1993, 65, 2389-2393.
49. Spengler, B.; Kaufmann, R. *Anal. Chem.* 1992, 20, 91-101.
50. Wang, B.H.; Dreisewerd, K.; Bahr, U.; Karas, M.; Hillenkamp, F. *J. Am. Soc. Mass Spectrom.* 1993, 4, 393-398.
51. Borsen, K.O.; Schar, M.; Gassmann, E.; Steiner, V. *Biol. Mass Spectrom.* 1991, 20, 471-478.

52. Beavis, R.C.; Chait, B.T.; Hillenkamp, F.; Karas, M. *Anal. Chem.* **1991**, *24*, 1193A-1202A.
53. Vorm, O.; Mann, M. *J. Am. Soc. Mass Spectrom.* **1994**, *5*, 955-958.
54. Caprioli, R.M.; Andren, P.E. *J. Mass Spectrom.* **1995**, *30*, 817-824.
55. Hercules, D.M.; Proctor, A.; Wilkinson, W.R.; Gusev, A.I. *Anal. Chem.* **1995**, *67*, 1034-1041.
56. Williams, P.; Thomas, R.M.; Nelson, R.W. *Rapid Commun. Mass Spectrom.* **1990**, *4*, 348-351.
57. Beavis, R.C.; Chait, B.T. *Rapid Commun. Mass Spectrom.* **1989**, *3*, 432-435.
58. Zhao, S.; Somayajula, K.V.; Sharkey, A.G.; Hercules, D.M.; Hillenkamp, F.; Karas, M.; Ingendoh, A. *Anal. Chem.* **1991**, *63*, 450-453.
59. Overberg, A.; Karas, M.; Bahr, U.; Kaufmann, R.; Hillenkamp, F. *Rapid Commun. Mass Spectrom.* **1990**, *4*, 293-296.
60. Gimon, M.E.; Preston-Schaffter, L.M.; Russell, D. in *Proceedings of the 42<sup>nd</sup> ASMS Conference on Mass Spectrometry and Allied Topics*. Chicago, IL, **1994**, 1347.
61. *MALDI Matrices Reference Guide*. Thermo Bioanalysis Limited: Hemel Hempstead, UK, **1995**.
62. Vargas, R. Ph.D. Dissertation. *Development of Laser Desorption Ionization on a Quadrupole Ion Trap Mass Spectrometer*. University of Florida, **1993**.
63. Raven, P.H.; Johnson, G.B. *Biology*. Times Mirror/Mosby Publishing: St Louis, **1986**, 906-908.
64. *Lasermat Users Guide*. Finnigan MAT: Hemel Hempstead, UK, **1991**.
65. Winograd, N. *Anal. Chem.* **1993**, *65*, 622A-629A.
66. Booth, M.M. Ph.D. Dissertation. *Matrix-Assisted Laser Desorption Ionization (MALDI) Tandem Mass Spectrometry (MS<sup>n</sup>) Using a Quadrupole Ion Trap*. University of Florida, **1996**.
67. Giddings, J.C. *Unified Separation Science*. John Wiley & Sons Inc.: New York, **1991**, 29-30.
68. Cottrell, T.S.; Mock, K.K. *Rapid Commun. Mass Spectrom.* **1992**, *6*, 233-238.

69. Paul, W.; Steinwedel, H. *U.S. Patent 2,939,952* filed December 21, 1954 (German Patent filed December 1953).
70. March, R.E.; Todd, J.F. *Practical Aspects of Ion Trap Mass Spectrometry Vol. I. Fundamentals of Ion trap Mass Spectrometry*. CRC Press: Boca Raton, 1995, 26-48.
71. Paul, W.; Reinhard, H.P.; Zahn, U. *Z. Phys.* 1958, 152, 143-182.
72. Wuerker, R.F.; Shelton, H.; Langmuir, R.V. *J. Appl. Phys.* 1959, 30, 342.
73. Major, F.G.; Dehmelt, H.G. *Phys. Rev.* 1968, 179, 91-107.
74. Fischer, E. *Z. Phys.* 1959, 156, 1-26.
75. Dawson, P.H.; Whetten, N.R. *J. Vac. Sci. Technol.* 1968, 5, 11-18.
76. Stafford, G.C.; Kelley, P.E.; Bradford, D.C. *Am. Lab.* 1983, 51-57.
77. Weber-Grabau, M.; Kelley, P.E.; Syka, J.E.P.; Bradshaw, S.C.; Hoekman, D.J. in *Proceedings of the 36<sup>th</sup> ASMS Conference on Mass Spectrometry and Allied Topics*. San Francisco, CA, 1988, 1106-1107.
78. Busch, K.L.; Glish, G.L.; McLuckey, S.A. *Mass Spectrometry/Mass Spectrometry: Techniques and Applications of Tandem Mass Spectrometry*. VCH: New York, 1988, 87-90.
79. Kaiser, R.E.; Louris, J.N.; Amy, J.W.; Cooks, R.G. *Rapid Commun. Mass Spectrom.* 1989, 3, 225-229.
80. Yates, N.A.; Yost, R.A.; Bradshaw, S.C.; Tucker, D.B. in *Proceedings of the 39<sup>th</sup> ASMS Conference on Mass Spectrometry and Allied Topics*. Nashville, TN, 1991, 132-133.
81. Gronowska, I.W.; Paradisio, C.; Traldi, P.; Vettori, U. *Rapid Commun. Mass Spectrom.* 1990, 4, 306-313.
82. Kaiser, R.E.; Cooks, R.G.; Syka, J.E.P.; Stafford, G.C. *Rapid Commun. Mass Spectrom.* 1990, 4, 30-35.
83. Duckworth, D.C.; Barschick, C.M. Smith, D.H.; McLuckey, S.A. *Anal. Chem.* 1994, 66, 92-98.



84. Louris, J.N.; Brodbelt, J.S.; Kaiser, R.E.; Cooks, R.G. in *Proceedings of the 35<sup>th</sup> ASMS Conference on Mass Spectrometry and Allied Topics*. Denver, CO, 1987, 766-767.
85. Weber-Grabau, M; Kelley, P.E.; Syka, J.E.P.; Bradshaw, S.C.; Brodbelt, J.S. in *Proceedings of the 35<sup>th</sup> ASMS Conference on Mass Spectrometry and Allied Topics*. Denver, CO, 1987, 769-770.
86. Van Berkel, F.J.; Glish, G.L.; McLuckey, S.A. *Anal. Chem.* 1990, 62, 1284-1295.
87. Knight, R.D.; *Int. J. Mass Spectrom. Ion Processes.* 1991, 106, 63-65.
88. Mathieu, E.J. *Math Pure Appl.* 1868, 13, 137.
89. Guidugli, F.; Traldi, P. *Rapid Commun. Mass Spectrom.* 1991, 5, 343-349.
90. Louris, J.; Stafford, G.; Syka, J.; Taylor, D. in *Proceedings of the 40<sup>th</sup> ASMS Conference on Mass Spectrometry and Allied Topics*. Washington, DC, 1992, 1003.
91. Johnson, J.V.; Pedder, R.E.; Yost, R.A. *Rapid Commun. Mass Spectrom.* 1992, 6, 760-764.
92. Kelly, P.E.; Hoekman, D.J.; Bradshaw, S.C. in *Proceedings of the 41<sup>st</sup> ASMS Conference on Mass Spectrometry and Allied Topics*. San Francisco, CA, 1993, 453.
93. Soni, M.H.; Cooks, R.G. *Anal. Chem.* 1994, 66, 2488-2496.
94. Schwartz, J.C.; Jardine, I. *Rapid Commun. Mass Spectrom.* 1992, 6, 313-317.
95. Kaiser, R.E.; Cooks, R.G.; Stafford, G.C.; Syka, J.E.P.; Hemberger, P.H. *Int. J. Mass Spectrom. Ion Processes.* 1991, 106, 79-85.
96. Cotter, R.; Heller, D.N.; Lys, I.; Uy, O.M. *Anal. Chem.* 1989, 61, 1083-1089.
97. Glish, G.L.; Goeringer, D.E.; McLuckey, S.A. *Int. J. Mass Spectrom. Ion Processes.* 1989, 94, 15-24.
98. Vargas, R.; Yost, R.A. in *Proceedings of the ASMS Sanibel Conference on Lasers in Mass Spectrometry*. Sanibel, FL, 1992.
99. Cotter, R.J.; Doroshenko, V.M.; Cornish, T.J. *Rapid Commun. Mass Spectrom.* 1992, 6, 753-757.

100. Vargas, R.; Yost, R.A. in *Proceedings of the Pittsburgh Conference on Analytical Chemistry and Applied Spectroscopy*. Atlanta, GA, 1992, 548.
101. Beavis, R.C.; Chait, B.T. *Chem. Phys. Letters*. 1991, 181, 479.
102. Glish, G.L.; Chambers, D.M.; Goeringer, D.E.; McLuckey, S.A. in *Proceedings of the 40<sup>th</sup> ASMS Conference on Mass Spectrometry and Allied Topics*. Washington, DC, 1992, 1747-1748.
103. Louris, J.N.; Amy, J.W.; Ridley, T.Y.; Cooks, R.G. *Int. J. Mass Spectrom. Ion Processes*. 1989, 88, 97.
104. Vargas, R.; Yost, R.A.; Lee, M.S.; Moon, S.; Rosenberg, I.E. in *Proceedings of the Pittsburgh Conference on Analytical Chemistry and Applied Spectroscopy*. Atlanta, GA, 1993, 1225.
105. Reddick, C.D.; Booth, M.M.; Yost, R.A. in *Proceedings of the 44<sup>th</sup> ASMS Conference on Mass Spectrometry and Allied Topics*. Portland, OR, 1988, 1366.
106. Zeman, H.D. *Rev. Sci. Instrum.* 1977, 48, 1079-1085.
107. Russell, D.H.; Hanson, D.H.; Castro, M.E. in *Proceedings of the 35<sup>th</sup> ASMS Conference on Mass Spectrometry and Allied Topics*. Denver, CO, 1988, 1152-1153.
108. Pedder, R.E.; Yost, R.A. in *Proceedings of the 37<sup>th</sup> ASMS Conference on Mass Spectrometry and Allied Topics*. Miami, FL, 1989, 468.
109. Pedder, R.E. Ph.D. Dissertation. *Fundamental Studies in a Quadrupole Ion Trap Mass Spectrometer*. University of Florida, 1992.
110. Griffin, T.P. Ph.D. Dissertation. *GC/MS/MS on the Quadrupole Ion Trap Mass Spectrometer: Software Development and the Examination of the Effects of Ion Population*. University of Florida, 1995.
111. Yates, N.A. Ph.D. Dissertation. *Methods for Gas Chromatography-Tandem Mass Spectrometry on the Quadrupole Ion Trap*. University of Florida, 1994.
112. Torrey, E.F. *Surviving Schizophrenia*. Harper Perennial: New York, 1995, 15-22.
113. Keefe, R.; Keefe, H. *Understanding Schizophrenia: A Guide to New Research on Causes and Treatment*. The Free Press: Toronto, 1994, 53-72.
114. Borne, R.F. *Drug Topics*. 1994, October 10, 108.

115. Escandon, N.A.; Zimmermann, D.C.; McCall, R.B. *J. Pharmacol. Exp. Ther.* **1994**, *268*, 441-447.
116. Wani, M.C.; Taylor, H.L.; Wall, M.E. *J. Am. Chem. Soc.* **1971**, *93*, 2325-2327.
117. Forastiere, A.A.; Rowinsky, E.K.; Chaudry, V. *Proc. of the Amer. Soc. of Clin. Onc. II.* **1992**, A-289, 117.
118. Rowinsky, E.K.; Donehower, R.C. *Cancer Treat. Rev.* **1993**, *19*, 63-78.
119. Nicolaou, K.C.; Guy, R.K.; Potier, P. *Sci. Amer.* **1996**, June, 94-98.
120. Schiff, P.B.; Horwitz, S.B. *Biochemistry.* **1981**, *20*(11), 3247-3252.
121. Lewis, R. *Biophotonics.* **1995**, July/August, 34-35.
122. Straubinger, R.M.; Sharma, A.; Mayhew, E. *Second National Cancer Institute Workshop on Taxol and Taxus.* **1992**, September 23-24, 115.
123. Fong, G.W.K.; Kho, B.T. *J. Liq. Chrom.* **1979**, *2*, 957-968.
124. Hart, K.J.; McLuckey, S.A.; Glish, G. *J. Am. Soc. Mass Spectrom.* **1992**, *3*, 549-557.
125. Harrison, A.G. *Chemical Ionization Mass Spectrometry.* CRC Press Inc.: Boca Raton, **1983**, 25-33.
126. Cotter, R.J. *Anal. Chem.* **1980**, *52*, 1767-1770.
127. Speir, J.P.; Gorman, G.S.; Amster, I. *J. Anal. Chem.* **1991**, *63*, 65-69.
128. van Breemen, R.B.; Snow, M.; Cotter, R.J. *Int. J. Mass Spectrom. Ion Processes.* **1983**, *49*, 35.
129. Perchalski, R. Ph.D. Dissertation. *Characteristics and Application of a Laser Ionization/Evaporation Source for Tandem Mass Spectrometry.* University of Florida, **1985**.
130. *Finnigan Mat 4500 Series GC/MS Operator's Manual.* Finnigan MAT: San Jose, CA, **1981**, 4-13.

## BIOGRAPHICAL SKETCH

Christopher Darrin Reddick was born in Washington, D.C., on April 19, 1970. Shortly after his eighth birthday, his parents moved the family to the suburbs of Silver Spring, Maryland. Growing up, Chris received most of his early education from staying up late with his parents while they studied for their undergraduate and graduate degrees. Because of this, Chris found his days in elementary school to be restrictive and rather boring. To offset the drudgeries of school, Chris became active in music and sports. By the age of thirteen he had learned to play several instruments in his junior high band and was playing for two basketball teams, the county soccer team, and the local YMCA football team. It should be pointed out that one of Chris's greatest achievements to date was scoring four touchdowns to win the county football championship in the 95 lb. and under division. The closest Chris came to science or engineering as a kid was dismantling and rebuilding bicycles during his BMX racing days.

Although Chris was able to do well in school when it counted, he had yet to reach his full academic potential. So in 1985, his parents enrolled him in St. John's Military Academy in Washington, D.C. Chris quickly adjusted and thrived in his new environment. By his senior year, Chris had reached the rank of captain, was sixteenth in his class, and was playing for his high school basketball team, which was ranked in the top ten in the country. After graduation, he attended Carnegie Mellon University in Pittsburgh. Chris initially started out as an aspiring music major, but quickly switched to the Math

Department. In his second semester he changed his major to chemistry because he thought that this was a more promising career path, but more importantly because he enjoyed tinkering in the lab. While at Carnegie Mellon, Chris interned at the Aluminum Company of America (ALCOA) just outside of Pittsburgh. It was at ALCOA that he was first introduced to analytical chemistry. Although his primary project involved developing supercritical-fluid chromatography (SFC) methods for contaminants in process lubricants, Chris realized early on that mass spectrometry was taking a commanding lead in analytical chemistry. On the advice of his supervisor Dr. Jerry Marks (a friend of Rick Yost's) and his mentor Dr. Robin Khosah, Chris applied to and was accepted at the University of Florida in August of 1992.

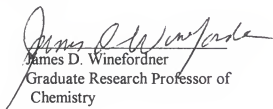
While in graduate school, Chris focused his research on using laser desorption ionization methods to analyze pharmaceutical drug compounds from biological tissues. This research eventually lead him to construct a new laser desorption mass spectrometer based on the quadrupole ion trap mass analyzer. For the final three years of his graduate research, Chris was supported on a grant from Bristol-Myers Squibb. Upon graduation, Chris will continue work in the pharmaceutical area at Bristol-Myers Squibb in New Brunswick, New Jersey.

I certify that I have read this study and that in my opinion it conforms to acceptable standards of scholarly presentation and is fully adequate, in scope and quality, as a dissertation for the degree of Doctor of Philosophy.



Richard A. Yost, Chair  
Professor of Chemistry

I certify that I have read this study and that in my opinion it conforms to acceptable standards of scholarly presentation and is fully adequate, in scope and quality, as a dissertation for the degree of Doctor of Philosophy.



James D. Winefordner  
Graduate Research Professor of  
Chemistry

I certify that I have read this study and that in my opinion it conforms to acceptable standards of scholarly presentation and is fully adequate, in scope and quality, as a dissertation for the degree of Doctor of Philosophy.



David H. Powell  
Associate Scientist of Chemistry

I certify that I have read this study and that in my opinion it conforms to acceptable standards of scholarly presentation and is fully adequate, in scope and quality, as a dissertation for the degree of Doctor of Philosophy.



James A. Deyrup  
Professor of Chemistry

I certify that I have read this study and that in my opinion it conforms to acceptable standards of scholarly presentation and is fully adequate, in scope and quality, as a dissertation for the degree of Doctor of Philosophy.



Howard M. Johnson  
Graduate Research Professor of  
Microbiology and Cell Science

This dissertation was submitted to the Graduate Faculty of the Department of Chemistry in the College of Liberal Arts and Sciences and to the Graduate School and was accepted as partial fulfillment of the requirements for the degree of Doctor of Philosophy.

August, 1997

---

Dean, Graduate School